

CHAPTER 4[†] THERMAL EVALUATION

The HI-STORM System is designed for long-term storage of spent nuclear fuel (SNF) in a vertical orientation. An array of HI-STORM Systems laid out in a rectilinear pattern will be stored on a concrete ISFSI pad in an open environment. In this section, compliance of the HI-STORM thermal performance to 10CFR72 requirements for outdoor storage at an ISFSI is established. Safe thermal performance during on-site loading, unloading and transfer operations utilizing the HI-TRAC transfer cask is also demonstrated. The analysis considers passive rejection of decay heat from the stored SNF assemblies to the environment under the most severe design basis ambient conditions. Effects of incident solar radiation (insolation) and partial radiation blockage due to the presence of neighboring casks at an ISFSI site are included in the analyses. Finally, the thermal margins of safety for long-term storage of both moderate burnup (up to 45,000 MWD/MTU) and high burnup spent nuclear fuel (greater than 45,000 MWD/MTU) in the HI-STORM 100 System are quantified.

The guidelines presented in NUREG-1536 [4.4.10] include eight specific acceptance criteria that should be fulfilled by the cask thermal design. These eight criteria are summarized here as follows:

1. The fuel cladding temperature at the beginning of dry cask storage should generally be below the anticipated damage-threshold temperatures for normal conditions and a minimum of 20 years of cask storage.
2. The fuel cladding temperature should generally be maintained below 570^oC (1058^oF) for accident, off-normal, and fuel transfer conditions.
3. The maximum internal pressure of the cask should remain within its design pressures for normal (1% rod rupture), off-normal (10% rod rupture), and accident (100% rod rupture) conditions.
4. The cask and fuel materials should be maintained within their minimum and maximum temperature criteria for normal, off-normal, and accident conditions.
5. For fuel assemblies proposed for storage, the cask system should ensure a very low probability of cladding breach during long-term storage.

[†] This chapter has been prepared in the format and section organization set forth in Regulatory Guide 3.61. However, the material content of this chapter also fulfills the requirements of NUREG-1536. Pagination and numbering of sections, figures, and tables are consistent with the convention set down in Chapter 1, Section 1.0, herein. Finally, all terms-of-art used in this chapter are consistent with the terminology of the glossary (Table 1.0.1) and component nomenclature of the Bill-of-Materials (Section 1.5).

6. Fuel cladding damage resulting from creep cavitation should be limited to 15% of the original cladding cross sectional area.
7. The cask system should be passively cooled.
8. The thermal performance of the cask should be within the allowable design criteria specified in FSAR Chapters 2 and 3 for normal, off-normal, and accident conditions.

As demonstrated in this chapter (see Subsections 4.4.6 and 4.5.6), the HI-STORM System is designed to comply with *all* eight criteria listed above. All thermal analyses to evaluate normal conditions of storage in a HI-STORM storage module are described in Section 4.4. All thermal analyses to evaluate normal handling and on-site transfer in a HI-TRAC transfer cask are described in Section 4.5. All analyses for off-normal conditions are described in Section 11.1. All analyses for accident conditions are described in Section 11.2. Sections 4.1 through 4.3 describe thermal analyses and input data that are common to all conditions. This FSAR chapter is in full compliance with NUREG-1536 requirements, subject to the exceptions and clarifications discussed in Chapter 1, Table 1.0.3.

This revision to the HI-STORM Safety Analysis Report, ~~the first since the HI-STORM 100 System was issued a Part 72 Certificate of Compliance~~, incorporates several features into the thermal analysis to respond to the changing needs of the U.S. nuclear power generation industry. The most significant changes are:

- *The Aluminum Heat Conduction Elements (AHCE), optional under CoC 1014-1, are eliminated from the design. Removing the AHCEs from the MPC eliminates the constriction to the downcomer flow (Figure 4.0.1) and accordingly boosts the thermal performance of the MPC.*
- *The whole spectrum of Regionalized storage of Spent Nuclear Fuel (SNF) for each MPC type has been analyzed to permit the user to select the heat load for region 2 (the outer region) and then determine the corresponding permissible heat load for region 1 (core region of the basket). The flexibility of selecting region 2 heat load afforded to the ISFSI owner by the analyses documented in this FSAR will permit MPCs to be loaded in the most effective manner to minimize the aggregate dose emitted from the totality of the casks arrayed on the pad.*
- *Certain storage scenarios, such as damaged fuel canister in region 2 and HI-TRAC placed in a deep pit (resulting in some restriction on heat dissipation to ambient) have been explicitly analyzed and reported in the FSAR.*
- *Certain elements of excessive conservatism in the mathematical model have been relaxed to retain a moderate level of conservatism. Subsection 4.4.6 documents conservatisms that apply to the thermal solution. A quantitative estimate of the consequences of each element of conservatism is provided in Appendix 4.B.*

- *The nominal helium fill pressure has been increased from 31.3 to 42.8 psig to facilitate increased heat dissipation from the MPC through the classical thermosiphon action (Figure 4.0.1).*
- ? ~~Post-core decay time (PCDT) limitations on high burnup fuel (burnup > 45,000 MWD/MTU) have been computed. The allowable cladding temperatures for high burnup PWR and BWR fuel, required to establish PCDT limits, are computed using a methodology consistent with ISG-11.~~
- ? ~~Both uniform and regionalized storage are permitted, the latter being particularly valuable in mitigating the dose emitted by the MPC by restricting "cold and old" SNF in the locations surrounding the core region of the basket (where the "hot and new" fuel is stored).~~
- ? ~~The effect of convective heat transfer in the MPC, originally included in the analysis but subsequently neglected to enable the NRC to make a more considered assessment of gravity-driven convective heat transfer in honeycomb basket equipped MPCs, is now reintroduced.~~
- ~~In the absence of the credit for convective (thermosiphon) effect, the previous analysis relied on the conduction heat transfer through the clearance between the basket and the MPC enclosure vessel. The conduction heat flow path was provided by the Aluminum Heat Conduction Elements (AHCE). The AHCE hardware is retained in the MPC and credit for ACHE heat dissipation is eliminated in the thermal analyses to maintain a solid margin of conservatism in the computed results. In a similar spirit of conservatism, the heat transfer in narrow cavities (the Rayleigh effect), approved by the SFPO in the previous analysis, is neglected in this revision.~~

Aside from the above-mentioned changes, this revision of this chapter is essentially identical to its predecessor.

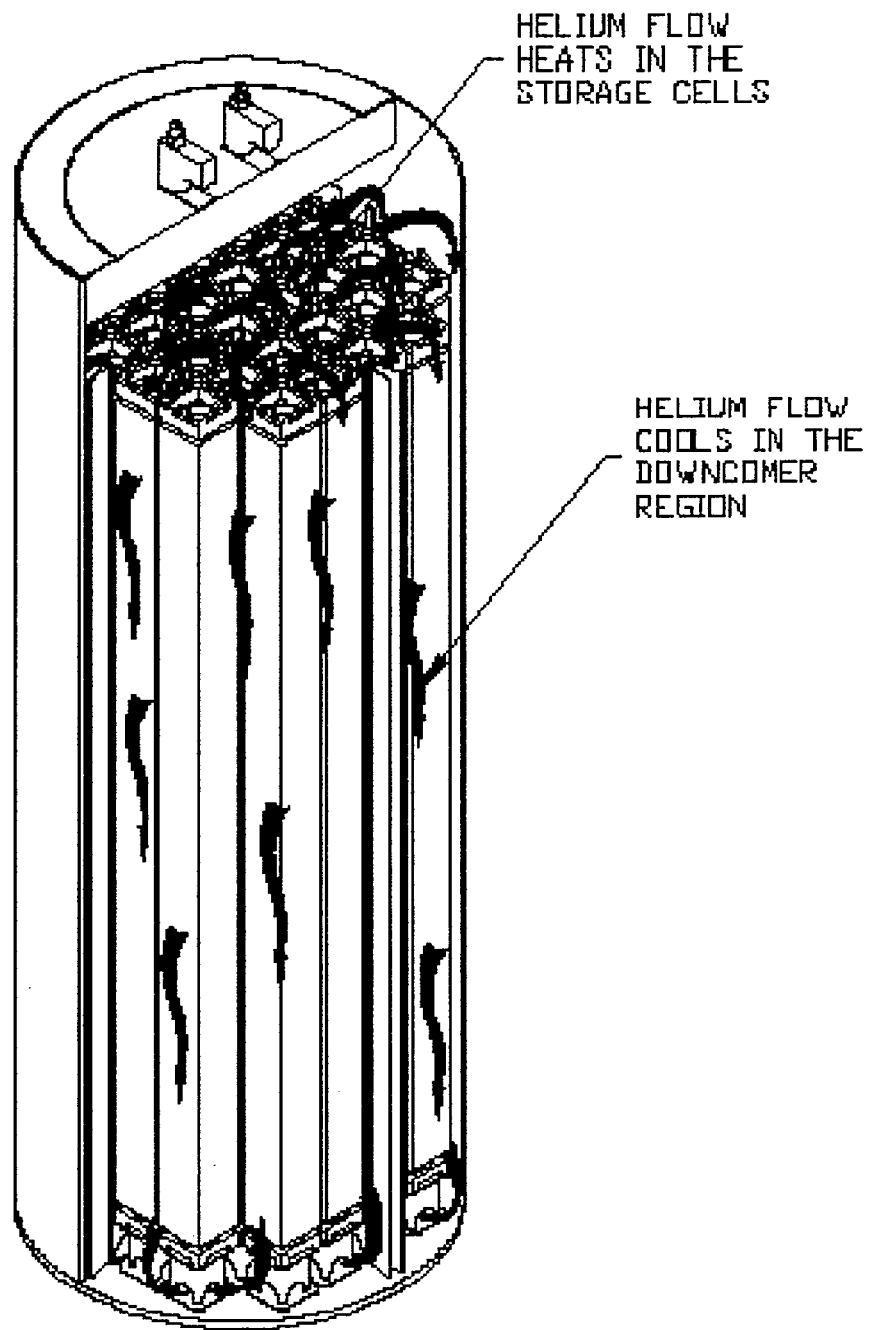


FIGURE 4.0.1: MPC INTERNAL HELIUM CIRCULATION

4.1 DISCUSSION

A sectional view of the HI-STORM dry storage system has been presented earlier (see Figure 1.2.1). The system consists of a sealed MPC situated inside a vertical ventilated storage overpack. Air inlet and outlet ducts that allow for air cooling of the stored MPC are located at the bottom and top, respectively, of the cylindrical overpack. The SNF assemblies reside inside the MPC, which is sealed with a welded lid to form the confinement boundary. The MPC contains an all-alloy honeycomb basket structure with square-shaped compartments of appropriate dimensions to allow insertion of the fuel assemblies prior to welding of the MPC lid and closure ring. Each box panel, with the exception of exterior panels on the MPC-68 and MPC-32, is equipped with a ~~Boral~~ (thermal neutron absorber) panel sandwiched between an alloy steel sheathing plate and the box panel, along the entire length of the active fuel region. The MPC is backfilled with helium up to the design-basis initial fill level (Table 1.2.2). This provides a stable, inert environment for long-term storage of the SNF. Heat is rejected from the SNF in the HI-STORM System to the environment by passive heat transport mechanisms only.

The helium backfill gas is an integral part of the MPC thermal design. The helium fills all the spaces between solid components and provides an improved conduction medium (compared to air) for dissipating decay heat in the MPC. Additionally, helium in the spaces between the fuel basket and the MPC shell is heated differentially and, therefore, subject to the "Rayleigh" effect which is discussed in detail later. For added conservatism, the increase in the heat transfer rate due to the Rayleigh effect contribution is neglected in this revision of the FSAR. To ensure that the helium gas is retained and is not diluted by lower conductivity air, the MPC confinement boundary is designed and fabricated to comply with the provisions of the ASME B&PV Code Section III, Subsection NB (to the maximum extent practical), as an all-seal-welded pressure vessel with redundant closures. It is demonstrated in Section 11.1.3 that the failure of one field-welded pressure boundary seal will not result in a breach of the pressure boundary. The helium gas is therefore retained and undiluted, and may be credited in the thermal analyses.

An important thermal design criterion imposed on the HI-STORM System is to limit the maximum fuel cladding temperature to within design basis limits (Table 4.3.7) for long-term storage of design basis SNF assemblies. An equally important design criterion is to minimize temperature gradients in the MPC so as to minimize thermal stresses. In order to meet these design objectives, the MPC baskets are designed to possess certain distinctive characteristics, which are summarized in the following.

The MPC design minimizes resistance to heat transfer within the basket and basket periphery regions. This is ensured by an uninterrupted panel-to-panel connectivity realized in the all-welded honeycomb basket structure. The MPC design incorporates top and bottom plenums with interconnected downcomer paths. The top plenum is formed by the gap between the bottom of the MPC lid and the top of the honeycomb fuel basket, and by elongated semicircular holes in each basket cell wall. The bottom plenum is formed by large elongated semicircular holes at the base of

all cell walls. The MPC basket is designed to eliminate structural discontinuities (i.e., gaps) which introduce large thermal resistances to heat flow. Consequently, temperature gradients are minimized in the design, which results in lower thermal stresses within the basket. Low thermal stresses are also ensured by an MPC design that permits unrestrained axial and radial growth of the basket. The possibility of stresses due to restraint on basket periphery thermal growth is eliminated by providing adequate basket-to-canister shell gaps to allow for basket thermal growth during heat-up to design basis temperatures.

It is heuristically apparent from the geometry of the MPC that the basket metal, the fuel assemblies, and the contained helium mass will be at their peak temperatures at or near the longitudinal axis of the MPC. The temperatures will attenuate with increasing radial distance from this axis, reaching their lowest values at the outer surface of the MPC shell. Conduction along the metal walls and radiant heat exchange from the fuel assemblies to the MPC metal mass would therefore result in substantial differences in the bulk temperatures of helium columns in different fuel storage cells. Since two fluid columns at different temperatures in communicative contact cannot remain in static equilibrium, the non-isotropic temperature field in the MPC internal space due to conduction and radiation heat transfer mechanisms guarantee the incipience of the third mode of heat transfer: natural convection.

The preceding paragraph introduced the internal helium thermosiphon feature engineered into the MPC design. It is recognized that the backfill helium pressure, in combination with low pressure drop circulation passages in the MPC design, induces a thermosiphon upflow through the multicellular basket structure to aid in removing the decay heat from the stored fuel assemblies. The decay heat absorbed by the helium during upflow through the basket is rejected to the MPC shell during the subsequent downflow of helium in the peripheral downcomers. This helium thermosiphon heat extraction process significantly reduces the burden on the MPC metal basket structure for heat transport by conduction, thereby minimizing internal basket temperature gradients and resulting thermal stresses.

The helium columns traverse the vertical storage cavity spaces, redistributing heat within the MPC. Elongated holes in the bottom of the cell walls, liberal flow space and elongated holes at the top, and wide-open downcomers along the outer periphery of the basket ensure a smooth helium flow regime. The most conspicuous beneficial effect of the helium thermosiphon circulation, as discussed above, is the mitigation of internal thermal stresses in the MPC. Another beneficial effect is reduction of the peak fuel cladding temperatures of the fuel assemblies located in the interior of the basket. ~~In the original HI-STORM licensing analyses, no credit for the thermosiphon action was taken. To partially compensate for the reduction in the computed heat rejection capability due to the complete neglect of the global thermosiphon action within the MPC, heat conduction elements made of aluminum were interposed in the large peripheral spaces between the MPC shell and the fuel basket. These heat conduction elements, shown in the MPC Drawings in Section 1.5, are engineered such that they can be installed in the peripheral spaces to create a nonstructural thermal connection between the basket and the MPC shell. In their installed condition, the heat conduction elements will~~

~~contact the MPC shell and the basket walls. MPC manufacturing procedures have been established to ensure that the thermal design objectives for the conduction elements set forth in this document are realized in the actual hardware. The presence of heat conduction elements in the canister design has been conservatively neglected in the thermal models of the HI-STORM 100 System in this revision of the Safety Analysis Report.~~

Four distinct MPC basket geometries are evaluated for thermal performance in the HI-STORM System. For intact PWR fuel storage, the MPC-24, MPC-24E, and MPC-32 designs are available. Four locations are designated for storing damaged PWR fuel in the MPC-24E design. A 68-cell MPC design (MPC-68, MPC-68F, and MPC-68FF) is available for storing BWR fuel (intact or damaged (including fuel debris)). All of the four basic MPC geometries (MPC-32, MPC-24, MPC-24E and MPC-68) are described in Chapter 1 wherein their design drawings can also be found.

The design maximum decay heat loads for storage of intact zircaloy clad fuel in the four MPCs are listed in Tables 4.4.20, 4.4.21, 4.4.28, and 4.4.29. Storage of intact stainless steel is evaluated in Subsection 4.3.2. Storage of zircaloy clad fuel with stainless steel clad fuel in an MPC is permitted. In this scenario, the zircaloy clad fuel is conservatively stipulated to meet the lower decay heat limits for stainless steel clad fuel. Storage of damaged, zircaloy clad fuel is evaluated in Subsection 4.4.1.1.4. The axial heat distribution in each fuel assembly is assumed to follow the burnup profiles set forth by Table 2.1.11.

Thermal analysis of the HI-STORM System is based on including all three fundamental modes of heat transfer, namely conduction, natural convection and radiation. Different combinations of these modes are active in different parts of the system. These modes are properly identified and conservatively analyzed within each part of the MPC, the HI-STORM storage overpack and the HI-TRAC transfer cask, to enable bounding calculations of the temperature distribution within the HI-STORM System to be performed. In addition to storage within the HI-STORM overpack, loaded MPCs will also be located for short durations inside the transfer cask (HI-TRAC) designed for moving MPCs into and out of HI-STORM storage modules.

Heat is dissipated from the outer surface of the storage overpack and HI-TRAC to the environment by buoyancy induced airflow (natural convection) and thermal radiation. Heat transport through the cylindrical wall of the storage overpack and HI-TRAC is solely by conduction. While stored in a HI-STORM overpack, heat is rejected from the surface of the MPC via the parallel action of thermal radiation to the inner shell of the overpack and convection to a buoyancy driven airflow in the annular space between the outer surface of the MPC and the inner shell of the overpack. This situation is similar to the familiar case of natural draft flow in furnace stacks. When placed into a HI-TRAC cask for transfer operations, heat is rejected from the surface of the MPC to the inner shell of the HI-TRAC by conduction and thermal radiation.

Within the MPC, heat is transferred between metal surfaces (e.g., between neighboring fuel rod surfaces) via a combination of conduction through a gaseous medium (helium) and thermal radiation.

Heat is transferred between the fuel basket and the MPC shell by thermal radiation and conduction. The heat transfer between the fuel basket external surface and the MPC shell inner surface is further influenced by the "Rayleigh" effect. This is discussed in Subsection 4.4.1.1.5. The heat transfer augmentation effect of this mechanism, as discussed earlier, is conservatively neglected.

As discussed later in this chapter, an array of conservative assumptions bias the results of the thermal analysis towards much reduced computed margins than would be obtained by a rigorous analysis of the problem. In particular, the thermal model employed in determining the MPC temperatures is consistent with the model presented in Rev. 9-0 of the HI-STAR FSAR submittal (Docket No. 72-1008).

As discussed in Chapter 2, the HI-STORM MPCs are identical to those utilized in the NRC-accepted HI-STAR System (Docket 72-1008 for storage). As such, many of the analysis methods utilized herein for performing thermal evaluations of the HI-STORM MPCs are identical to those already accepted for the HI-STAR System. Specifically, the analysis methods for evaluation of the following items are identical to those for the HI-STAR System:

- i. fuel assembly effective thermal conductivity
- ii. MPC fuel basket composite wall effective thermal conductivity
- iii. MPC fuel basket effective thermal conductivity
- iv. MPC fuel basket peripheral region effective thermal conductivity
- v. ~~aluminum heat conduction elements effective thermal conductivity~~
- vi. MPC internal cavity free volume
- vii. MPC contents effective heat capacity and density
- viii. bounding fuel rod internal pressures and hoop stresses

In addition, thermal properties for all materials common to both the HI-STORM and HI-STAR systems are identical, including stainless and carbon steels, zircaloy, UO₂, ~~aluminum alloy 1100~~, ~~Boral neutron absorber material~~, Holtec-A, helium, air and paint.

The complete thermal analysis is performed using the industry standard ANSYS finite element modeling package [4.1.1] and the finite volume Computational Fluid Dynamics (CFD) code FLUENT [4.1.2]. ANSYS has been previously used and accepted by the NRC on numerous dockets [4.4.10, 4.V.5.a]. The FLUENT CFD program is independently benchmarked and validated with a wide class of theoretical and experimental studies reported in the technical journals. Additionally, Holtec has confirmed the code's capability to reliably predict temperature fields in dry storage applications using independent full-scale test data from a loaded cask [4.1.3]. This study concluded that FLUENT can be used to model all modes of heat transfer, namely, conduction, convection, and radiation in dry cask systems. A series of Holtec topical reports, culminating in "Topical report on the HI-STAR/HI-STORM thermal model and its benchmarking with full-size cask test data", Holtec Report HI-992252, Rev. 1, document the comparison of the Holtec thermal model against the full-size cask test data [4.1.3]. In reference [4.1.3], the Holtec thermal model is shown to overpredict the

measured fuel cladding temperature by a modest amount for every test set. In early 2000, PNL evaluated the thermal performance of HI-STORM 100 at discrete ambient temperatures using the COBRA-SFS Code. (Summary report communicated by T.E. Michener to J. Guttman (NRC staff) dated May 31, 2000 titled "TEMPEST Analysis of the Utah ISFSI Private Fuel Storage Facility and COBRA-SFS Analysis of the Holtec HI-STORM 100 Storage System"). The above-mentioned topical report has been updated to include a comparison of the Holtec thermal model results with the PNL solution. Once again, the Holtec thermal model is uniformly conservative, albeit by small margins. The benchmarking of the Holtec thermal model against the EPRI test data [4.1.3] and PNL COBRA-SFS study validate the suitability of the thermal model employed to evaluate the thermal performance of the HI-STORM 100 System in this document.

4.2 SUMMARY OF THERMAL PROPERTIES OF MATERIALS

Materials present in the MPCs include stainless steels (Alloy X), Boral-neutron absorber (*Boral* or *METAMIC*), aluminum Alloy 1100 heat-conduction elements, and helium. Materials present in the HI-STORM storage overpack include carbon steels and concrete. Materials present in the HI-TRAC transfer cask include carbon steels, lead, Holtite-A neutron shield, and demineralized water. In Table 4.2.1, a summary of references used to obtain cask material properties for performing all thermal analyses is presented.

Individual thermal conductivities of the alloys that comprise the Alloy X materials and the bounding Alloy X thermal conductivity are reported in Appendix 1.A of this report. Tables 4.2.2, and 4.2.3 and 4.2.9 provide numerical thermal conductivity data of materials at several representative temperatures. Thermal conductivity data for Boral components (i.e., B₄C core and aluminum cladding) is provided in Table 4.2.8. *Boral is a compressed neutron absorbing core clad with thin layer of aluminum on both sides. Because of its sandwich construction, its conduction properties are directionally dependent (i.e. non-isotropic). In contrast to Boral, METAMIC is a homogeneous neutron absorbing material with thermal conductivity that is higher than the Boral neutron absorbing B₄C core (See Figure 4.2.3) but lower than Boral's aluminum cladding. The equivalent conductivity of a Boral panel, defined as the Square Root of the Mean Sum of Squares (SRMSS) conductivity in two principal directions (through thickness and width) is closely matched by METAMIC[†]. Therefore, the two materials are considered thermally equivalent.* The temperature dependence of the thermal conductivities of helium and air is shown in Figure 4.2.1.

For the HI-STORM overpack, the thermal conductivity of concrete and the emissivity/absorptivity of painted surfaces are particularly important. Recognizing the considerable variations in reported values for these properties, we have selected values that are conservative with respect to both authoritative references and values used in analyses on previously licensed cask docket. Specific discussions of the conservatism of the selected values are included in the following paragraphs.

As specified in Table 4.2.1, the concrete thermal conductivity is taken from Marks' Standard Handbook for Mechanical Engineers, which is conservative compared to a variety of recognized concrete codes and references. Neville, in his book "Properties of Concrete" (4th Edition, 1996), gives concrete conductivity values as high as 2.1 Btu/(hr×ft×°F). For concrete with siliceous aggregates, the type to be used in HI-STORM overpacks, Neville reports conductivities of at least 1.2 Btu/(hr×ft×°F). Data from Loudon and Stacey, extracted from Neville, reports conductivities of 0.980 to 1.310 Btu/(hr×ft×°F) for normal weight concrete protected from the weather. ACI-207.1R provides thermal conductivity values for seventeen

structures (mostly dams) at temperatures from 50-150°F. Every thermal conductivity value reported in ACI-207.1R is greater than the 1.05 Btu/(hr×ft×°F) value used in the HI-STORM thermal

[†] For example, at 482°F, the through-thickness and width direction conductivities of Boral (B₄C thickness fraction = 0.82) is computed as 52.9 and 58.2 Btu/ft-hr-°F respectively. The SRMSS conductivity = $[(52.9^2 + 58.2^2)/2]^{0.5}$ is 55.61 BTU/ft/hr-°F compared to lowerbound METAMIC conductivity (Figure 4.2.3) of 55.68 Btu/ft-hr-°F (@482°F).

analyses.

Additionally, the NRC has previously approved analyses that use higher conductivity values than those applied in the HI-STORM thermal analysis. For example, thermal calculations for the NRC approved Vectra NUHOMS cask system (June 1996, Rev. 4A) used thermal conductivities as high as 1.17 Btu/(hr×ft×°F) at 100°F. Based on these considerations, the concrete thermal conductivity value stipulated for HI-STORM thermal analyses is considered to be conservative.

Holtite-A is a composite material consisting of approximately 37 wt% epoxy polymer, 1% B₄C and 62% Aluminum trihydrate. Thermal conductivity of the polymeric component is low because polymers are generally characterized by a low conductivity (0.05 to 0.2 Btu/ft-hr-°F). Addition of fillers in substantial amounts raises the mixture conductivity up to a factor of ten. Thermal conductivity of epoxy filled resins with Alumina is reported in the technical literature† as approximately 0.5 Btu/ft-hr-°F and higher. In the HI-STORM FSAR, a conservatively postulated conductivity of 0.3 Btu/ft-hr-°F is used in the thermal models for the neutron shield region (in the HI-TRAC transfer cask). As the thermal inertia of the neutron shield is not credited in the analyses, the density and heat capacity properties are not reported herein.

Surface emissivity data for key materials of construction are provided in Table 4.2.4. The emissivity properties of painted external surfaces are generally excellent. Kern [4.2.5] reports an emissivity range of 0.8 to 0.98 for a wide variety of paints. In the HI-STORM thermal analysis, an emissivity of 0.85^{††} is applied to painted surfaces. A conservative solar absorptivity coefficient of 1.0 is applied to all exposed overpack surfaces.

In Table 4.2.5, the heat capacity and density of the different overpack materials are presented. These properties are used in performing transient (i.e., hypothetical fire accident condition) analyses. The temperature dependence of the viscosities of helium and air are provided in Table 4.2.6 and plotted in Figure 4.2.2.

The heat transfer coefficient for exposed surfaces is calculated by accounting for both natural convection and thermal radiation heat transfer. The natural convection coefficient depends upon the product of Grashof (Gr) and Prandtl (Pr) numbers. Following the approach developed by Jakob and Hawkins [4.2.9], the product Gr ∅ Pr is expressed as $L^3 \Delta T Z$, where L is height of the overpack, ΔT is overpack surface temperature differential and Z is a parameter based on air properties, which are known functions of temperature, evaluated at the average film temperature. The temperature dependence of Z is provided in Table 4.2.7.

† "Principles of Polymer Systems", F. Rodriguez, Hemisphere Publishing Company (Chapter 10).
†† This is conservative with respect to prior cask industry practice, which has historically utilized higher emissivities. For example, a higher emissivity for painted surfaces ($\epsilon = 0.95$) is used in the previously licensed TN-32 cask TSAR (Docket 72-1021).

Table 4.2.1

**SUMMARY OF HI-STORM SYSTEM MATERIALS
THERMAL PROPERTY REFERENCES**

Material	Emissivity	Conductivity	Density	Heat Capacity
Helium	N/A	Handbook [4.2.2]	Ideal Gas Law	Handbook [4.2.2]
Air	N/A	Handbook [4.2.2]	Ideal Gas Law	Handbook [4.2.2]
Zircaloy	EPRI [4.2.3]	NUREG [4.2.6], [4.2.7]	Rust [4.2.4]	Rust [4.2.4]
UO ₂	Not Used	NUREG [4.2.6], [4.2.7]	Rust [4.2.4]	Rust [4.2.4]
Stainless Steel	Kern [4.2.5]	ASME [4.2.8]	Marks' [4.2.1]	Marks' [4.2.1]
Carbon Steel	Kern [4.2.5]	ASME [4.2.8]	Marks' [4.2.1]	Marks' [4.2.1]
Boral [†]	Not Used <i>Marks' [4.2.1]</i>	Test Data	Test Data	Test Data
Holtite-A	Not Used	Lower Bound Value Used	Not Used	Not Used
Concrete	Not Used	Marks' [4.2.1]	Marks' [4.2.1]	Handbook [4.2.2]
Lead	Not Used	Handbook [4.2.2]	Handbook [4.2.2]	Handbook [4.2.2]
Water	Not Used	ASME [4.2.10]	ASME [4.2.10]	ASME [4.2.10]
Aluminum Alloy 1100 (Heat Conduction Elements)	Handbook [4.2.2]	ASME [4.2.8]	ASME [4.2.8]	ASME [4.2.8]
METAMIC [‡]	<i>Marks' [4.2.1]</i>	<i>Test Data</i>	<i>Test Data</i>	<i>Test Data</i>

[†] AAR Structures Boral thermophysical test data.

[‡] Test data provided by METAMIC, Inc..

Table 4.2.2

SUMMARY OF HI-STORM SYSTEM MATERIALS
THERMAL CONDUCTIVITY DATA

Material	@ 200°F (Btu/ft-hr-°F)	@ 450°F (Btu/ft-hr-°F)	@ 700°F (Btu/ft-hr-°F)
Helium	0.0976	0.1289	0.1575
Air [§]	0.0173	0.0225	0.0272
Alloy X	8.4	9.8	11.0
Carbon Steel	24.4	23.9	22.4
Concrete ^{††}	1.05	1.05	1.05
Lead	19.4	17.9	16.9
Water	0.392	0.368	N/A

§ At lower temperatures, Air conductivity is between 0.0139 Btu/ft-hr-°F (at 32°F) and 0.0176 Btu/ft-hr-°F at 212°F.

†† Assumed constant for the entire range of temperatures.

Table 4.2.3

SUMMARY OF FUEL ELEMENT COMPONENTS
THERMAL CONDUCTIVITY DATA

Zircaloy Cladding		Fuel (UO ₂)	
Temperature (°F)	Conductivity (Btu/ft-hr-°F)	Temperature (°F)	Conductivity (Btu/ft-hr-°F)
392	8.28 [†]	100	3.48
572	8.76	448	3.48
752	9.60	570	3.24
932	10.44	793	2.28 [†]

[†] Lowest values of conductivity used in the thermal analyses for conservatism.

Table 4.2.4

SUMMARY OF MATERIALS SURFACE EMISSIVITY DATA

Material	Emissivity
Zircaloy	0.80
Painted surfaces	0.85
Stainless steel	0.36
Carbon Steel	0.66
Sandblasted Aluminum	0.40
<i>Neutron Absorber Panels</i>	<i>0.26**</i>

Note: The emissivity of a metal surface is a function of the surface finish. In general, oxidation of a metal surface increases the emissivity. As stated in Marks' Standard Handbook for Mechanical Engineers: "Unless extraordinary pains are taken to prevent oxidation, however, a metallic surface may exhibit several times the emittance or absorptance of a polished specimen." This general statement is substantiated with a review of tabulated emissivity data from several standard references. These comparisons show that oxidized metal surfaces do indeed have higher emissivities than clean surfaces.

** From Marks' Handbook (Oxidized Aluminum Surface)

Table 4.2.5

DENSITY AND HEAT CAPACITY PROPERTIES SUMMARY

Material	Density (lbm/ft ³)	Heat Capacity (Btu/lbm-°F)
Helium	(Ideal Gas Law)	1.24
Zircaloy	409	0.0728
Fuel (UO ₂)	684	0.056
Carbon steel	489	0.1
Stainless steel	501	0.12
Boral	154.7	0.13
Concrete	142 [†]	0.156
Lead	710	0.031
Water	62.4	0.999
Aluminum Alloy 1100 (Heat Conduction Elements)	169.9	0.23
<i>METAMIC</i>	<i>163.4 – 166.6</i>	<i>0.22 – 0.29</i>

[†] A minimum allowable density for concrete is specified as 146 lb/ft³ in Appendix 1.D. For conservatism in transient heatup calculations, a lower value of concrete density compared to the Appendix 1.D value is specified here.

Table 4.2.6

GASES VISCOSITY[†] VARIATION WITH TEMPERATURE

Temperature (°F)	Helium Viscosity (Micropoise) ^{††}	Temperature (°F)	Air Viscosity (Micropoise)
167.4	220.5	32.0	172.0
200.3	228.2	70.5	182.4
297.4	250.6	260.3	229.4
346.9	261.8	-	-
463.0	288.7	-	-
537.8	299.8	-	-
737.6	338.8	-	-

[†] Obtained from Rohsenow and Hartnett [4.2.2].

^{††} This data is also provided in graphical form in Figure 4.2.2.

Table 4.2.7

VARIATION OF NATURAL CONVECTION PROPERTIES
PARAMETER "Z" FOR AIR WITH TEMPERATURE[†]

Temperature (°F)	Z (ft ⁻³ °F ⁻¹)
40	2.1×10 ⁶
140	9.0×10 ⁵
240	4.6×10 ⁵
340	2.6×10 ⁵
440	1.5×10 ⁵

[†] Obtained from Jakob and Hawkins [4.2.9].

Table 4.2.8

BORAL COMPONENT MATERIALS[†]
THERMAL CONDUCTIVITY DATA

Temperature (°F)	B ₄ C Core Conductivity (Btu/ft-hr-°F)	Aluminum Cladding Conductivity (Btu/ft-hr-°F)
212	48.09	100.00
392	48.03	104.51
572	47.28	108.04
752	46.35	109.43

[†] Both B₄C and aluminum cladding thermal conductivity values are obtained from AAR Structures Boral thermophysical test data.

Table 4.2.9

[INTENTIONALLY DELETED]
~~HEAT CONDUCTION ELEMENTS (ALUMINUM ALLOY 1100)~~
~~THERMAL CONDUCTIVITY DATA~~

Temperature (°F)	Conductivity (Btu/ft-hr-°F)
100	131.8
200	128.5
300	126.2
400	124.5

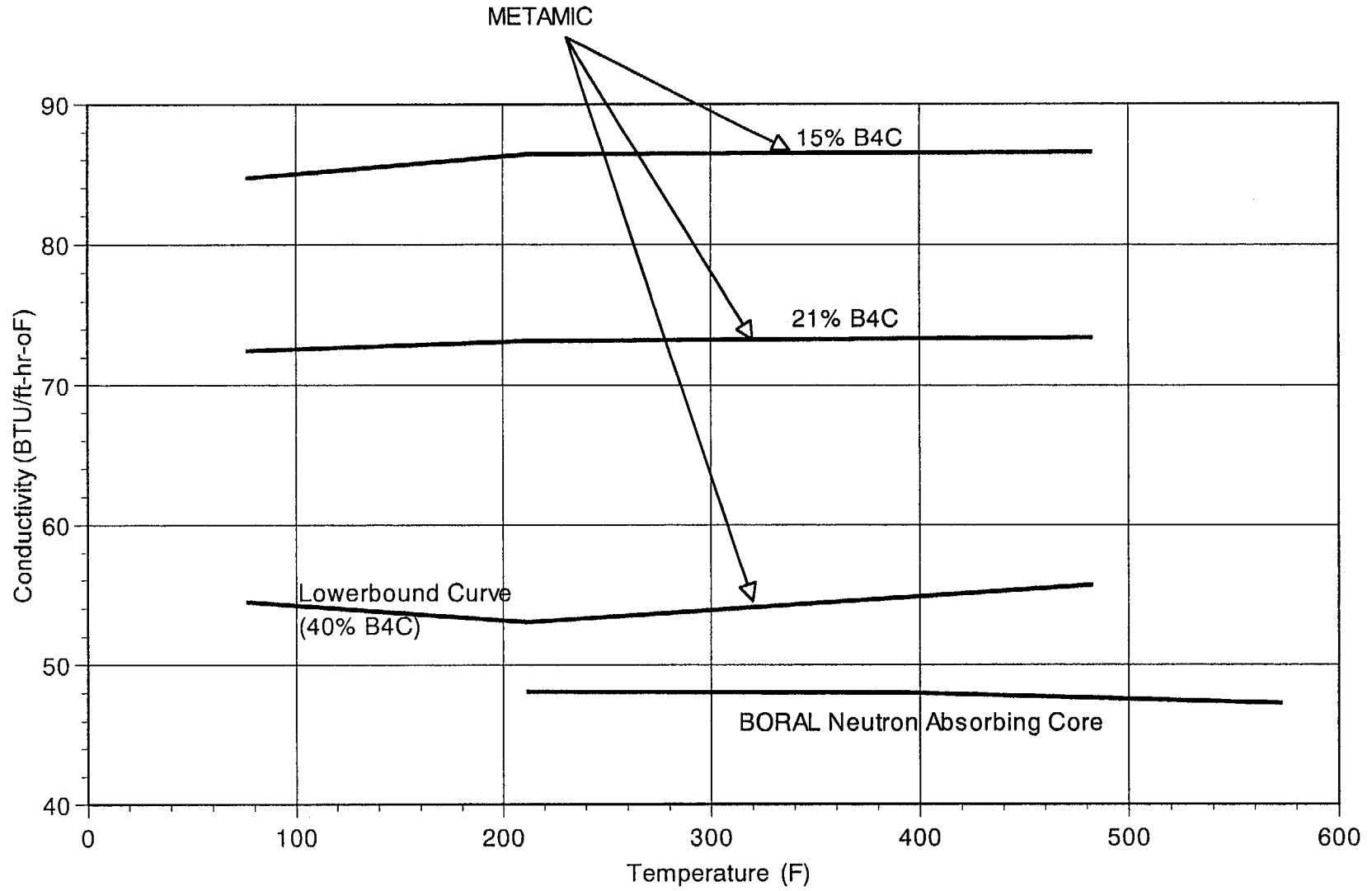


FIGURE 4.2.3: COMPARISON OF THERMAL CONDUCTIVITY OF METAMIC AND THE CERMET CORE OF A BORAL NEUTRON ABSORBER

4.3 SPECIFICATIONS FOR COMPONENTS

HI-STORM System materials and components designated as "Important to Safety" (i.e., required to be maintained within their safe operating temperature ranges to ensure their intended function) which warrant special attention are summarized in Table 4.3.1. The neutron shielding ability of Holtite-A neutron shield material used in the HI-TRAC onsite transfer overpack is ensured by demonstrating that the material exposure temperatures are maintained below the maximum allowable limit. Long-term integrity of SNF is ensured by the HI-STORM System thermal performance that demonstrates that fuel cladding temperatures are maintained below design basis limits. *Neutron absorber materials (Boral or METAMIC) used in MPC baskets for criticality control (a composite material composed of B_4C and aluminum (See Sub-Section 1.2.1.3.1)) is* are stable up to 1000°F[†] for short-term and 850°F for long-term dry storage[‡]. However, for conservatism, a significantly lower maximum temperature limit is imposed. The overpack concrete, the primary function of which is shielding, will maintain its structural, thermal and shielding properties provided that American Concrete Institute (ACI) temperature limits are not exceeded.

Compliance to 10CFR72 requires, in part, identification and evaluation of short-term off-normal and severe hypothetical accident conditions. The inherent mechanical stability characteristics of cask materials and components ensure that no significant functional degradation is possible due to exposure to short-term temperature excursions outside the normal long-term temperature limits. For evaluation of HI-STORM System thermal performance under off-normal or hypothetical accident conditions, material temperature limits for short-duration events are provided in Table 4.3.1.

4.3.1 Evaluation of Moderate Burnup Zircaloy Clad Fuel

Demonstration of fuel cladding integrity against the potential for degradation and gross rupture throughout the entire dry cask storage period is mandated by the Code of Federal Regulations (Part 72, Section 72.122(h)). The specific criteria required to establish fuel cladding integrity, set forth in NUREG-1536 (4.0,IV,5&6) are:

- i. For each fuel type proposed for storage, the dry cask storage system should ensure a very low probability of cladding breach during long-term storage.
- ii. Fuel cladding damage resulting from creep cavitation should be limited to 15% of the original cladding cross sectional area during dry storage.

Consistent with the NUREG-1536 criteria, the HI-STORM System is designed to preclude gross fuel cladding failures during the entire duration of storage. A method for establishing the peak cladding temperature limits in accordance with the diffusion-controlled cavity growth (DCCG) methodology

[†] B_4C is a refractory material that is unaffected by high temperature and aluminum is solid at temperatures in excess of 1000°F.

[‡] AAR Advanced Structures Boral thermophysical test data.

was proposed by the Lawrence Livermore National Laboratory [4.3.5]. Recent NRC guidelines^{††}, applicable for high burnup fuel (greater than 45,000 MWD/MTU), require that alternate methods be adopted for computing peak cladding temperature limits (see Appendix 4.A). For the FSAR request for approval for fuel burnups up to 45,000 MWD/MTU, the PNL-6189 [4.3.1] creep rupture criteria has been conservatively adopted in accord with the latest NRC guidelines so as to develop more restrictive permissible peak fuel cladding temperatures for the HI-STORM System. A discussion of the DCCG and PNL criteria for establishing allowable cladding temperatures is provided in the balance of the section.

4.3.1.1 Cladding Temperature Limits (DCCG Criteria)

For SNF of a given age (decay time), the permissible peak cladding temperature is a direct function of the cladding hoop stress, which in turn depends on the radius-to-thickness ratio of the fuel rod and its internal pressure. The rod internal pressure P_i is a function of the maximum initial fill pressures (Tables 4.3.2 and 4.3.5) and fuel burnup dependent fission gas release. The free rod volumes in the third column of Tables 4.3.2 and 4.3.5 are defined as free rod volumes in each fuel rod available for pressurization with fill gas. The free rod volume is the cumulative sum of the open top plenum space, the pellet-to-cladding annular space and the inter-pellet junction space. As a lower bound value of the free rod volume is conservative for cladding stress at operating temperatures, only the nominal gas plenum space is shown. The plenum length for miscellaneous BWR fuel assemblies is set to 12 inches. The radius-to-thickness ratio r^* is determined based on rod nominal dimension values (Tables 4.3.3 and 4.3.6), with consideration of maximum cladding thickness loss due to in-reactor oxidation, as reported by PNL [4.3.4].

The data presented in Tables 4.3.2 and 4.3.5 are combined with theoretical bounding fuel rod internal gas pressures from published technical sources [4.3.1 and 4.3.6], to absolutely ensure that bounding clad hoop stress values are used in the determination of gross cladding integrity. These bounding pressures are so large that they approach physical upper bounds for some fuel assemblies, as the corresponding hoop stresses approach the yield stress of zircaloy (approximately 172 MPa at 750°F [4.3.7]). The theoretical bounding rod internal pressure for PWR assemblies is compared, in Figure 4.3.1, to the published test data for assemblies from two different plants. From this figure, the large conservatism in the theoretical bounding pressure is evident.

These theoretical bounding pressures, from two sources, are provided below for PWR and BWR fuel:

PWR: 2416 psia [4.3.1], 16 MPa (2320 psia) [4.3.6]

BWR: 1094 psia [4.3.1], 70 atm (1029 psia) [4.3.6]

The coincident gas plenum temperatures reported in the PNL report [4.3.1] are 387°C for PWR assemblies and 311°C for BWR assemblies at reactor operating conditions. It can be seen in Figures

^{††} Interim Staff Guidance-11, "Storage of Spent Fuel Having Burnups in Excess of 45,000 MWD/MtU", USNRC.

4.4.16 and 4.4.17 that the temperature distribution of gas in the fuel rods, a great bulk of which is located in the top gas plenum, is well below the in-core condition gas temperatures reported above (PWR fuel) and for the most part in the BWR fuel. In the interest of conservatism, no credit is taken for the substantially lower gas plenum temperatures that prevail during dry storage. Furthermore, the greater of the literature pressure data listed above is adopted for performing peak clad temperature limit calculations. The values utilized for P_i are 2416 psia for PWR[†] assemblies and 1094 psia for BWR assemblies.

By utilizing P_i and r^* , the cladding stress for various PWR fuel types is calculated from Lamé's formula and summarized in Table 4.3.3. For certain outlier fuel types (PWR), the stress calculations are provided in Table 4.3.9. An inspection of cladding stress data summarized in Tables 4.3.9 and 4.3.3 indicates 152.7 MPa as the theoretical bounding value of cladding stress (σ_{max}) for the PWR SNF. Corresponding fill gas data and calculations of cladding stress for the various BWR SNF types are summarized in Tables 4.3.5 and 4.3.6, respectively. An inspection of the cladding stress data in Table 4.3.6 indicates that the theoretical bounding value of the cladding hoop stress for the BWR SNF is 72.7 MPa. The theoretical bounding values of σ_{max} for the array of PWR and BWR SNF types are thus 152.7 MPa and 72.7 MPa, respectively.

In this manner, the maximum conceivable values of cladding hoop stress are calculated for use in subsequent DCCG method calculations. As an additional conservatism, the peak fuel rod cladding hoop stresses are conservatively held constant throughout the dry storage period. In practice, the rod cladding hoop stresses are the maximum when the casks are initially loaded and monotonically decrease with the time-decreasing heat load and temperature. The Ideal Gas Law governs the decrease in pressure with decreasing temperature.

As stated earlier, the value of σ_{max} is required to establish the peak cladding temperature limit using the DCCG method. The DCCG model-based zircaloy cladding temperature limit computation, in accordance with the LLNL procedure [4.3.5], requires a solution to the following equation expressed in terms of the area fraction of de-cohesion (A):

$$\int_{A_i}^{A_f} \frac{dA}{f(A)} = \int_{t_0}^{t_0 + t_s} G(t) dt$$

where:

- A_i = initial area fraction of de-cohesion
- A_f = end of storage life area fraction of de-cohesion (limited to 0.15)
- t_0 = age of fuel prior to dry cask storage (years)
- t_s = dry cask storage period (40 years)
- $f(A)$ = area fraction of de-cohesion function
- $G(t)$ = damage function

The term on the left-hand side of this equation represents the area fraction of de-cohesion that occurs

[†] Certain outlier fuels (Table 4.3.9) are stipulated to be below a postulated limiting rod pressure.

over the dry storage period. The term on the right-hand side represents the cumulative damage over the same period. The area fraction of de-cohesion function and the damage function, $f(A)$ and $G(t)$ respectively, are:

$$f(A) = \frac{[1 - (\frac{A_i}{A})^{1/2}](1 - A)}{A^{1/2} [\frac{1}{2} \ell n \frac{1}{A} - \frac{3}{4} + A(1 - \frac{A}{4})]}$$

$$G(t) = \frac{32}{3\pi^{1/2}} \frac{F_B^{3/2}(\alpha)}{F_V(\alpha)} \frac{\Omega \delta \sigma_{\infty}(t)}{K \lambda^3} \frac{D_{GB}[T(t)]}{T(t)}$$

where:

$$F_B(\alpha) = \pi \sin^2(\alpha)$$

$$F_V(\alpha) = \frac{2\pi}{3} (2 - 3 \cos \alpha + \cos^3 \alpha)$$

$T(t)$ = time-dependent peak cladding temperature
 K = Boltzmann constant (1.38053×10^{-23} J/K)

A discussion on the balance of parameters in the damage function $G(t)$ is provided below.

Cladding Hoop Stress ($\sigma_{\infty}(t)$)

The cladding hoop stress is principally dependent upon the specific fuel rod dimensions, initial fill rod pressure, time-dependent storage temperature, and fuel burnup dependent fission gas release from the fuel pellets into the rod plenum space. The peak fuel rod pressure for various analyzed PWR and BWR fuel types at the start of the dry storage period are summarized in Tables 4.3.3 and 4.3.6. The highest peak rod stress among the various PWR and BWR fuel types, previously defined as σ_{max} , are conservatively applied as constant (time-independent) cladding hoop stresses in the DCCG model-based damage function.

Grain Boundary Cavity Dihedral Angle (α)

The LLNL report [4.3.5] has determined the dihedral angle (α) for pure metals to be 75° . To account for possible non-ideal conditions, a conservatively lower α equal to 60° is applied to the DCCG model.

Zirconium Atomic Volume (Ω)

The zirconium atomic volume estimated from several literature sources as documented in the LLNL report [4.3.5] is in the range of $2.31 \times 10^{-29} \text{ m}^3$ to $3.37 \times 10^{-29} \text{ m}^3$. In the interest of conservatism, the maximum estimated atomic volume equal to $3.37 \times 10^{-29} \text{ m}^3$ is used for the analysis.

Grain Boundary Thickness (δ)

The LLNL report [4.3.5] has recommended a grain boundary thickness of three Burgers vectors to be adequate for the analysis. Thus, $\delta = 3 (3.23 \times 10^{-10}) = 9.69 \times 10^{-10}$ m is used in the analysis.

Average Cavity Spacing (λ)

The type of nucleation mechanism and the density of nucleation sites control cavity spacing. The LLNL report [4.3.5] references an experimental study that found that the cavity spacing is in the range of 10×10^{-6} to 20×10^{-6} m. In the interest of conservatism, the minimum reported cavity spacing equal to 10×10^{-6} m is used in the analysis.

Grain Boundary Diffusion Rate (D_{GB})

Two grain boundary diffusion rate correlations for zirconium are reported in the LLNL report [4.3.5]. The two correlations provide diffusion rate estimates that are approximately two orders of magnitude apart from each other. Consequently, the more conservative correlation that provides a higher estimate of the grain boundary diffusion rate is used in the analysis. This more conservative correlation, yielding units of m^2/sec , is:

$$D_{GB} = 5.9 \times 10^{-6} \exp [-131,000/RT]$$

where R is the universal gas constant in J/mol \times K units.

Time-Dependent Peak Cladding Temperature ($T(t)$)

The peak cladding temperature during long-term storage is principally dependent upon the thermal heat load from the stored fuel assemblies, which is imposed on the cask. It is well established that the rate of radioactive decay in a fuel assembly exponentially attenuates with the age of fuel. Consequently, the peak cladding temperature during long-term storage will also attenuate rapidly as a direct consequence of the heat load reduction with time, which is modeled using the data provided in USNRC Regulatory Guide 3.54 [4.3.3]. To confirm the applicability of the Reg. Guide 3.54 data, comparisons with the ORIGEN-S source term calculation results discussed in Chapter 5 of this FSAR were performed. Figures 4.3.2 and 4.3.3 present graphical comparisons of the decay heat versus decay time profiles from the Reg. Guide data with the profiles from the ORIGEN-S calculations. For the design-basis maximum decay heat load (which is approached with 5-year old fuel), the Reg. Guide data agrees favorably with the ORIGEN-S calculation results. The Reg. Guide data is, in fact, slightly conservative with respect to the ORIGEN-S calculations.

It should be noted that the area fraction of de-cohesion function $f(A)$ approaches zero in the limit as $A \rightarrow A_i$. Consequently, the mathematical singularity in the integral $\int_{A_i}^A \frac{dA}{f(A)}$ is numerically accommodated by using an alternate form given below:

$$\int_{A_i}^A \frac{dA}{f(A)} = \text{Limit } \varepsilon \rightarrow 0 \int_{A_i+\varepsilon}^{A_f} \frac{A^{1/2} \left[\frac{1}{2} \ln \frac{1}{A} - \frac{3}{4} + A \left(1 - \frac{A}{4}\right) \right] dA}{\left[1 - \left(\frac{A_i}{A}\right)^{1/2}\right] (1-A)}$$

The allowable area fraction of de-cohesion using $A_i = 0.05$, $\varepsilon = 0.0001$, and $A_f = 0.15$ is determined to be equal to 0.15211.

This is consistent with an alternate form of the DCCG model reported in the PNL study [4.3.1, Appendix D] as reproduced below:

$$A_f = \int_0^{t_f} G(t) dt \leq 0.15$$

The cumulative damage $G(t)$ can be evaluated as a function of the initial fuel cladding temperature and corresponding cladding stress, which are the two primary constituents of the damage function. The initial cladding hoop stress at a bounding storage temperature has already been determined. All other parameters in the $G(t)$ function (except for the initial peak cladding temperature limit T_0) have been defined as discussed previously in this section. The cumulative cladding damage experienced during the 40-year dry cask storage period is determined by integrating the $G(t)$ function. The initial peak cladding temperature limit parameter T_0 is iteratively adjusted to limit the cumulative damage to 15% as required by the NUREG-1536 Criterion (ii) discussed earlier in this section. The initial peak cladding temperature limits for the bounding PWR and BWR fuel assemblies are provided in Table 4.3.7.

4.3.1.2 Permissible Cladding Temperatures (PNL Method)

In this subsection, the permissible peak clad temperature limits for the HI-STORM System are computed using the so-called “generic CSFM temperature limits” data provided in a PNL report [4.3.1]. The generic CSFM temperature limits, known to be more conservative than the previously discussed DCCG method, define the maximum permissible initial storage temperature (T_p) of cladding as a function of initial cladding stress (σ_{max}) and fuel age (τ_f) at the start of dry storage. The stress developed in cladding is a function of rod diameter-to-thickness ratio (d_c) and the internal rod gas pressure (P_0) which prevails during dry storage conditions. In the previous subsection, the W-14x14 and GE-7x7 fuel types were identified to have the highest d_c in the class of PWR† and BWR

† Certain outlier fuels are excluded from this class as the cladding stress is bounded by the design basis W 14x14 fuel (Table 4.3.9).

fuels, respectively. The cladding thickness data in Tables 4.3.3 and 4.3.6 is the corroded wall thickness after including maximum oxidation loss during reactor operation. The d_c for bounding PWR and BWR SNF is 18.3 and 19.3, respectively.

The cladding stress in a fuel rod is principally dependent upon the rod internal pressure P_o which is postulated to reasonably bound rod pressures of SNF during dry storage. PNL [4.3.2] and EPRI [4.3.4] provide in-core irradiation rod pressures information which are theoretical upper bounds. For reference, they are provided herein in Subsection 4.3.1.1. Other robust sources† which authoritatively deal with this matter report peak rod pressures of 1600 psia (PWR) and 900 psia (BWR) during in-core irradiation. The conservatism in the in-core irradiation rod pressures for bounding rods pressure during dry cask storage is illustrated in Figure 4.3.1. From published test data on rods pressure measured from two different plants, the projected rods pressure in dry storage is significantly lower than the in-core irradiation pressure (~1350 psia for PWR). For computing permissible cladding temperatures for SNF storage in the HI-STORM System, a conservatively postulated P_o of 2000 psia (PWR) and 1000 psia (BWR) are employed in this work.

The dry storage rod pressure P_o for PWR and BWR types is postulated as 2000 psia and 1000 psia, respectively. Having obtained P_o , the cladding stress (σ_{max}) is readily obtained by the product of P_o and d_c and dividing the result by 2 (Lame's formula). The cladding stress computed in this manner is 18,300 psi (126.1 MPa) and 9,650 psia (66.5 MPa) for PWR and BWR fuel, respectively. From the generic CSFM temperature limits table in the PNL report [4.3.1, page 3-19] and σ_{max} , the permissible peak clad temperature limit (T_p) as a function of τ_f is readily obtained. The T_p vs. τ_f results for PWR and BWR fuel are presented in Table 4.3.7. The peak clad temperature limits (DCCG criteria) and permissible cladding temperature limits (PNL criteria) data are graphically depicted in Figure 4.3.4. The more restrictive results (PNL criteria) are applied to the HI-STORM System. In Table 4.3.8, permissible (PNL criteria) temperatures for an outlier fuel type (Dresden-1 thin clad) are evaluated at a conservatively bounding stress (94.1 MPa, Table 4.3.6). These temperatures are applicable to Low Heat Emitting (LHE) fuel evaluated in Subsection 4.4.1.1.13.

4.3.2 Evaluation of Stainless Steel Clad Fuel

Approximately 2,200 PWR and BWR fuel assemblies stored in the United States were manufactured with stainless steel cladding. All stainless steel cladding materials are of the austenitic genre with the ASTM alloy compositions being principally type 304 and 348H. For long-term storage conditions, a recent EPRI/PNL study [4.3.4] recommends a 430°C (806°F) peak stainless steel cladding temperature limit. This temperature limit is substantially higher than the peak fuel cladding temperatures calculated for the HI-STORM System with design-basis maximum decay heat loads and zircaloy clad fuel (see Tables 4.4.9 and 4.4.10).

It is recognized that the peak cladding temperature of stainless fuel will differ from zircaloy clad fuel principally due to the following differences:

† NRC SER for HI-STORM System (Docket 72-1014)

- i. Differences in decay heat levels
- ii. Differences in cladding emissivity
- iii. Differences in cladding conductivity
- iv. Differences in fuel rod array dimensions

The net planar thermal resistance of the equivalent homogenized axisymmetric MPC basket containing stainless steel clad fuel is greater than that with zircaloy clad fuel. The higher resistance arises principally from the significantly lower emissivity of the stainless steel cladding. This factor is, however, offset by significantly lower design-basis heat loads prescribed for a HI-STORM System containing stainless steel clad fuel. A 20% (MPC-68, MPC-24, and MPC-24E) and 25% (MPC-32) or greater reduction in the design basis heat duty for stainless steel fuel (i.e., 20%-25% lower than zircaloy clad fuel) bounds the nominal percentage decrease in MPC basket effective thermal conductivity[†] (stainless steel fueled baskets are between 9% (MPC-68) to 25% (MPC-32) less conducting, as shown in Table 4.4.3). The design basis maximum allowable decay heat for MPCs fueled with stainless steel clad fuel are conservatively set to be 20% lower than zircaloy-fueled basket maximum heat load for MPC-24, MPC-24E, and MPC-68 (25% lower for MPC-32).. Therefore, it is concluded that the peak cladding temperature for stainless steel clad fuel will be bounded by zircaloy clad fuel results. Consequently, in view of the conservative heat loads prescribed for stainless steel clad fuel, a separate thermal analysis to demonstrate the adequacy of stainless steel cladding integrity for storage in the HI-STORM System is not necessary.

4.3.3 Short-Term Cladding Temperature Limit

For short-term durations, relatively high fuel cladding temperature limits have been historically accepted. For example, the Safety Analysis Report of the STC transport cask (Docket No. 71-9235), recently certified by the USNRC, permits 1200°F (approximately 649°C) as the maximum value of the peak cladding temperature, T_{max} , for transport of SNF with up to 45,000 MWD/MTU burnup. NUREG-1536 and PNL test data [4.3.2], limiting themselves to medium burnup levels (28,800 MWD/MTU), endorse a somewhat lower T_{max} ($T_{max} = 570^{\circ}\text{C}$ or 1058°F). Based on the published industry test data, guidance in the literature, and analytical reasoning, we herein prescribe 570°C as the admissible value of T_{max} for SNF, with accumulated burnups up to 45,000 MWD/MTU, in the HI-STORM System.

A Brookhaven report written for EPRI [4.3.6] asserts that fuel cladding rupture becomes “virtually absent at stresses below about 200 MPa”. It can be readily deduced that the peak cladding stress for the limiting condition of 570°C cladding temperature will be below 200 MPa for the SNF burnup levels considered in this FSAR. Recalling that $\sigma_{max} = 152.7$ MPa (Table 4.3.3) at a 387°C average rod gas temperature, the cladding circumferential stress σ_{peak} at 570°C is obtained by direct proportionality in absolute gas temperature:

[†] The term “effective conductivity” of the fuel basket is defined in Section 4.4.1.

$$\sigma_p = \sigma_{\max} \times (570 + 273)/(387 + 273) = 195.0 \text{ MPa}$$

Therefore, a short-term fuel cladding temperature limit $T_{\max} = 570^\circ\text{C}$ is considered safe to preclude fuel cladding failure. For fuel claddings which have been exposed to higher levels of in-core irradiation, the irradiation process progressively hardens the cladding material, making high burnup fuel less susceptible to stress-induced creep and fracture at these stress levels (up to 200 MPa). A recent high burnup fuel cladding integrity study by German researchers[†] corroborates this physical reasoning. In the German study, fuel rods with up to 64,000 MWD/MTU burnup were tested at substantially higher stresses (~400 MPa and 600 MPa) without cladding failure.

The EPRI report [4.3.6] cites experiments on fourteen irradiated Turkey Point Unit 3 rods carried out by Einziger et al.^{††} in 1982 which showed no breach in cladding even after as much as 7% strain was accumulated in elevated temperatures lasting for 740-1,000 hours. Einziger's test data corroborates our selection of $T_{\max} = 570^\circ\text{C}$ as the short duration limiting temperature.

[†] "Short-time Creep and Rupture Tests on High Burnup Fuel Rod Cladding", by W. Goll, E. Toscano and H. Spilker.

^{††} "High Temperature Post Irradiation Materials Performance of Spent Pressurized Water Reactor Fuel Rods under Dry Storage Conditions," by R.E. Einziger, S.D. Atkin, D.E. Stallrecht, and V.S. Pasupathi, Nuclear Technology, 57:65-80 (1982).

Table 4.3.1

HI-STORM SYSTEM MATERIAL TEMPERATURE LIMITS

Material	Normal Long-Term Temperature Limits [°F]	Short-Term Temperature Limits [°F]
Zircaloy fuel cladding	(Moderate [†] Burnup) See Table 4.3.7	1058
Stainless steel fuel cladding	806	1058
Boral ^{‡‡} <i>Neutron Absorbers (Boral or METAMIC)</i>	800	950
Holtite-A ^{†††}	300	300
Concrete	200	350
Water	307 ^{††††}	N/A

[†] High burnup fuel storage limits are established in Appendix 4.A.

^{‡‡} ~~Based on AAR Structures Boral thermophysical test data.~~

^{†††} See Section 1.2.1.3.2.

^{††††} Saturation temperature at HI-TRAC water jacket design pressure.

Table 4.3.2

SUMMARY OF PWR ASSEMBLY RODS INITIAL GAS FILL DATA

Assembly Type	Rods Per Assembly	Free Rod Volume (in ³)	Fill Pressure (psig) at 70°F	Fill Gas Volume at STP [†]	
				Per Rod (Liters)	Per Assembly (Liters)
W-14×14 Std.	179	0.67 ^{††}	0-460	0.845	151.2
W-15×15 Std.	204	0.67 ^{††}	0-475	0.633	129.1
W-17×17 Std.	264	0.59 ^{††}	275-500	0.666	175.8
B&W-15×15 Mark B	208	1.308	415	0.582	121.1
B&W-17×17 Mark C	264	0.819	435	0.381	100.6
CE-14×14 Std.	164	1.693	300-450	0.814	133.5
CE-16×16 Std.	220	1.411	300-450	0.678	149.2
B&W-15×15 Mark B-11	208	1.260	415	0.560	116.5
CE-14×14 (MP2)	176	1.728	300-450	0.831	146.2

[†] STP stands for standard temperature (0°C) and pressure (1 atmosphere).

^{††} Bounding low values verified from Holtec's proprietary information database.

Table 4.3.3

BOUNDING VALUES OF FUEL CLADDING STRESS FOR PWR SNF

	W- 14×14 Std.	W- 15×15 Std.	W- 17×17 Std.	B&W- 15×15 Mark B	B&W- 17×17 Mark C	CE- 14×14 Std.	CE- 16×16 Sys 80	CE-14×14 (MP2)
Fresh Fuel Rods O.D. (inch)	0.4220	0.422	0.374	0.430	0.379	0.440	0.382	0.440
End of Life Oxidation Thickness (inch) [†]	0.0027	0.0027	0.0027	0.0027	0.0027	0.0027	0.0027	0.0027
End of Life Rods O.D. (inch)	0.4166	0.4166	0.3686	0.4246	0.3736	0.4346	0.3766	0.4346
Rods I.D. (inch)	0.3734	0.373	0.329	0.377	0.331	0.384	0.332	0.388
Average Tube Diameter (inch)	0.3950	0.3948	0.3488	0.4008	0.3523	0.4093	0.3493	0.4113
Wall Thickness (inch)	0.0216	0.0218	0.0198	0.0238	0.0213	0.0253	0.0223	0.0233
Theoretical Bounding Rod Pressure (MPa gage) ^{††}	16.7	16.7	16.7	16.7	16.7	16.7	16.7	16.7
Bounding Cladding Stress (MPa)	152.7	151.2	147.1	140.6	138.1	135.0	130.8	147.4

[†] PNL-4835 [4.3.2] reported maximum cladding thickness loss due to in-reactor oxidation.

^{††} PNL-6189 [4.3.1] data.

Table 4.3.4

INTENTIONALLY DELETED.

Table 4.3.5
SUMMARY OF BWR ASSEMBLY RODS INITIAL GAS FILL DATA

Assembly Type	Rods Per Assembly	Free Rod Volume (in ³)	Fill Pressure (psig) at 70°F	Fill Gas Volume at STP	
				Per Rod (liters)	Per Assembly (liters)
GE-7x7 (1966)	49	2.073	0-44.1 [†]	0.126	6.17
GE-7x7 (1968)	49	2.073	0-44.1	0.126	6.17
GE-7x7R	49	1.991	0-44.1	0.121	5.93
GE-8x8	60	1.504	0-44.1	0.0915	5.49
GE-8x8R	60	1.433	0-147 ^{††}	0.240	14.4
Exxon-9x9	79	1.323	58.8-88.2 ^{†††}	0.141	11.1
6x6 GE Dresden-1	36	2.304	58.8-88.2	0.245	8.82
6x6 Dresden-1 MOX	36	2.286	58.8-88.2	0.243	8.75
6x6 GE Humboldt Bay	36	2.346	58.8-88.2	0.250	9.0
7x7 GE Humboldt Bay	49	1.662	58.8-88.2	0.177	8.67
8x8 GE Dresden-1	64	1.235	58.8-88.2	0.131	8.38
8x8 SPC	63	1.615	58.8-88.2	0.172	10.8
9x9 SPC-2 water rods	79	1.248	58.8-88.2	0.133	10.5
9x9 SPC-1 water rod	80	1.248	58.8-88.2	0.133	10.6
9x9 GE11/GE13	74	1.389	58.8-88.2	0.150	11.1
9x9 Atrium 9B SPC	72	1.366	58.8-88.2	0.145	10.4
10x10 SVEA-96	96	1.022	58.8-88.2	0.109	10.5
10x10 GE12	92	1.167	58.8-88.2	0.124	11.4
6x6 Dresden-1	36	2.455	58.8-88.2	0.261	9.4
7x7 Oyster Creek	49	2.346	58.8-88.2	0.250	12.2
8x8 Oyster Creek	64	1.739	58.8-88.2	0.185	11.8
8x8 Quad + Westinghouse	64	1.201	58.8-88.2	0.128	8.2
8x8 TVA Browns Ferry	61	1.686	58.8-88.2	0.179	10.9
9x9 SPC-5	76	1.249	58.8-88.2	0.133	10.1
ANF 8x8	62	1.61	58.8-88.2	0.172	10.7
ANF-9X (9x9)	72	1.249	58.8-88.2	0.133	9.6

[†] Conservatively bounding for GE-7x7 (1966), GE-7x7 (1968), GE-7x7R and GE-8x8 (ORNL/TM-9591/V1-R1).

^{††} Conservatively bounding initial fill pressure. ORNL/TM-9591/V1-R1 reports GE-8x8R pre-pressurized to 3 atm.

^{†††} BWR fuel rods internal pressurization between 4 to 6 atm (PNL-4835).

Table 4.3.6

BOUNDING VALUES OF FUEL CLADDING STRESS FOR BWR SNF

	GE-7x7 (1966)	GE-7x7 (1968)	GE-7x7R	GE-8x8	GE-8x8R	Exxon-9x9
Fresh Fuel Rods O.D. (inch)	0.563	0.570	0.563	0.493	0.483	0.42
End of Life Oxidation Thickness (inch)	0.0047	0.0047	0.0047	0.0047	0.0047	0.0047
End of Life Rods O.D. (inch)	0.5536	0.5606	0.5536	0.4836	0.4736	0.4106
Rods I.D. (inch)	0.499	0.499	0.489	0.425	0.419	0.36
Average Tube Diameter (inch)	0.5263	0.5298	0.5213	0.4543	0.4463	0.3853
Wall Thickness (inch)	0.0273	0.0308	0.0323	0.0293	0.0273	0.0253
Theoretical Bounding Rod Pressure (MPa gage) [†]	7.54	7.54	7.54	7.54	7.54	7.54
Bounding Cladding Stress (MPa)	72.7	64.8	60.8	58.5	61.6	57.4

[†] PNL-6189 [4.3.1] data.

Table 4.3.6 (continued)

BOUNDING VALUES OF FUEL CLADDING STRESS FOR BWR SNF

	6x6 GE Dresden-1	6x6 MOX Dresden-1	6x6 GE Humboldt Bay	7x7 GE Humboldt Bay	8x8 GE Dresden-1	8x8 SPC
Fresh Fuel Rods O.D. (inch)	0.5645	0.5625	0.563	0.486	0.412	0.484
End of Life Oxidation Thickness (inch)	0.0047	0.0047	0.0047	0.0047	0.0047	0.0047
End of Life Rods O.D. (inch)	0.5551	0.5531	0.5536	0.4766	0.4026	0.4746
Rods I.D. (inch)	0.4945	0.4925	0.499	0.4204	0.362	0.414
Average Tube Diameter (inch)	0.5248	0.5228	0.5263	0.4485	0.3813	0.4443
Wall Thickness (inch)	0.0303	0.0303	0.0273	0.0281	0.0203	0.0303
Theoretical Bounding Rod Pressure (MPa gage) [†]	7.54	7.54	7.54	7.54	7.54	7.54
Bounding Cladding Stress (MPa)	65.3	65.0	72.7	60.1	70.8	55.3

[†] PNL-6189 [4.3.1] data.

Table 4.3.6 (continued)

BOUNDING VALUES OF FUEL CLADDING STRESS FOR BWR SNF

	9x9 SPC-2 water rods	9x9 SPC-1 water rod	9x9 GE-11/13	9x9 SPC Atrium 9B	10x10 SVEA- 96	10x10 GE12
Fresh Fuel Rods O.D. (inch)	0.424	0.423	0.44	0.433	0.379	0.404
End of Life Oxidation Thickness (inch)	0.0047	0.0047	0.0047	0.0047	0.0047	0.0047
End of Life Rods O.D. (inch)	0.4146	0.4136	0.4306	0.4236	0.3696	0.3946
Rods I.D. (inch)	0.364	0.364	0.384	0.3808	0.3294	0.352
Average Tube Diameter (inch)	0.3893	0.3888	0.4073	0.4022	0.3495	0.3733
Wall Thickness (inch)	0.0253	0.0248	0.0233	0.0214	0.0201	0.0213
Theoretical Bounding Rod Pressure (MPa gage) [†]	7.54	7.54	7.54	7.54	7.54	7.54
Bounding Cladding Stress (MPa)	58.0	59.1	65.9	70.9	65.6	66.1

[†] PNL-6189 [4.3.1] data.

Table 4.3.6 (continued)

BOUNDING VALUES OF FUEL CLADDING STRESS FOR BWR SNF

	6x6 Dresden-1† Thin Clad	7x7 Oyster Creek	8x8 Oyster Creek	8x8 Quad†
Fresh fuel Rods O.D. (inch)	0.5625	0.57	0.5015	0.4576
End-of-Life Oxidization Thin Clad (inch)	0.0047	0.0047	0.0047	0.0047
End-of-Life Rods O.D. (inch)	0.5531	0.5606	0.4921	0.4482
Rods I.D. (inch)	0.5105	0.499	0.4295	0.3996
Average Tube Diameter (inch)	0.5318	0.5298	0.4608	0.4239
Wall Thickness (inch)	0.0213	0.0308	0.0313	0.0243
Theoretical Boundary Rod Pressure (MPa gauge)	7.54	7.54	7.54	7.54
Bounding Cladding Stress (MPa)	94.1	64.5	55.5	65.8

† Outlier fuel type evaluated in Table 4.3.8.

Table 4.3.6 (continued)

BOUNDING VALUES OF FUEL CLADDING STRESS FOR BWR SNF

	8x8 TVA Browns Ferry	9x9 SPC-5	ANF 8x8	ANF-9X (9x9)
O.D. Inch	0.483	0.417	0.484	0.424
End-of-Life Oxidation Thickness (inch)	0.0047	0.0047	0.0047	0.0047
End-of-Life Rods O.D. (inch)	0.4736	0.4076	0.4746	0.4146
Rods I.D. (inch)	0.423	0.364	0.414	0.364
Average Tube Diameter (inch)	0.4483	0.3858	0.4443	0.3893
Wall Thickness (inch)	0.0253	0.0218	0.0303	0.0253
Theoretical Bounding Rod Pressure (MPa)	7.54	7.54	7.54	7.54
Bounding Cladding Stress (MPa)	66.8	66.7	55.3	58.0

Table 4.3.7

ZIRCALOY CLADDING TEMPERATURE LIMITS AND PERMISSIBLE TEMPERATURES

Fuel Age (years)	PWR SNF (°C) [°F]		BWR SNF (°C) [°F]	
	DCCG Limit	Permissible PNL Limit	DCCG Limit	Permissible PNL Limit
5	419.4 [787]	366.0 [691]	440.2 [824]	393.2 [740]
6	416.7 [782]	358.0 [676]	436.2 [817]	377.9 [712]
7	397.0 [747]	335.0 [635]	416.4 [781]	353.7 [669]
10	379.4 [715]	329.6 [625]	398.9 [750]	347.9 [658]
15	370.2 [698]	323.2 [614]	390.2 [734]	341.1 [646]

Table 4.3.8

PERMISSIBLE TEMPERATURES FOR OUTLIER FUEL TYPES

Fuel Age (Years)	6x6 Dresden-1 Thin Clad (°C) [°F] (BWR)	
5	383.7	[723]
6	370.9	[700]
7	347.7	[658]
10	342.1	[648]
15	334.9	[635]

Table 4.3.9

BOUNDING CLADDING STRESS FOR OUTLIER PWR FUEL

	B&W 15x15 Mark B-11
Fresh Fuel Rods O.D. (inch)	0.414
End of Life Oxidation Thickness (inch)	0.0027
End of Life Rods O.D. (inch)	0.4086
Rods I.D. (inch)	0.370
Average Rod Diameter (inch)	0.3893
Limiting Rod Pressure (MPa)	15 [†]
Bounding Cladding Stress (MPa)	151.3

[†] Rod pressure to be limited to 2175 psia at 387°C gas plenum temperature.

4.4 THERMAL EVALUATION FOR NORMAL CONDITIONS OF STORAGE

Under long-term storage conditions, the HI-STORM System (i.e., HI-STORM overpack and MPC) thermal evaluation is performed with the MPC cavity backfilled with helium. Thermal analysis results for the long-term storage scenarios are obtained and reported in this section.

4.4.1 Thermal Model

The MPC basket design consists of four distinct geometries to hold 24 or 32 PWR, or 68 BWR fuel assemblies. The basket is a matrix of square compartments designed to hold the fuel assemblies in a vertical position. The basket is a honeycomb structure of alloy steel (Alloy X) plates with full-length edge-welded intersections to form an integral basket configuration. All individual cell walls, except outer periphery cell walls in the MPC-68 and MPC-32, are provided with ~~Boral~~ neutron absorber sandwiched between the box wall and a stainless steel sheathing plate over the full length of the active fuel region.

The design basis decay heat generation (per PWR or BWR assembly) for long-term normal storage is specified in Table 2.1.6. The decay heat is conservatively considered to be non-uniformly distributed over the active fuel length based on the design basis axial burnup distributions provided in Chapter 2 (Table 2.1.11).

Transport of heat from the interior of the MPC to its outer surface is accomplished by a combination of conduction through the MPC basket metal grid structure, and conduction and radiation heat transfer in the relatively small helium gaps between the fuel assemblies and basket cell walls. Heat dissipation across the gap between the MPC basket periphery and the MPC shell is by a combination of helium conduction, natural convection (by means of the "Rayleigh" effect)[†] and radiation across the gap and conduction in the aluminum alloy 1100 heat conduction elements*. MPC internal helium circulation is recognized in the thermal modeling analyses reported herein. Heat rejection from the outer surface of the MPC to the environment is primarily accomplished by convective heat transfer to a buoyancy driven airflow through the MPC-to-overpack annular gap. Inlet and outlet ducts in the overpack cylinder at its bottom and top, respectively, allow circulation of air through the annulus. A secondary heat rejection path from the outer surface of the MPC to the environment involves thermal radiation heat transfer across the annular gap, radial conduction through the overpack cylinder, and natural convection and thermal radiation from the outer surface of the overpack to the atmosphere.

4.4.1.1 Analytical Model - General Remarks

Transport of heat from the heat generation region (fuel assemblies) to the outside environment (ambient air or ground) is analyzed broadly in terms of three interdependent thermal models.

1. The first model considers transport of heat from the fuel assembly to the basket cell walls. This model recognizes the combined effects of conduction (through helium) and radiation,

[†] Neglected in the thermal analyses for conservatism.

* ~~Neglected in the thermal analyses for conservatism.~~

and is essentially a finite element technology based update of the classical Wootton & Epstein [4.4.1] (which considered radiative heat exchange between fuel rod surfaces) formulation.

2. The second model considers heat transport within an MPC cross section by conduction and radiation. The effective cross sectional thermal conductivity of the basket region, obtained from a combined fuel assembly/basket heat conduction-radiation model developed on ANSYS, is applied to an axisymmetric thermal model of the HI-STORM System on the FLUENT [4.1.2] code.
3. The third model deals with the transmission of heat from the MPC exterior surface to the external environment (heat sink). The upflowing air stream in the MPC/cask annulus extracts most of the heat from the external surface of the MPC, and a small amount of heat is radially deposited on the HI-STORM inner surface by conduction and radiation. Heat rejection from the outside cask surfaces to ambient air is considered by accounting for natural convection and radiative heat transfer mechanisms from the vertical (cylindrical shell) and top cover (flat) surfaces. The reduction in radiative heat exchange between cask outside vertical surfaces and ambient air, because of blockage from the neighboring casks arranged for normal storage at an ISFSI pad as described in Section 1.4, is recognized in the analysis. The overpack top plate is modeled as a heated surface in convective and radiative heat exchange with air and as a recipient of heat input through insolation. Insolation on the cask surfaces is based on 12-hour levels prescribed in 10CFR71, averaged over a 24-hour period, after accounting for partial blockage conditions on the sides of the overpack.

Subsections 4.4.1.1.1 through 4.4.1.1.9 contain a systematic description of the mathematical models devised to articulate the temperature field in the HI-STORM System. The description begins with the method to characterize the heat transfer behavior of the prismatic (square) opening referred to as the “fuel space” with a heat emitting fuel assembly situated in it. The methodology utilizes a finite element procedure to replace the heterogeneous SNF/fuel space region with an equivalent solid body having a well-defined temperature-dependent conductivity. In the following subsection, the method to replace the “composite” walls of the fuel basket cells with an equivalent “solid” wall is presented. Having created the mathematical equivalents for the SNF/fuel spaces and the fuel basket walls, the method to represent the MPC cylinder containing the fuel basket by an equivalent cylinder whose thermal conductivity is a function of the spatial location and coincident temperature is presented.

Following the approach of presenting descriptions starting from the inside and moving to the outer region of a cask, the next subsections present the mathematical model to simulate the overpack. Subsection 4.4.1.1.9 concludes the presentation with a description of how the different models for the specific regions within the HI-STORM System are assembled into the final FLUENT model.

4.4.1.1.1 Overview of the Thermal Model

Thermal analysis of the HI-STORM System is performed by assuming that the system is subject to its maximum heat duty with each storage location occupied and with the heat generation rate in each stored fuel assembly equal to the design-basis maximum value. While the assumption of equal heat generation imputes a certain symmetry to the cask thermal problem, the thermal model must incorporate three attributes of the physical problem to perform a rigorous analysis of a fully loaded cask:

- i. While the rate of heat conduction through metals is a relatively weak function of temperature, radiation heat exchange is a nonlinear function of surface temperatures.
- ii. Heat generation in the MPC is axially non-uniform due to non-uniform axial burnup profiles in the fuel assemblies.
- iii. Inasmuch as the transfer of heat occurs from inside the basket region to the outside, the temperature field in the MPC is spatially distributed with the maximum values reached in the central core region.

It is clearly impractical to model every fuel rod in every stored fuel assembly explicitly. Instead, the cross section bounded by the inside of the storage cell, which surrounds the assemblage of fuel rods and the interstitial helium gas, is replaced with an "equivalent" square (solid) section characterized by an effective thermal conductivity. Figure 4.4.1 pictorially illustrates the homogenization concept. Further details of this procedure for determining the effective conductivity are presented in Subsection 4.4.1.1.2; it suffices to state here that the effective conductivity of the cell space will be a function of temperature because the radiation heat transfer (a major component of the heat transport between the fuel rods and the surrounding basket cell metal) is a strong function of the temperatures of the participating bodies. Therefore, in effect, every storage cell location will have a different value of effective conductivity (depending on the coincident temperature) in the homogenized model. The temperature-dependent fuel assembly region effective conductivity is determined by a finite volume procedure, as described in Subsection 4.4.1.1.2.

In the next step of homogenization, a planar section of MPC is considered. With each storage cell inside space replaced with an equivalent solid square, the MPC cross section consists of a metallic gridwork (basket cell walls with each square cell space containing a solid fuel cell square of effective thermal conductivity, which is a function of temperature) circumscribed by a circular ring (MPC shell). There are ~~five~~ *four* distinct materials in this section, namely the homogenized fuel cell squares, the Alloy X structural materials in the MPC (including ~~Boral~~-sheathing), ~~Boral~~*neutron absorber*, ~~Alloy 1100 aluminum heat conduction elements~~, and helium gas. Each of the ~~five~~ *four* constituent materials in this section has a different conductivity. It is emphasized that the conductivity of the homogenized fuel cells is a strong function of temperature.

In order to replace this thermally heterogeneous MPC section with an equivalent conduction-only region, resort to the finite element procedure is necessary. Because the rate of transport of heat within the MPC is influenced by radiation, which is a temperature-dependent effect, the equivalent conductivity of the MPC region must also be computed as a function of temperature. Finally, it is

recognized that the MPC section consists of two discrete regions, namely, the basket region and the peripheral region. The peripheral region is the space between the peripheral storage cells and the MPC shell. This space is essentially full of helium surrounded by Alloy X plates and optionally Alloy 1100 aluminum heat conduction elements. Accordingly, as illustrated in Figure 4.4.2 for MPC-68, the MPC cross section is replaced with two homogenized regions with temperature-dependent conductivities. In particular, the effective conductivity of the fuel cells is subsumed into the equivalent conductivity of the basket cross section. The finite element procedure used to accomplish this is described in Subsection 4.4.1.1.4. The ANSYS finite element code is the vehicle for all modeling efforts described in the foregoing.

In summary, appropriate finite-element models are used to replace the MPC cross section with an equivalent two-region homogeneous conduction lamina whose local conductivity is a known function of coincident absolute temperature. Thus, the MPC cylinder containing discrete fuel assemblies, helium, ~~Boral~~ neutron absorber and Alloy X, is replaced with a right circular cylinder whose material conductivity will vary with radial and axial position as a function of the coincident temperature. Finally, HI-STORM is simulated as a radially symmetric structure with a buoyancy-induced flow in the annular space surrounding the heat generating MPC cylinder.

The thermal analysis procedure described above makes frequent use of equivalent thermal properties to ease the geometric modeling of the cask components. These equivalent properties are rigorously calculated values based on detailed evaluations of actual cask system geometries. All these calculations are performed conservatively to ensure a bounding representation of the cask system. This process, commonly referred to as submodeling, yields accurate (not approximate) results. Given the detailed nature of the submodeling process, experimental validation of the individual submodels is not necessary.

Internal circulation of helium in the sealed MPC is modeled as flow in a porous media in the fueled region containing the SNF (including top and bottom plenums). The basket-to-MPC shell clearance space is modeled as a helium filled radial gap to include the downcomer flow in the thermal model. The downcomer region, as illustrated in Figure 4.4.2, consists of an azimuthally varying gap formed by the square-celled basket outline and the cylindrical MPC shell. At the locations of closest approach a differential expansion gap (a small clearance on the order of 1/10 of an inch) is engineered to allow free thermal expansion of the basket. At the widest locations, the gaps are on the order of the fuel cell opening (~6" (BWR) and ~9" (PWR) MPCs). It is heuristically evident that heat dissipation by conduction is maximum at the closest approach locations (low thermal resistance path) and that convective heat transfer is highest at the widest gap locations (large downcomer flow). In the FLUENT thermal model, a radial gap that is large compared to the basket-to-shell clearance and small compared to the cell opening is used. As a relatively large gap penalizes heat dissipation by conduction and a small gap throttles convective flow, the use of a single gap in the FLUENT model understates both conduction and convection heat transfer in the downcomer region. Heat dissipation by the inclusion of aluminum heat conduction elements, as stated earlier, is conservatively neglected in the HI-STORM thermal modeling.

The FLUENT thermal modeling methodology has been benchmarked with full-scale cask test data (EPRI TN-24P cask testing), as well as with PNNL's COBRA-SFS modeling of the HI-STORM

SHADED TEXT INDICATES CONFIDENTIAL INFORMATION PURSUANT TO 10 CFR 2.790

System. The benchmarking work has been documented in a Holtec topical report HI-992252 (“Topical Report on the HI-STAR/HI-STORM Thermal Model and Its Benchmarking with Full-Size Cask Test Data”).

In this manner, a loaded MPC standing upright on the ISFSI pad in a HI-STORM overpack is replaced with a right circular cylinder with spatially varying temperature-dependent conductivity. Heat is generated within the basket space in this cylinder in the manner of the prescribed axial burnup distribution. In addition, heat is deposited from insolation on the external surface of the overpack. Under steady state conditions the total heat due to internal generation and insolation is dissipated from the outer cask surfaces by natural convection and thermal radiation to the ambient environment and from heating of upward flowing air in the annulus. Details of the elements of mathematical modeling are provided in the following.

4.4.1.1.2 Fuel Region Effective Thermal Conductivity Calculation

Thermal properties of a large number of PWR and BWR fuel assembly configurations manufactured by the major fuel suppliers (i.e., Westinghouse, CE, B&W, and GE) have been evaluated for inclusion in the HI-STORM System thermal analysis. Bounding PWR and BWR fuel assembly configurations are determined using the simplified procedure described below. This is followed by the determination of temperature-dependent properties of the bounding PWR and BWR fuel assembly configurations to be used for cask thermal analysis using a finite volume (FLUENT) approach.

To determine which of the numerous PWR assembly types listed in Table 4.4.1 should be used in the thermal model for the PWR fuel baskets (MPC-24, MPC-24E, MPC-32), we must establish which assembly type has the maximum thermal resistance. The same determination must be made for the MPC-68, out of the menu of SNF types listed in Table 4.4.2. For this purpose, we utilize a simplified procedure that we describe below.

Each fuel assembly consists of a large array of fuel rods typically arranged on a square layout. Every fuel rod in this array is generating heat due to radioactive decay in the enclosed fuel pellets. There is a finite temperature difference required to transport heat from the innermost fuel rods to the storage cell walls. Heat transport within the fuel assembly is based on principles of conduction heat transfer combined with the highly conservative analytical model proposed by Wooton and Epstein [4.4.1]. The Wooton-Epstein model considers radiative heat exchange between individual fuel rod surfaces as a means to bound the hottest fuel rod cladding temperature.

Transport of heat energy within any cross section of a fuel assembly is due to a combination of radiative energy exchange and conduction through the helium gas that fills the interstices between the fuel rods in the array. With the assumption of uniform heat generation within any given horizontal cross section of a fuel assembly, the combined radiation and conduction heat transport effects result in the following heat flow equation:

$$Q = \sigma C_o F_e A [T_C^4 - T_B^4] + 13.5740 L K_{cs} [T_C - T_B]$$

where:

$F_\epsilon = \text{Emissivity Factor}$

$$= \frac{1}{\left(\frac{1}{\epsilon_C} + \frac{1}{\epsilon_B} - 1\right)}$$

$\epsilon_C, \epsilon_B =$ emissivities of fuel cladding, fuel basket (see Table 4.2.4)

$C_o = \text{Assembly Geometry Factor}$

$$= \frac{4N}{(N+1)^2} \text{ (when } N \text{ is odd)}$$

$$= \frac{4}{N+2} \text{ (when } N \text{ is even)}$$

$N =$ Number of rows or columns of rods arranged in a square array

$A =$ fuel assembly "box" heat transfer area = 4 × width × length

$L =$ fuel assembly length

$K_{cs} =$ fuel assembly constituent materials volume fraction weighted mixture conductivity

$T_C =$ hottest fuel cladding temperature ($^{\circ}\text{R}$)

$T_B =$ box temperature ($^{\circ}\text{R}$)

$Q =$ net radial heat transport from the assembly interior

$\sigma =$ Stefan-Boltzmann Constant (0.1714×10^{-8} Btu/ft²-hr- $^{\circ}\text{R}^4$)

In the above heat flow equation, the first term is the Wooten-Epstein radiative heat flow contribution while the second term is the conduction heat transport contribution based on the classical solution to the temperature distribution problem inside a square shaped block with uniform heat generation [4.4.5]. The 13.574 factor in the conduction term of the equation is the shape factor for two-dimensional heat transfer in a square section. Planar fuel assembly heat transport by conduction occurs through a series of resistances formed by the interstitial helium fill gas, fuel cladding and enclosed fuel. An effective planar mixture conductivity is determined by a volume fraction weighted sum of the individual constituent material resistances. For BWR assemblies, this formulation is applied to the region inside the fuel channel. A second conduction and radiation model is applied between the channel and the fuel basket gap. These two models are combined, in series, to yield a total effective conductivity.

The effective conductivity of the fuel for several representative PWR and BWR assemblies is presented in Tables 4.4.1 and 4.4.2. At higher temperatures (approximately 450°F and above), the zircaloy clad fuel assemblies with the lowest effective thermal conductivities are the W-17×17 OFA (PWR) and the GE11-9×9 (BWR). A discussion of fuel assembly conductivities for some of the recent vintage 10×10 array and certain plant specific BWR fuel designs is presented near the end of this subsection. As noted in Table 4.4.2, the Dresden 1 (intact and damaged) fuel assemblies are excluded from consideration. The design basis decay heat load for Dresden-1 intact and damaged fuel (Table 2.1.7) is approximately 58% lower than the MPC-68 design-basis maximum heat load (Table 2.1.6). Examining Table 4.4.2, the effective conductivity of the damaged Dresden-1 fuel assembly in a damaged fuel container is approximately 40% lower than the bounding (GE-11 9×9)

fuel assembly. Consequently, the fuel cladding temperatures in the HI-STORM System with Dresden-1 intact or damaged fuel assemblies will be bounded by design basis fuel cladding temperatures. Based on this simplified analysis, the W-17x17 OFA PWR and GE11-9x9 BWR fuel assemblies are determined to be the bounding configurations for analysis of zircaloy clad fuel at design basis maximum heat loads. As discussed in Section 4.3.1, stainless clad fuel assemblies with significantly lower decay heat emission characteristics are not deemed to be bounding.

For the purpose of determining axial flow resistance for inclusion of MPC thermosiphon effect in the HI-STORM system modeling, equivalent porous media parameters for the W-17x17OFA and GE11-9x9 fuels are computed. Theoretically bounding expansion and contraction loss factors are applied at the grid spacer locations to conservatively maximize flow resistance. As an additional measure of conservatism, the grids are modeled by postulating that they are formed using thick metal sheets which have the effect of artificially throttling flow. Heat transfer enhancement by grid spacers turbulence is conservatively ignored in the analysis.

Having established the governing (most resistive) PWR and BWR SNF types, we use a finite-volume code to determine the effective conductivities in a conservative manner. Detailed conduction-radiation finite-volume models of the bounding PWR and BWR fuel assemblies developed on the FLUENT code are shown in Figures 4.4.3 and 4.4.4, respectively. The PWR model was originally developed on the ANSYS code, which enables individual rod-to-rod and rod-to-basket wall view factor calculations to be performed using the AUX12 processor. Limitations of radiation modeling techniques implemented in ANSYS do not permit taking advantage of quarter symmetry of the fuel assembly geometry. Unacceptably long CPU time and large workspace requirements necessary for performing gray body radiation calculations for a complete fuel assembly geometry on ANSYS prompted the development of an alternate simplified model on the FLUENT code. The FLUENT model is benchmarked with the ANSYS model results for a Westinghouse 17x17 fuel assembly geometry for the case of black body radiation (emissivities = 1). The FLUENT model is found to yield conservative results in comparison to the ANSYS model for the "black" surface case. The FLUENT model benchmarked in this manner is used to solve the gray body radiation problem to provide the necessary results for determining the effective thermal conductivity of the governing PWR fuel assembly. The same modeling approach using FLUENT is then applied to the governing BWR fuel assembly, and the effective conductivity of GE-11 9x9 fuel determined.

The combined fuel rods-helium matrix is replaced by an equivalent homogeneous material that fills the basket opening by the following two-step procedure. In the first step, the FLUENT-based fuel assembly model is solved by applying equal heat generation per unit length to the individual fuel rods and a uniform boundary temperature along the basket cell opening inside periphery. The temperature difference between the peak cladding and boundary temperatures is used to determine an effective conductivity as described in the next step. For this purpose, we consider a two-dimensional cross section of a square shaped block with an edge length of $2L$ and a uniform volumetric heat source (q_g), cooled at the periphery with a uniform boundary temperature. Under the assumption of constant material thermal conductivity (K), the temperature difference (ΔT) from the center of the cross section to the periphery is analytically given by [4.4.5]:

$$\Delta T = 0.29468 \frac{q_g L^2}{K}$$

This analytical formula is applied to determine the effective material conductivity from a known quantity of heat generation applied in the FLUENT model (smeared as a uniform heat source, q_g) basket opening size and ΔT calculated in the first step.

As discussed earlier, the effective fuel space conductivity must be a function of the temperature coordinate. The above two-step analysis is carried out for a number of reference temperatures. In this manner, the effective conductivity as a function of temperature is established.

In Table 4.4.5, 10×10 array type BWR fuel assembly conductivity results from a simplified analysis are presented to determine the most resistive fuel assembly in this class. The Atrium-10 fuel type is determined to be the most resistive in this class of fuel assemblies. A detailed finite-element model of this assembly type was developed to rigorously quantify the heat dissipation characteristics. The results of this study are presented in Table 4.4.6 and compared to the BWR bounding fuel assembly conductivity depicted in Figure 4.4.5. The results of this study demonstrate that the bounding fuel assembly conductivity is conservative with respect to the 10×10 class of BWR fuel assemblies.

Table 4.4.23 summarizes plant specific fuel types' effective conductivities. From these analytical results, SPC-5 is determined to be the most resistive fuel assembly in this group of fuel. A finite element model of the SPC-5 fuel assembly was developed to confirm that its in-plane heat dissipation characteristics are bounded from below by the Design Basis BWR fuel conductivities used in the HI-STORM thermal analysis.

Temperature-dependent effective conductivities of PWR and BWR design basis fuel assemblies (most resistive SNF types) are shown in Figure 4.4.5. The finite volume results are also compared to results reported from independent technical sources. From this comparison, it is readily apparent that FLUENT-based fuel assembly conductivities are conservative. The FLUENT computed values (not the published literature data) are used in the MPC thermal analysis presented in this document.

4.4.1.1.3 Effective Thermal Conductivity of ~~Boral~~Neutron Absorber /Sheathing/Box Wall Sandwich

Each MPC basket cell wall (except the MPC-68 and MPC-32 outer periphery cell walls) is manufactured with a ~~Boral~~-neutron absorbing plate for criticality control. Each ~~Boral~~-neutron absorbing plate is sandwiched in a sheathing-to-basket wall pocket. A schematic of the "Box Wall-~~Boral~~neutron absorber-Sheathing" sandwich geometry of an MPC basket is illustrated in Figure 4.4.6. During fabrication, a uniform normal pressure is applied to each "Box Wall- ~~Boral~~neutron absorber-Sheathing" sandwich in the assembly fixture during welding of the sheathing periphery on the box wall. This ensures adequate surface-to-surface contact for elimination of any macroscopic air gaps. The mean coefficient of linear expansion of the ~~Boral~~-neutron absorber is higher than the thermal expansion coefficients of the basket and sheathing materials. Consequently, basket heat-up from the stored SNF will further ensure a tight fit of the ~~Boral~~-neutron absorber plate in the sheathing-to-box pocket. The presence of small microscopic gaps due to less than perfect surface

finish characteristics requires consideration of an interfacial contact resistance between the ~~Boral neutron absorber~~ and box-sheathing surfaces. A conservative contact resistance resulting from a 2 mil ~~Boral neutron absorber~~ to pocket air-gap is applied in the analysis. Note that this gap would actually be filled with helium, so this is very conservative. In other words, no credit is taken for the interfacial pressure between ~~Boral neutron absorber plate~~ and stainless plate/sheet stock produced by the fixturing and welding process. Furthermore, no credit is taken for the presence of helium in and radiative heat exchange across the ~~Boral to sheathing or Boral to box wall gaps~~.

Heat conduction properties of a composite “Box Wall-~~Boral neutron absorber~~-Sheathing” sandwich in the two principal basket cross sectional directions as illustrated in Figure 4.4.6 (i.e., lateral “out-of-plane” and longitudinal “in-plane”) are unequal. In the lateral direction, heat is transported across layers of sheathing, ~~air-helium gap, Boral neutron absorber (B₄C and cladding layers)~~ and box wall resistances that are essentially in series (except for the small helium filled end regions shown in Figure 4.4.7). Heat conduction in the longitudinal direction, in contrast, is through an array of essentially parallel resistances comprised of these several layers listed above. Resistance network models applicable to the two directions are illustrated in Figure 4.4.7. It is noted that, in addition to the essentially series and parallel resistances of the composite wall layers for the “out-of-plane” and “in-plane” directions respectively, the effect of small helium filled end regions is also included in the resistance network analogy. For the ANSYS based MPC basket thermal model, corresponding non-isotropic effective thermal conductivities in the two orthogonal sandwich directions are determined and applied in the analysis.

4.4.1.1.4 Finite Element Modeling of Basket In-Plane Conductive Heat Transport

The heat rejection capability of each MPC basket design (i.e., MPC-24, MPC-68, MPC-32 and MPC-24E) is evaluated by developing a thermal model of the combined fuel assemblies and composite basket walls geometry on the ANSYS finite element code. The ANSYS model includes a geometric layout of the basket structure in which the basket “Box Wall-~~Boral neutron absorber~~-Sheathing” sandwich is replaced by a “homogeneous wall” with an equivalent thermal conductivity. Since the thermal conductivity of the Alloy X material is a weakly varying function of temperature, the equivalent “homogeneous wall” must have a temperature-dependent effective conductivity. Similarly, as illustrated in Figure 4.4.7, the conductivities in the “in-plane” and “out-of-plane” directions of the equivalent “homogeneous wall” are different. Finally, as discussed earlier, the fuel assemblies and the surrounding basket cell openings are modeled as homogeneous heat generating regions with an effective temperature dependent in-plane conductivity. The methodology used to reduce the heterogeneous MPC basket - fuel assemblage to an equivalent homogeneous region with effective thermal properties is discussed in the following.

Consider a cylinder of height, L , and radius, r_o , with a uniform volumetric heat source term, q_g , insulated top and bottom faces, and its cylindrical boundary maintained at a uniform temperature, T_c . The maximum centerline temperature (T_h) to boundary temperature difference is readily obtained from classical one-dimensional conduction relationships (for the case of a conducting region with uniform heat generation and a constant thermal conductivity K_s):

$$(T_h - T_c) = q_g r_o^2 / (4 K_s)$$

Noting that the total heat generated in the cylinder (Q_t) is $\pi r_o^2 L q_g$, the above temperature rise formula can be reduced to the following simplified form in terms of total heat generation per unit length (Q_t/L):

$$(T_h - T_c) = (Q_t / L) / (4 \pi K_s)$$

This simple analytical approach is employed to determine an effective basket cross-sectional conductivity by applying an equivalence between the ANSYS finite element model of the basket and the analytical case. The equivalence principle employed in the thermal analysis is depicted in Figure 4.4.2. The 2-dimensional ANSYS finite element model of the MPC basket is solved by applying a uniform heat generation per unit length in each basket cell region (depicted as Zone 1 in Figure 4.4.2) and a constant basket periphery boundary temperature, T_c . Noting that the basket region with uniformly distributed heat sources and a constant boundary temperature is equivalent to the analytical case of a cylinder with uniform volumetric heat source discussed earlier, an effective MPC basket conductivity (K_{eff}) is readily derived from the analytical formula and ANSYS solution leading to the following relationship:

$$K_{eff} = N (Q_f'/L) / (4 \pi [T_h' - T_c'])$$

where:

N = number of fuel assemblies

(Q_f'/L) = per fuel assembly heat generation per unit length applied in ANSYS model

T_h' = peak basket cross-section temperature from ANSYS model

Cross sectional views of MPC basket ANSYS models are depicted in Figures 4.4.9 and 4.4.10. Notice that many of the basket supports and all shims have been conservatively neglected in the models. This conservative geometry simplification, coupled with the conservative neglect of thermal expansion that would minimize the gaps, yields conservative gap thermal resistances. Temperature-dependent equivalent thermal conductivities of the fuel regions and composite basket walls, as determined from analysis procedures described earlier, are applied to the ANSYS model. The planar ANSYS conduction model is solved by applying a constant basket periphery temperature with uniform heat generation in the fuel region. Table 4.4.3 summarizes effective thermal conductivity results of each basket design obtained from the ANSYS models. The effective calculated basket cross sectional conductivity and the effective axial direction effective conductivity are assumed to be equal in the comprehensive HI-STORM System thermal model. It is recalled that the equivalent thermal conductivity values presented in Table 4.4.3 are lower bound values because, among other elements of conservatism, the effective conductivity of the most resistive SNF types (Tables 4.4.1 and 4.4.2) is used in the MPC finite element simulations.

The basket in-plane conductivities are computed for intact fuel storage and containerized fuel stored in Damaged Fuel Containers (DFCs). The MPC-24E is provided with four enlarged cells designated for storing damaged fuel. The MPC-68 has sixteen peripheral locations for damaged fuel storage in generic DFC designs. As a substantial fraction of the basket cells are occupied by intact fuel, the overall effect of DFC fuel storage on the basket heat dissipation rate is quite small. Including the

effect of reduced conductivity of the DFC cells in MPC-24E, the basket conductivity is computed to drop slightly (~0.6%). ~~In a bounding calculation in which all cells of MPC 68 are assumed occupied by fuel in DFC, the basket conductivity drops by about 5%. In a bounding evaluation in which the sixteen outer cells are occupied with damaged fuel, the effect of reduced conductivity on the PCT is computed to be negligible (less than 1°F). Therefore, DFCs do not pose a limitation on safe storage of fuel. Conservatively, assuming 95% of intact fuel basket heat load adequately covers damaged fuel storage in the MPC 24E and MPC 68.~~

4.4.1.1.5 Heat Transfer in MPC Basket Peripheral Region

Both of the MPC designs for storing PWR or BWR fuel are provided with relatively large regions, formed between the relatively cooler MPC shell and hot basket peripheral panels, filled with helium gas. Heat transfer in these helium-filled regions corresponds to the classical case of heat transfer in a differentially heated closed cavity. Many investigators, including Eckert and Carlson (Int. J. Heat Mass Transfer, vol. 2, p. 106, 1961) and Elder (J. Fluid Mech., vol. 23, p. 77, 1965) have performed experimental studies of this arrangement. The peripheral region between the basket and MPC inner surface is simulated as a tall fluid-filled cavity of height H formed between two differentially heated surfaces (ΔT) separated by a small distance L. In a closed cavity, an exchange of hot and cold fluids occurs near the top and bottom ends of the cavity, resulting in a net transport of heat across the gap. The rate of heat transfer across the cavity is characterized by a Rayleigh number, Ra_L , defined as:

$$Ra_L = \frac{C_p \rho^2 g \beta \Delta T L^3}{\mu K}$$

where:

C_p	=	fluid heat capacity
ρ	=	fluid density
g	=	acceleration due to gravity
β	=	coefficient of thermal expansion (equal to reciprocal of absolute temperature for gases)
ΔT	=	temperature difference between the hot and cold surfaces
L	=	spacing between the hot and cold surfaces
μ	=	fluid viscosity
K	=	fluid conductivity

Hewitt et al. [4.4.6] recommends the following Nusselt number correlation for heat transport in tall cavities:

$$Nu_L = 0.42 Ra_L^{1/4} Pr^{0.012} \left(\frac{H}{L}\right)^{-0.3}$$

where Pr is the Prandtl number of the cavity fill gas.

A Nusselt number of unity implies heat transfer by fluid conduction only, while a higher than unity Nusselt number is due to the "Rayleigh" effect which monotonically increases with increasing Rayleigh number. Nusselt numbers applicable to helium-filled PWR and BWR fueled HI-STORM MPC peripheral voids used in the original licensing analysis are provided in Table 4.4.4. For

conservatism, however, the contribution of the Rayleigh effect is ignored in the thermal model of the MPC.

4.4.1.1.6 Effective Thermal Conductivity of MPC Basket-to-Shell Aluminum Heat Conduction Elements

Aluminum heat conduction elements, required hardware in FSAR Revision 0 and optional hardware in FSAR Revision 1, are eliminated in Revision 2. Accordingly text in this sub-section is deleted.

~~As shown in HI-STORM System MPC drawings in Section 1.5, an option for insertion of full-length heat conduction elements fabricated from thin aluminum Alloy 1100 sheet metal is shown in the MPC design drawings. Due to the high thermal conductivity of aluminum Alloy 1100 (about 15 times that of Alloy X), a significant rate of net heat transfer is possible along thin plates. Figure 4.4.11 shows the mathematical idealization of a typical conduction element inserted in a basket periphery panel to MPC shell space. The aluminum heat conduction element is shown to cover the MPC basket Alloy X peripheral panel and MPC shell (Regions I and III depicted in Figure 4.4.11) surfaces along the full length of the basket. Heat transport to and from the aluminum heat conduction element is conservatively postulated to occur across a thin helium gap as shown in the figure (i.e., no credit is taken for contact between the aluminum heat conduction element and the Alloy X fuel basket). Aluminum surfaces inside the hollow region are sandblasted prior to fabrication to result in a rough surface finish which has a significantly higher emissivity compared to smooth surfaces of rolled aluminum. The untreated aluminum surfaces directly facing Alloy X panels have a smooth finish to minimize contact resistance.~~

~~Net heat transfer resistance from the hot basket periphery panel to the relatively cooler MPC shell along the aluminum heat conduction element pathway is a sum of three individual resistances, in regions labeled I, II, and III in Figure 4.4.11. In Region I, heat is transported from the basket to the aluminum heat conduction element surface directly facing the basket panel across a thin helium resistance gap. Longitudinal transport of heat (in the z direction) in the aluminum plate (in Region I) will result in an axially non-uniform temperature distribution. Longitudinal one-dimensional heat transfer in the Region I aluminum plate was analytically formulated to result in the following ordinary differential equation for the non-uniform temperature distribution:~~

$$\del t K_{Al} \frac{\partial^2 T}{\partial z^2} = \frac{K_{He}}{h} (T_h - T)$$

Boundary Conditions

$$\del \frac{\partial T}{\partial z} = 0 \text{ at } z = 0$$
$$\del T = T_h \text{ ' at } z = P$$

~~where (see Figure 4.4.11):~~

- ~~T(z) = non-uniform aluminum metal temperature distribution~~
- ~~t = heat conduction element thickness~~
- ~~K_{Al} = heat conduction element conductivity~~
- ~~K_{He} = helium conductivity~~

SHADED TEXT INDICATES CONFIDENTIAL INFORMATION PURSUANT TO 10 CFR 2.790

h = helium gap thickness

T_h = hot basket temperature

T_h' = heat conduction element Region I boundary temperature at $z = P$

P = heat conduction element Region I length

Solution of this ordinary differential equation subject to the imposed boundary condition is:

$$(T_h - T) = (T_h - T_h') \left[\frac{e^{\frac{z}{\sqrt{\alpha}}} + e^{-\frac{z}{\sqrt{\alpha}}}}{e^{\frac{P}{\sqrt{\alpha}}} + e^{-\frac{P}{\sqrt{\alpha}}}} \right]$$

where α is a dimensional parameter equal to $(h \times t \times K_{Al} / K_{He})$. The net heat transfer (Q_I) across the Region I helium gap can be determined by the following integrated heat flux to a heat conduction element of length L as:

$$Q_I = \int_0^P \frac{K_{He}}{h} (T_h - T) dz$$

Substituting the analytical temperature distribution result obtained in Equation c, the following expression for net heat transfer is obtained:

$$Q_I = \frac{K_{He} L \sqrt{\alpha}}{h} \left(1 - \frac{1}{e^{\frac{P}{\sqrt{\alpha}}} + e^{-\frac{P}{\sqrt{\alpha}}}} \right) (T_h - T_h')$$

Based on this result, an expression for Region I resistance is obtained as shown below:

$$R_I = \frac{T_h - T_h'}{Q_I} = \frac{h}{K_{He} L \sqrt{\alpha}} \left(1 - \frac{1}{e^{\frac{P}{\sqrt{\alpha}}} + e^{-\frac{P}{\sqrt{\alpha}}}} \right)^{-1}$$

The Region II resistance expression can be developed from the following net heat transfer equation in the vertical leg of the conduction element as shown below:

$$Q_{II} = \frac{K_{Al} L t}{W} (T_h' - T_c')$$

where W is the conduction element Region II length.

$$R_{II} = \frac{T_h' - T_c'}{Q_{II}} = \frac{W}{K_{Al} L t}$$

Similarly, a Region III resistance expression can be analytically determined as shown below:

$$R_{III} = \frac{(T_c' - T_c)}{Q_{III}}$$
$$= \frac{h}{K_{He} L \sqrt{\alpha}} \left(1 - \frac{1}{e^{\frac{P}{\sqrt{\alpha}}} + e^{-\frac{P}{\sqrt{\alpha}}}} \right)^{-1}$$

~~This completes the analysis for the total thermal resistance attributable to the heat conduction elements, which is equal to the sum of the three individual resistances. The total heat conduction element resistance is smeared across the basket to MPC shell region as an effective uniform annular gap conductivity (see Figure 4.4.2). We note that heat transport along the conduction elements is an independent conduction path in parallel with conduction and radiation mechanisms in the large helium gaps. Helium conduction and radiation in the MPC basket to MPC shell peripheral gaps is accounted for separately in the ANSYS models for the MPCs, described earlier. Therefore, the net conductivity of the MPC basket to MPC shell peripheral gap region is will be the sum of the heat conduction elements effective conductivity and the helium gap conduction radiation effective conductivity. For conservatism, however, the contribution of the heat conduction elements is ignored in the HI-STORM thermal analyses.~~

4.4.1.1.7 Annulus Air Flow and Heat Exchange

The HI-STORM storage overpack is provided with four inlet ducts at the bottom and four outlet ducts at the top. The ducts are provided to enable relatively cooler ambient air to flow through the annular gap between the MPC and storage overpack in the manner of a classical “chimney”. Hot air is vented from the top outlet ducts to the ambient environment. Buoyancy forces induced by density differences between the ambient air and the heated air column in the MPC-to-overpack annulus sustain airflow through the annulus.

In contrast to a classical chimney, however, the heat input to the HI-STORM annulus air does not occur at the bottom of the stack. Rather, the annulus air picks up heat from the lateral surface of the MPC shell as it flows upwards. The height dependent heat absorption by the annulus air must be properly accounted for to ensure that the buoyant term in the Bernoulli equation is not overstated making the solution unconservative. To fix ideas, consider two cases of stack heat input; Case A where the heat input to the rising air is all at the bottom (the “fireplace” scenario), and Case B, where the heat input is uniform along the entire height (more representative of the ventilated cask conditions). In both cases, we will assume that the air obeys the perfect gas law; i.e., at constant pressure, $\rho = C/T$ where ρ and T are the density and the absolute temperature of the air and C is a constant.

Case A: Entire Heat Input at the Bottom

In a stack of height H , where the temperature of the air is raised from T_i to T_o at the bottom (Figure 4.4.12; Case A), the net fluid “head” p_1 is given by:

$$p_1 = \rho_i H - \rho_o H$$

ρ_i and ρ_o are the densities of air corresponding to absolute temperatures T_i and T_o , respectively.

Since $\rho_i = \frac{C}{T_i}$ and $\rho_o = \frac{C}{T_o}$, we have:

$$p_1 = CH \left(\frac{1}{T_i} - \frac{1}{T_o} \right)$$

or

$$p_1 = \frac{CH \Delta T}{T_i T_o}$$

where: $\Delta T = T_o - T_i$

Let $\Delta T \ll T_i$, then we can write:

$$\begin{aligned} \frac{1}{T_o} &= \frac{1}{T_i \left(1 + \frac{\Delta T}{T_i}\right)} \\ &= \frac{1}{T_i} \left[1 - \frac{\Delta T}{T_i} + \dots \right] \end{aligned}$$

Substituting in the above we have:

$$p_1 = \frac{CH}{T_i} \delta (1 - \delta + \dots)$$

where $\delta = \frac{\Delta T}{T_i}$ (dimensionless temperature rise)

or $p_1 = \rho_i H \delta - O(\delta^2)$.

Case B: Uniform Heat Input

In this case, the temperature of air rises linearly from T_i at the bottom to T_o at the top (Figure 4.4.12; Case B):

$$T_o = T_i + \zeta h; 0 \leq h \leq H$$

where:

$$\zeta = \frac{T_o - T_i}{H} = \frac{\delta T_i}{H}$$

The total buoyant head, in this case, is given by:

$$\begin{aligned}
 p_2 &= \rho_i H - \int_0^H \rho \, dh \\
 &= \rho_i H - C \int_0^H \frac{1}{T} \, dh \\
 &= \rho_i H - C \int_0^H \frac{dh}{(T_i + \zeta h)} \\
 &= \rho_i H - \frac{C}{\zeta} \ln(1 + \delta)
 \end{aligned}$$

Using the logarithmic expansion relationship and simplifying we have:

$$p_2 = \frac{\rho_i H \delta}{2} - O(\delta^2)$$

Neglecting terms of higher order, we conclude that p_2 is only 50% of p_1 , i.e., the buoyancy driver in the case of uniformly distributed heat input to the air is half of the value if the heat were all added at the bottom.

In the case of HI-STORM, the axial heat input profile into the annulus air will depend on the temperature difference between the MPC cylindrical surface and the rising air along the height (Case C in Figure 4.4.12). The MPC surface temperature profile, of course, is a strong function of the axial decay heat generation profile in the SNF. Previous analyses show that the HI-STORM “chimney” is less than 50% as effective as a classical chimney. As we explain in Subsection 4.4.1.1.9, this fact is fully recognized in the global HI-STORM thermal model implementation of FLUENT.

4.4.1.1.8 Determination of Solar Heat Input

The intensity of solar radiation incident on an exposed surface depends on a number of time varying terms. The solar heat flux strongly depends upon the time of the day as well as on latitude and day of the year. Also, the presence of clouds and other atmospheric conditions (dust, haze, etc.) can significantly attenuate solar intensity levels. Rapp [4.4.2] has discussed the influence of such factors in considerable detail.

Consistent with the guidelines in NUREG-1536 [4.4.10], solar input to the exposed surfaces of the HI-STORM overpack is determined based on 12-hour insolation levels recommended in 10CFR71 (averaged over a 24-hour period) and applied to the most adversely located cask after accounting for partial blockage of incident solar radiation on the lateral surface of the cask by surrounding casks. In reality, the lateral surfaces of the cask receive solar heat depending on the azimuthal orientation of the sun during the course of the day. In order to bound this heat input, the lateral surface of the cask is assumed to receive insolation input with the solar insolation applied horizontally into the cask array. The only reduction in the heat input to the lateral surface of the cask is due to partial blockage

offered by the surrounding casks. In contrast to its lateral surface, the top surface of HI-STORM is fully exposed to insolation without any mitigation effects of blockage from other bodies. In order to calculate the view factor between the most adversely located HI-STORM system in the array and the environment, a conservative geometric simplification is used. The system is reduced to a concentric cylinder model, with the inner cylinder representing the HI-STORM unit being analyzed and the outer shell representing a reflecting boundary (no energy absorption).

Thus, the radius of the inner cylinder (R_i) is the same as the outer radius of a HI-STORM overpack. The radius of the outer cylinder (R_o) is set such that the rectangular space ascribed to a cask is preserved. This is further explained in the next subsection. It can be shown that the view factor from the outer cylinder to the inner cylinder (F_{o-i}) is given by [4.4.3]:

$$F_{o-i} = \frac{1}{R} - \frac{1}{\pi R} \times \left[\cos^{-1}\left(\frac{B}{A}\right) - \frac{1}{2L} \left\{ \sqrt{(A+2)^2 - (2R)^2} \times \cos^{-1}\left(\frac{B}{RA}\right) + B \sin^{-1}\left(\frac{1}{R}\right) - \frac{\pi A}{2} \right\} \right]$$

where:

- F_{o-i} = View Factor from the outer cylinder to the inner cylinder
- R = Outer Cylinder Radius to Inner Cylinder Radius Ratio (R_o/R_i)
- L = Overpack Height to Radius Ratio
- $A = L^2 + R^2 - 1$
- $B = L^2 - R^2 + 1$

Applying the theorem of reciprocity, the view factor (F_{i-a}) from outer overpack surface, represented by the inner cylinder, to the ambient can be determined as:

$$F_{i-a} = 1 - F_{o-i} \frac{R_o}{R_i}$$

Finally, to bound the quantity of heat deposited onto the HI-STORM surface by insolation, the absorptivity of the cask surfaces is assumed to be unity.

4.4.1.1.9 FLUENT Model for HI-STORM

In the preceding subsections, a series of analytical and numerical models to define the thermal characteristics of the various elements of the HI-STORM System are presented. The thermal modeling begins with the replacement of the Spent Nuclear Fuel (SNF) cross section and surrounding fuel cell space with a solid region with an equivalent conductivity. Since radiation is an important constituent of the heat transfer process in the SNF/storage cell space, and the rate of radiation heat transfer is a strong function of the surface temperatures, it is necessary to treat the equivalent region conductivity as a function of temperature. Because of the relatively large range of temperatures in a loaded HI-STORM System under the design basis heat loads, the effects of variation in the thermal conductivity of the Alloy X basket wall with temperature are included in the

numerical analysis model. The presence of significant radiation effects in the storage cell spaces adds to the imperative to treat the equivalent storage cell lamina conductivity as temperature-dependent.

Numerical calculations and FLUENT finite-volume simulations have been performed to establish the equivalent thermal conductivity as a function of temperature for the limiting (thermally most resistive) BWR and PWR spent fuel types. Utilizing the most limiting SNF (established through a simplified analytical process for comparing conductivities) ensures that the numerical idealization for the fuel space effective conductivity is conservative for all non-limiting fuel types.

Having replaced the fuel spaces by solid square blocks with a temperature-dependent conductivity essentially renders the basket into a non-homogeneous three-dimensional solid where the non-homogeneity is introduced by the honeycomb basket structure composed of interlocking basket panels. The basket panels themselves are a composite of Alloy X cell wall, ~~Boral~~ neutron absorber, and Alloy X sheathing metal. A conservative approach to replace this composite section with an equivalent "solid wall" was described earlier.

In the next step, a planar section of the MPC is considered. The MPC contains a non-symmetric basket lamina wherein the equivalent fuel spaces are separated by the "equivalent" solid metal walls. The space between the basket and the MPC, called the peripheral gap, is filled with helium gas. At this stage in the thermal analysis, the SNF/basket/MPC assemblage has been replaced with a two-zone (Figure 4.4.2) cylindrical solid whose thermal conductivity is a strong function of temperature.

The fuel assembly and MPC basket effective conductivity evaluations are performed for two distinct scenarios described earlier in this section. In the first scenario, the MPC cavity is backfilled with helium only. In the second scenario, gaseous fission products from a hypothetical rupture of 10% of the stored fuel rods dilute the backfill helium gas. As previously stated, thermal analysis results for both scenarios are obtained and reported in this section.

The thermal model for the HI-STORM overpack is prepared as a three-dimensional axisymmetric body. For this purpose, the hydraulic resistances of the inlet ducts and outlet ducts, respectively, are represented by equivalent axisymmetric porous media. Two overpack configurations are evaluated – HI-STORM 100 and a shorter variation (HI-STORM 100S) overpack. HI-STORM 100S features a smaller inlet duct-to-outlet duct separation and an optional enhanced gamma shield cross plat. Since the optional gammas shield cross plate flow resistance is bounding, the optional design was conservatively evaluated in the thermal analysis. The fuel cladding temperatures for MPC emplaced in a HI-STORM 100S overpack are confirmed to be bounded by the HI-STORM 100 System thermal model solution. Thus, separate table summaries for HI-STORM 100S overpack are not provided.

The axial resistance to airflow in the MPC/overpack annulus (which includes longitudinal channels to "cushion" the stresses in the MPC structure during a postulated non-mechanistic tip-over event) is replaced by a hydraulically equivalent annulus. The surfaces of the ducts and annulus are assumed to have a relative roughness (ϵ) of 0.001. This value is appropriate for rough cast iron, wood stave and concrete pipes, and is bounding for smooth painted surfaces (all internal and external HI-STORM overpack carbon steel surfaces are painted). Finally, it is necessary to describe the external boundary conditions to the overpack situated on an ISFSI pad. An isolated HI-STORM will take suction of

cool air from and reject heated air to, a semi-infinite half-space. In a rectilinear HI-STORM array, however, the unit situated in the center of the grid is evidently hydraulically most disadvantaged, because of potential interference to air intake from surrounding casks. To simulate this condition in a conservative manner, we erect a hypothetical cylindrical barrier around the centrally local HI-STORM. The radius of this hypothetical cylinder, R_o , is computed from the equivalent cask array downflow hydraulic diameter (D_h) which is obtained as follows:

$$D_h = \frac{4 \times \text{Flow Area}}{\text{Wetted Perimeter}}$$

$$= \frac{4 \left(A_o - \frac{\pi}{4} d_o^2 \right)}{\pi d_o}$$

where:

- A_o = Minimum tributary area ascribable to one HI-STORM (see Figure 4.4.24).
- d_o = HI-STORM overpack outside diameter

The hypothetical cylinder radius, R_o , is obtained by adding half D_h to the radius of the HI-STORM overpack. In this manner, the hydraulic equivalence between the cask array and the HI-STORM overpack to hypothetical cylindrical annulus is established.

For purposes of the design basis analyses reported in this chapter, the tributary area A_o is assumed to be equal to 346 sq. ft. Sensitivity studies on the effect of the value of A_o on the thermal performance of the HI-STORM System shows that the system response is essentially insensitive to the assumed value of the tributary area. For example, a thermal calculation using $A_o = 225$ sq. ft. (corresponding to 15 ft. square pitch) and design basis heat load showed that the peak cladding temperature is less than 1°C greater than that computed using $A_o = 346$ sq. ft. Therefore, the distance between the vertically arrayed HI-STORMs in an ISFSI should be guided by the practical (rather than thermal) considerations, such as personnel access to maintain air ducts or painting the cask external surfaces.

The internal surface of the hypothetical cylinder of radius R_o surrounding the HI-STORM module is conservatively assumed to be insulated. Any thermal radiation heat transfer from the HI-STORM overpack to this insulated surface will be perfectly reflected, thereby bounding radiative blocking from neighboring casks. Then, in essence, the HI-STORM module is assumed to be confined in a large cylindrical "tank" whose wall surface boundaries are modeled as zero heat flux boundaries. The air in the "tank" is the source of "feed air" to the overpack. The air in the tank is replenished by ambient air from above the top of the HI-STORM overpacks. There are two sources of heat input to the exposed surface of the HI-STORM overpack. The most important source of heat input is the internal heat generation within the MPC. The second source of heat input is insolation, which is conservatively quantified in the manner of the preceding subsection.

The FLUENT model consisting of the axisymmetric 3-D MPC space, the overpack, and the enveloping tank is schematically illustrated in Figure 4.4.13. The HI-STORM thermosiphon-enabled solution is computed in a two-step process. In the first step, a HI-STORM overpack thermal model computes the ventilation effect from annulus heating by MPC decay heat. In this model, heat dissipation is conservatively restricted to the MPC shell (i.e., heat dissipation from MPC lid and baseplate completely neglected. This modeling assumption has the effect of overstating the MPC shell, annulus air and concrete temperatures. In the next step, the temperature of stored fuel in a pressurized helium canister (thermosiphon model) is determined using the overpack thermal solution in the first step to fashion a bounding MPC shell temperature profile for the MPC thermal model. The modeling details are provided in the Holtec benchmarking report [4.4.12].

A summary of the essential features of this model is presented in the following:

- A conservatively lower bound canister pressure of 5.7 atm is postulated for the thermosiphon modeling.
- Heat input due to insolation is applied to the top surface and the cylindrical surface of the overpack with a bounding maximum solar absorbtivity equal to 1.0.
- The heat generation in the MPC is assumed to be uniform in each *region in the* horizontal plane, but to vary in the axial direction to correspond to the axial power distribution listed in Chapter 2.
- The most disadvantageously placed cask (i.e., the one subjected to maximum radiative blockage), is modeled.
- The bottom surface of the overpack, in contact with the ISFSI pad, rejects heat through the pad to the constant temperature (77°F) earth below. For some scenarios, the bottom surface of the overpack is conservatively assumed to be adiabatic.

The finite-volume model constructed in this manner will produce an axisymmetric temperature distribution. The peak temperature will occur at the centerline and is expected to be above the axial location of peak heat generation. As will be shown in Subsection 4.4.2, the results of the finite-volume solution bear out these observations.

THIS PAGE INTENTIONALLY BLANK

To summarize, the HI-STORM 100 System is evaluated for two fuel storage scenarios. In one scenario, designated as uniform loading, every basket cell is assumed to be occupied with fuel producing heat at the maximum rate. Storage of moderate burnup and high burnup fuels are analyzed for this loading scenario. In another scenario, denoted as regionalized loading, a two-region fuel loading configuration is stipulated. The two regions are defined as an inner region (for storing hot fuel) and an outer region with low decay heat fuel physically enveloping the inner region. This scenario is depicted in Figure 4.4.25. The inner region is shown populated with fuel having a heat load of q_1 and post-core decay time (PCDT) or age τ , and the outer region with fuel of heat load q_2 and age τ_2 , where $q_1 > q_2$. For conservatism the outer region fuel permissible cladding temperature (T_2) is assumed to be that of old fuel ($\tau = 15$ years). By ensuring that the interface boundary temperature is less than or equal to T_2 ensures that fuel in the outer region is below permissible temperatures for any fuel age. To permit hot fuel storage in the inner region, a uniform low decay heat rate is stipulated for the outer region fuel. The maximum allowable heat load for inner region fuel (q_1), then, is a function of fuel age-dependent permissible temperature set forth in Table 4.3.7 and Appendix 4.A for moderate and high burnup fuels, respectively. For the regionalized loading scenario, the most restrictive of the two burnups dependent permissible temperature limits is used in the thermal evaluation. In the HI-STORM 100 System, four central locations in the MPC-24 and MPC-24E, twelve inner cells in MPC-32 and 32 in MPC-68 are designated as inner region locations in the regionalized fuel-loading scenario. Results of thermal evaluations for both scenarios are present in Subsection 4.4.2.

4.4.1.1.10 Effect of Fuel Cladding Crud Resistance

In this subsection, a conservatively bounding estimate of temperature drop across a crud film adhering to a fuel rod during dry storage conditions is determined. The evaluation is performed for a BWR fuel assembly based on an upper bound crud thickness obtained from the PNL-4835 report ([4.3.2], Table 3). The crud present on the fuel assemblies is predominately iron oxide mixed with small quantities of other metals such as cobalt, nickel, chromium, etc. Consequently, the effective conductivity of the crud mixture is expected to be in the range of typical metal alloys. Metals have thermal conductivities several orders of magnitude larger than that of helium. In the interest of extreme conservatism, however, a film of helium with the same thickness replaces the crud layer.

The calculation is performed in two steps. In the first step, a crud film resistance is determined based on a bounding maximum crud layer thickness replaced with a helium film on the fuel rod surfaces. This is followed by a peak local cladding heat flux calculation for the GE 7x7 array fuel assembly postulated to emit a conservatively bounding decay heat equal to 0.51 kW. The temperature drop across the crud film obtained as a product of the heat flux and crud resistance terms is determined to be less than 0.24°F. The calculations are presented below.

Bounding Crud Thickness(s) = 130μm (4.26x10⁻⁴ ft) (PNL-4835)
 Crud Conductivity (K) = 0.1 Btu/ft-hr-°F (conservatively assumed as helium)
 GE 7x7 Fuel Assembly:

Rod O.D. = 0.563"
 Active Fuel Length = 150"
 Heat Transfer Area = (7x7) x (πx0.563) x (150/144) = 90.3 ft²
 Axial Peaking Factor = 1.195 (Burnup distribution Table 2.1.11)
 Decay Heat = 500 1000 W (conservative assumption)

$$\text{Crud Resistance} = \frac{\delta}{K} = \frac{4.26 \times 10^{-4}}{0.1} = 4.26 \times 10^{-3} \frac{\text{ft}^2 \cdot \text{hr} \cdot ^\circ\text{F}}{\text{Btu}}$$

$$\begin{aligned} \text{Peak Heat Flux} &= \frac{(1000 \times 3.417) \text{ Btu/hr}}{90.3 \text{ ft}^2} \times 1.195 \\ &= 37.84 \times 1.195 = 45.2 \frac{\text{Btu}}{\text{ft}^2 \cdot \text{hr}} \end{aligned}$$

Temperature drop (ΔT_c) across crud film

$$\begin{aligned} &= 4.26 \times 10^{-3} \frac{\text{ft}^2 \cdot \text{hr} \cdot ^\circ\text{F}}{\text{Btu}} \times 45.2 \frac{\text{Btu}}{\text{ft}^2 \cdot \text{hr}} \\ &= 0.192^\circ\text{F} \end{aligned}$$

(i.e., less than 0.2°F)

Therefore, it is concluded that deposition of crud does not materially change the SNF cladding temperature.

4.4.1.1.11 Thermal Conductivity Calculations with Diluted Backfill Helium

In this subsection, the thermal conductivities of mixtures of the helium backfill gas and the gaseous fission products released from a hypothetical rupture of 10% of the stored fuel rods are evaluated. The gaseous fission products release fractions are stipulated in NUREG-1536. The released gases will mix with the helium backfill gas and reduce its thermal conductivity. These reduced thermal conductivities are applied to determine fuel assembly, and MPC fuel basket and basket periphery effective conductivities for thermal evaluation of the HI-STORM System.

Appendix C of NUREG/CR-0497 [4.4.7] describes a method for calculating the effective thermal conductivity of a mixture of gases. The same method is also described by Rohsenow and Hartnett

[4.2.2]. The following expression is provided by both references:

$$k_{mix} = \sum_{i=1}^n \left(\frac{k_i x_i}{x_i + \sum_{j=1}^n \varphi_{ij} x_j} \right)$$

where:

- k_{mix} = thermal conductivity of the gas mixture (Btu/hr-ft-°F)
- n = number of gases
- k_i = thermal conductivity of gas component i (Btu/hr-ft-°F)
- x_i = mole fraction of gas component i

In the preceding equation, the term φ_{ij} is given by the following:

$$\varphi_{ij} = \phi_{ij} \left[1 + 2.41 \frac{(M_i - M_j)(M_i - 0.142 \cdot M_j)}{(M_i + M_j)^2} \right]$$

where M_i and M_j are the molecular weights of gas components i and j , and ϕ_{ij} is:

$$\phi_{ij} = \frac{\left[1 + \left(\frac{k_i}{k_j} \right)^{\frac{1}{2}} \left(\frac{M_i}{M_j} \right)^{\frac{1}{4}} \right]^2}{2^{\frac{3}{2}} \left(1 + \frac{M_i}{M_j} \right)^{\frac{1}{2}}}$$

Table 4.4.7 presents a summary of the gas mixture thermal conductivity calculations for the MPC-24 and MPC-68 MPC designs containing design basis fuel assemblies.

Having calculated the gas mixture thermal conductivities, the effective thermal conductivities of the design basis fuel assemblies are calculated using the finite-volume model described in Subsection 4.4.1.1.2. Only the helium gas conductivity is changed, all other modeling assumptions are the same. The fuel assembly effective thermal conductivities with diluted helium are compared to those with undiluted helium in Table 4.4.8.

Next, the effective thermal conductivities of the MPC-24 and MPC-68 fuel basket and basket periphery regions are determined as described in Subsection 4.4.1.1.4. This calculation incorporates both the diluted helium thermal conductivity and the effective thermal conductivity of the fuel assembly with diluted helium. The MPC fuel basket and basket periphery effective thermal conductivities with diluted helium are compared to those with undiluted helium in Table 4.4.8. From

this table, it is observed that a 10% rod rupture condition has a relatively minor impact on the basket effective conductivity.

4.4.1.1.12 Effects of Hypothetical Low Fuel Rod Emissivity

The value of emissivity (ϵ) utilized in this FSAR was selected as 0.8 based on:

- i. the recommendation of an EPRI report [4.1.3]
- ii. Holtec's prior licensing experience with the HI-STAR 100 System
- iii. other vendors' cask licensing experience with the NRC
- iv. authoritative literature citations

The table below provides relevant third party information to support the emissivity value utilized in this FSAR.

Source	Reference	Zircaloy Emissivity
EPRI	[4.1.3]	0.8
TN-68 TSAR	Docket 72-1027	0.8
TN-40	Prairie Island Site Specific ISFSI	0.8
TN-32	Docket 72-1021	0.8
Todreas & Mantuefel	[4.4.8]	0.8
DOE SNF Report	[4.4.9]	0.8

The appropriateness of the selected value of ϵ is further supported by the information provided by PNL-4835 [4.3.2] and NUREG/CR-0497 [4.4.7]. PNL-4835 reports cladding oxidation thickness in U.S. Zircaloy LWR SNF assemblies (20 μm for PWR and 30 μm for BWR fuel). If these oxide thickness values are applied to the mathematical formulas presented for emissivity determination in [4.4.7], then the computed values are slightly higher than our assumed value of 0.8. It should be recognized that the formulas in [4.4.7] include a conservative assumption that depresses the value of computed emissivity, namely, absence of crud. Significant crud layers develop on fuel cladding surfaces during in-core operation. Crud, which is recognized by the above-mentioned NUREG document as having a boosting effect on ϵ , is completely neglected.

The above discussion provides a reasonable rationale for our selection of 0.8 as the value for ϵ . However, to determine the effect of a hypothetical low emissivity of 0.4, an additional thermal analysis adopting this value has been performed. In this analysis, each fuel rod of a fuel assembly is stipulated to have this uniformly low $\epsilon = 0.4$ and the effective fuel thermal conductivity is recalculated. In the next step, all cells of an MPC basket are assumed to be populated with this low ϵ

fuel that is further assumed to be emitting decay heat at design basis level. The effective conductivity of this basket populated with low ϵ fuel is recalculated. Using the recalculated fuel basket conductivity, the HI-STORM system temperature field is recomputed. This exercise is performed for the MPC-24 basket because, as explained in the next paragraph, this basket design, which accommodates a fewer number of fuel assemblies (compared to the MPC-68 and MPC-32) has a higher sensitivity to the emissivity parameter. This analysis has determined that the impact of a low ϵ assumption on the peak cladding temperature is quite small (about 5°C). It is noted that these sensitivity calculations were performed under the completely suppressed helium thermosiphon cooling assumption. Consequently, as the burden of heat dissipation shouldered by radiation heat transfer under this assumption is much greater, the resultant computed sensitivity is a conservative upper bound for the HI-STORM system.

The relatively insignificant increase in the computed peak clad temperature as a result of applying a large penalty in ϵ (50%) is consistent with the findings in a German Ph.D. dissertation [4.4.11]. Dr. Anton's study consisted of analyzing a cask containing 4 fuel assemblies with a total heat load of 17 kW and helium inside the fuel cavity. For an emissivity of 0.8, the calculated peak cladding temperature was 337°C. In a sensitivity study, wherein the emissivity was varied from 0.7 to 0.9, the temperature changed only by 5°C, i.e. to 342°C and 332°C. Dr. Anton ascribed two reasons for this low impact of emissivity on computed temperatures. Although the radiative heat emission by a surface decreases with lower emissivity, the fraction of heat reflected from other surfaces increases. In other words, the through-assembly heat dissipation by this means increases thereby providing some compensation for the reduced emission. Additionally, the fourth power of temperature dependence of thermal radiation heat transfer reduces the impact of changes in the coefficients on computed temperatures. For storage containers with larger number of fuel assemblies (like the HI-STORM System), an even smaller impact would be expected, since a larger fraction of the heat is dissipated via the basket conduction heat transfer.

4.4.1.1.13 HI-STORM Temperature Field with Low Heat Emitting Fuel

The HI-STORM 100 thermal evaluations for BWR fuel are grouped in two categories of fuel assemblies proposed for storage in the MPC-68. The two groups are classified as Low Heat Emitting (LHE) fuel assemblies and Design Basis (DB) fuel assemblies. The LHE group of fuel assemblies are characterized by low burnup, long cooling time, and short active fuel lengths. Consequently, their heat loads are dwarfed by the DB group of fuel assemblies. The Dresden-1 (6x6 and 8x8), Quad+, and Humboldt Bay (7x7 and 6x6) fuel assemblies are grouped as the LHE fuel. This fuel is evaluated when encased in Damaged Fuel Containers (DFC). As a result of interruption of radiation heat exchange between the fuel assembly and the fuel basket by the DFC boundary, this configuration is bounding for thermal evaluation. In Table 4.4.2, two canister types for encasing LHE fuel are evaluated – a Holtec design and an existing canister in which some of the Dresden-1 fuel is currently stored (Transnuclear D-1 canister). The most resistive LHE fuel assembly (Dresden- 1 8x8) is considered for thermal evaluation (see Table 4.4.2) in a DFC container. The MPC-68 basket effective conductivity, loaded with the most resistive fuel assembly (encased in a canister) is provided in Table 4.4.3. To this basket, LHE decay heat is applied and a HI-STORM 100 System thermal solution computed. The peak cladding temperature is computed as 513°F, which is substantially below the temperature limit for long cooled fuel (~635°F).

A thoria rod canister designed for holding a maximum of twenty fuel rods arrayed in a 5x4 configuration is currently stored at the Dresden-1 spent fuel pool. The fuel rods were originally constituted as part of an 8x8 fuel assembly and used in the second and third cycle of Dresden-1 operation. The maximum fuel burnup of these rods is quite low (~14,400 MWD/MTU). The thoria rod canister internal design is a honeycomb structure formed from 12-gage stainless steel plates. The rods are loaded in individual square cells. This long cooled, part assembly (18 fuel rods) and very low fuel burnup thoria rod canister renders it a miniscule source of decay heat. The canister all-metal internal honeycomb construction serves as an additional means of heat dissipation in the fuel cell space. In accordance with fuel loading stipulation in the Technical Specifications, long cooled fuel is loaded toward the basket periphery (i.e., away from the hot central core of the fuel basket). All these considerations provide ample assurance that these fuel rods will be stored in a benign thermal environment and, therefore, remain protected during long-term storage.

4.4.1.2 Test Model

A detailed analytical model for thermal design of the HI-STORM System was developed using the FLUENT CFD code and the industry standard ANSYS modeling package, as discussed in Subsection 4.4.1.1. As discussed throughout this chapter and specifically in Section 4.4.6, the analysis incorporates significant conservatism so as to compute bounding fuel cladding temperatures. Furthermore, compliance with specified limits of operation is demonstrated with adequate margins. In view of these considerations, the HI-STORM System thermal design complies with the thermal criteria set forth in the design basis (Sections 2.1 and 2.2) for long-term storage under normal conditions. Additional experimental verification of the thermal design is therefore not required.

4.4.2 Maximum Temperatures

All four MPC-basket designs developed for the HI-STORM System have been analyzed to determine temperature distributions under long-term normal storage conditions, and the results summarized in this subsection. A cross-reference of HI-STORM thermal analyses at other conditions with associated subsection of the FSAR summarizing obtained results is provided in Table 4.4.22. The MPC baskets are considered to be fully loaded with design basis PWR or BWR fuel assemblies, as appropriate. The systems are arranged in an ISFSI array and subjected to design basis normal ambient conditions with insolation.

As discussed in Subsection 4.4.1.1.1, the thermal analysis is performed using a submodeling process where the results of an analysis on an individual component are incorporated into the analysis of a larger set of components. Specifically, the submodeling process yields directly computed fuel temperatures from which fuel basket temperatures are then calculated. This modeling process differs from previous analytical approaches wherein the basket temperatures were evaluated first and then a basket-to-cladding temperature difference calculation by Wooten-Epstein or other means provided a basis for cladding temperatures. Subsection 4.4.1.1.2 describes the calculation of an effective fuel assembly thermal conductivity for an equivalent homogenous region. It is important to note that the result of this analysis is a function of thermal conductivity versus temperature. This function for fuel

thermal conductivity is then input to the fuel basket effective thermal conductivity calculation described in Subsection 4.4.1.1.4. This calculation uses a finite-element methodology, wherein each fuel cell region containing multiple finite-elements has temperature-varying thermal conductivity properties. The resultant temperature-varying fuel basket thermal conductivity computed by this basket-fuel composite model is then input to the fuel basket region of the FLUENT cask model.

Because the FLUENT cask model incorporates the results of the fuel basket submodel, which in turn incorporates the fuel assembly submodel, the peak temperature reported from the FLUENT model is the peak temperature in any component. In a dry storage cask, the hottest components are the fuel assemblies. It should be noted that, because the fuel assembly models described in Subsection 4.4.1.1.2 include the fuel pellets, the FLUENT calculated peak temperatures reported in Tables 4.4.9 and 4.4.10 are actually peak pellet centerline temperatures which bound the peak cladding temperatures, and are therefore conservatively reported as the cladding temperatures.

Applying the radiative blocking factor applicable for the worst case cask location, conservatively bounding axial temperatures at the most heated fuel cladding are shown in Figures 4.4.16 and 4.4.17 for MPC-24 and MPC-68 to depict the thermosiphon effect in PWR and BWR SNF. From these plots, the upward movement of the hot spot is quite evident. As discussed in this chapter, these calculated temperature distributions incorporate many conservatisms. The maximum fuel clad temperatures for zircaloy clad fuel assemblies are listed in Tables 4.4.9, 4.4.10, 4.4.26, and 4.4.27, which also summarize maximum calculated temperatures in different parts of the MPCs and HI-STORM overpack (Table 4.4.36).

Figures 4.4.19 and 4.4.20, respectively, depict radial temperature distribution in the PWR (MPC-24) and the BWR (MPC-68) at the horizontal plane where maximum fuel cladding temperature occurs. Finally, axial variations of the ventilation air temperatures and that of the inner shell surface are depicted in Figure 4.4.26 for a bounding heat load.

The following additional observations can be derived by inspecting the temperature field obtained from the finite volume analysis:

- The fuel cladding temperatures are in compliance with the temperature limits determined using both the DCCG methodology [4.3.5] and the PNL CSFM methodology [4.3.1].
- The maximum temperature of the basket structural material is within the stipulated design temperature.
- The maximum temperature of the ~~Boral~~ neutron absorber is below ~~the material supplier's recommended limit.~~ *design temperature limit.*
- The maximum temperatures of the MPC pressure boundary materials are well below their respective ASME Code limits.
- The maximum temperatures of concrete are within the NRC's recommended limits [4.4.10] (See Table 4.3.1.)

Noting that the permissible peak cladding temperature is a function of fuel age, parametric peak fuel cladding temperature versus total decay heat load information is computed from the FLUENT thermal model solution. The allowable fuel cladding temperature limits are presented in Section 4.3 for moderate burnup fuel and in Appendix 4.A for high-burnup fuel.

Because the peak clad temperature limits are dependent on burnup and the fuel age at the start of dry storage, the allowable decay heat load is also dependent on these parameters. Tables 4.4.20, 4.4.21, 4.4.28, and 4.4.29, for the MPC-24 and MPC-68, MPC-32 and MPC-24E, respectively, present the allowable decay heat load as a function of fuel age for moderate burnup fuel. Tables 4.4.32 through 4.4.35 present the results for high burnup fuel. Burnup and cooling-time curves, developed ~~in from~~ source-term calculations in Chapter 5 and reported in Chapter 2, are generated from the heat load limits in those tables. ~~It is noted that the burnup and cooling time curves are developed for the most limiting fuel assembly[†] of each type (PWR and BWR), but are applied to all assemblies of each type. By definition, the limiting fuel assembly emits more heat than any other assembly of its type at a given burnup and cooling time does. Thus, if the limiting fuel assembly meets the allowable clad temperature limit by a certain margin, then the other fuel assemblies of its type with equal burnup and cooling time will meet the clad temperature limit by an even greater margin. The added margin can be quite considerable. For example, the design basis PWR assembly is the B&W 15x15, which is used to determine Technical Specification limits for burnup in the HI-STORM System. For certain Westinghouse fuel types, the decay heat loads corresponding to these burnup limits will be about 15% less than that of the design basis assembly. This decay heat over prediction for other than design basis assemblies renders the predicted peak temperatures extremely conservative for those assemblies.~~

For the regionalized loading scenario as depicted in Figure 4.4.25, *certain permissible range of outer region decay heat limits are stipulated in Table 4.4.30. The inner region heat load limit will be governed by the peak cladding temperature limit for the hot fuel, provided that the interface cladding temperature limit for long cooled fuel is not exceeded. The MPC-32 and MPC-68 heat load limits are determined by analysis to be governed by this requirement. In the MPC-24 and MPC-24E regionalized loading scenarios, the interface cladding temperature limit is reached first for certain fuel cooling times. Thus, the peak cladding temperatures for these MPCs are below their permissible values by a greater margin. As explained in Sub-Section 4.4.1.1.9, the inner region heat load limits are provided in Table 4.4.31 a function of the outer region heat load and the process of determining the inner region heat load is described.*

The calculated temperatures are based on a series of analyses, described previously in this chapter, that incorporate many conservatisms. A list of the significant conservatisms is provided in Subsection 4.4.6. As such, the calculated temperatures are upper bound values that would exceed actual temperatures.

[†] The limiting fuel assembly (also referred to as the design basis assembly) is defined as that assembly which is the most heat emissive of its type (PWR or BWR) as a given burnup and cooling time.

The above observations lead us to conclude that the temperature field in the HI-STORM System with a fully loaded MPC containing design-basis heat emitting SNF complies with all regulatory and industry temperature limits. In other words, the thermal environment in the HI-STORM System will be conducive to long-term safe storage of spent nuclear fuel.

4.4.3 Minimum Temperatures

In Table 2.2.2 of this report, the minimum ambient temperature condition for the HI-STORM storage overpack and MPC is specified to be -40°F. If, conservatively, a zero decay heat load with no solar input is applied to the stored fuel assemblies, then every component of the system at steady state would be at a temperature of -40°F. All HI-STORM storage overpack and MPC materials of construction will satisfactorily perform their intended function in the storage mode at this minimum temperature condition. Structural evaluations in Chapter 3 show the acceptable performance of the overpack and MPC steel and concrete materials at low service temperatures. Criticality and shielding evaluations (Chapters 5 and 6) are unaffected by temperature.

4.4.4 Maximum Internal Pressure

The MPC is initially filled with dry helium after fuel loading and drying prior to installing the MPC closure ring. During normal storage, the gas temperature within the MPC rises to its maximum operating basis temperature as determined based on the thermal analysis methodology described earlier. The gas pressure inside the MPC will also increase with rising temperature. The pressure rise is determined based on the ideal gas law, which states that the absolute pressure of a fixed volume of gas is proportional to its absolute temperature. Tables 4.4.12, 4.4.13, 4.4.24, and 4.4.25 present summaries of the calculations performed to determine the net free volume in the MPC-24, MPC-68, MPC-32, and MPC-24E, respectively.

The MPC maximum gas pressure is considered for a postulated accidental release of fission product gases caused by fuel rod rupture. For these fuel rod rupture conditions, the amounts of each of the release gas constituents in the MPC cavity are summed and the resulting total pressures determined from the Ideal Gas Law. Based on fission gases release fractions (per NUREG 1536 criteria [4.4.10]), net free volume and initial fill gas pressure, the bounding maximum gas pressures with 1% (normal), 10% (off-normal) and 100% (accident condition) rod rupture are given in Table 4.4.14. The maximum gas pressures listed in Table 4.4.14 are all below the MPC internal design pressure listed in Table 2.2.1.

The inclusion of PWR non-fuel hardware (BPRA control elements and thimble plugs) to the PWR baskets influences the MPC internal pressure through two distinct effects. The presence of non-fuel hardware increases the effective basket conductivity, thus enhancing heat dissipation and lowering fuel temperatures as well as the temperature of the gas filling the space between fuel rods. The gas volume displaced by the mass of non-fuel hardware lowers the cavity free volume. These two effects, namely, temperature lowering and free volume reduction, have opposing influence on the MPC cavity pressure. The first effect lowers gas pressure while the second effect raises it. In the HI-STORM thermal analysis, the computed temperature field (with non-fuel hardware excluded) has been determined to provide a conservatively bounding temperature field for the PWR baskets (MPC-

SHADED TEXT INDICATES CONFIDENTIAL INFORMATION PURSUANT TO 10 CFR 2.790

24, MPC-24E, and MPC-32). The MPC cavity free space is computed based on volume displacement by the heaviest fuel (bounding weight) with non-fuel hardware included.

During in-core irradiation of BPRAs, neutron capture by the B-10 isotope in the neutron absorbing material produces helium. Two different forms of the neutron absorbing material are used in BPRAs: Borosilicate glass and B₄C in a refractory solid matrix (Al₂O₃). Borosilicate glass (primarily a constituent of Westinghouse BPRAs) is used in the shape of hollow pyrex glass tubes sealed within steel rods and supported on the inside by a thin-walled steel liner. To accommodate helium diffusion from the glass rod into the rod internal space, a relatively high void volume (~40%) is engineered in this type of rod design. The rod internal pressure is thus designed to remain below reactor operation conditions (2,300 psia and approximately 600°F coolant temperature). The B₄C- Al₂O₃ neutron absorber material is principally used in B&W and CE fuel BPRAs designs. The relatively low temperature of the poison material in BPRAs rods (relative to fuel pellets) favor the entrapment of helium atoms in the solid matrix.

Several BPRAs designs are used in PWR fuel that differ in the number, diameter, and length of poison rods. The older Westinghouse fuel (W-14x14 and W-15x15) has used 6, 12, 16, and 20 rods per assembly BPRAs and the later (W-17x17) fuel uses up to 24 rods per BPRAs. The BPRAs rods in the older fuel are much larger than the later fuel and, therefore, the B-10 isotope inventory in the 20-rod BPRAs bounds the newer W-17x17 fuel. Based on bounding BPRAs rods internal pressure, a large hypothetical quantity of helium (7.2 g-moles/BPRAs) is assumed to be available for release into the MPC cavity from each fuel assembly in the PWR baskets. The MPC cavity pressures (including helium from BPRAs) are summarized in Table 4.4.14.

4.4.5 Maximum Thermal Stresses

Thermal expansion induced mechanical stresses due to non-uniform temperature distributions are reported in Chapter 3 of this report. Table 4.4.15 provides a summary of HI-STORM System component temperature inputs for structural evaluation. Table 4.4.19 provides a summary of confinement boundary temperatures during normal storage conditions. Structural evaluation in Section 3.4.4 references these temperature results to demonstrate confinement boundary integrity.

4.4.6 Evaluation of System Performance for Normal Conditions of Storage

The HI-STORM System thermal analysis is based on a detailed and complete heat transfer model that conservatively accounts for all modes of heat transfer in various portions of the MPC and overpack. The thermal model incorporates many conservative features that render the results for long-term storage to be extremely conservative:

1. The most severe levels of environmental factors for long-term normal storage, which are an ambient temperature of 80°F and 10CFR71 insolation levels, were coincidentally imposed on the system.
2. ~~A hypothetical rupture of 10% of the stored fuel rods was conservatively considered for determining the thermal conductivity of the diluted helium backfill gas.~~

SHADED TEXT INDICATES CONFIDENTIAL INFORMATION PURSUANT TO 10 CFR 2.790

- 3.2. The most adversely located HI-STORM System in an ISFSI array was considered for analysis.
- 4.3. A conservative assessment of thermosiphon effect in the MPC, which is intrinsic to the HI-STORM fuel basket design is included in the thermal analyses.
- ~~5. Radiation heat transfer and the presence of helium within the Boral sheathing space are neglected.~~
- 6.4. No credit was considered for contact between fuel assemblies and the MPC basket wall or between the MPC basket and the basket supports. The fuel assemblies and MPC basket were conservatively considered to be in concentric alignment.
- 7.5. The MPC is assumed to be loaded with the SNF type which has the maximum equivalent thermal resistance of all fuel types in its category (BWR or PWR), as applicable.
- 8.6. The design basis maximum decay heat loads are used for all thermal-hydraulic analyses. For casks loaded with fuel assemblies having decay heat generation rates less than design basis, additional thermal margins of safety will exist. ~~This is assured by defining the burnup limits, as a function of age, for the fuel assemblies based on the bounding (i.e., most heat emissive) fuel assembly types within each class (PWR or BWR). As demonstrated in the source term calculations described Chapter 5, the B&W 15x15 and GE 7x7 are the governing PWR and BWR fuel assemblies, respectively. For all other fuel types, the heat emission rates at the design basis burnup levels will be below the design basis heat emission rate.~~
- ~~9. The interstitial space between Boral, and the Alloy X pocket in which it is contained, will be filled with helium. However, for conservatism, the conductivity of air is used instead.~~
- 10.7. The enhancement of heat transfer owing to the so-called "Rayleigh effect" in the basket/MPC interface region, which was included in the analyses underlying the original CoC on the HI-STORM 100 System, is neglected in this revision of the SAR for conservatism.
- ~~11. Aluminum heat conduction elements ignored in the thermal analyses.~~
8. *The flow resistance factors used to simulate flow through MPC 3-D continuum are conservative bounding values.*
9. *Axial heat transfer through fuel pellets is neglected.*
10. *The upflow of Helium through the MPC is assumed to be laminar (high flow resistance, low heat transfer).*
11. *Turbulation of flow at grid spacers, top & bottom fittings are neglected.*
12. *Insolation heating with a bounding absorbtivity (= 1.0).*

13. *Permissible cladding temperature used to determine design basis heat loads is less than the computed value for either high burnup or low burnup fuel of a given age (see Figure 4.B.9).*
14. *MPC is assumed to be loaded with the most thermally resistive fuel type in its category (BWR or PWR) as applicable.*

Temperature distribution results obtained from this highly conservative thermal model show that the maximum fuel cladding temperature limits are met with adequate margins. Expected margins during normal storage will be much greater due to the many conservative assumptions incorporated in the analysis. The long-term impact of decay heat induced temperature levels on the HI-STORM System structural and neutron shielding materials is considered to be negligible. The maximum local MPC basket temperature level is below the recommended limits for structural materials in terms of susceptibility to stress, corrosion and creep-induced degradation. Furthermore, stresses induced due to imposed temperature gradients are within Code limits. Therefore, it is concluded that the HI-STORM System thermal design is in compliance with 10CFR72 requirements.

Table 4.4.1

SUMMARY OF PWR FUEL ASSEMBLY EFFECTIVE
THERMAL CONDUCTIVITIES

Fuel	@ 200°F (Btu/ft-hr-°F)	@ 450°F (Btu/ft-hr-°F)	@ 700°F (Btu/ft-hr-°F)
W - 17×17 OFA	0.182	0.277	0.402
W - 17×17 Standard	0.189	0.286	0.413
W - 17×17 Vantage	0.182	0.277	0.402
W - 15×15 Standard	0.191	0.294	0.430
W - 14×14 Standard	0.182	0.284	0.424
W - 14×14 OFA	0.175	0.275	0.413
B&W - 17×17	0.191	0.289	0.416
B&W - 15×15	0.195	0.298	0.436
CE - 16×16	0.183	0.281	0.411
CE - 14×14	0.189	0.293	0.435
HN [†] - 15×15 SS	0.180	0.265	0.370
W - 14×14 SS	0.170	0.254	0.361
B&W-15x15 Mark B-11	0.187	0.289	0.424
CE-14x14 (MP2)	0.188	0.293	0.434
IP-1 (14x14) SS	0.125	0.197	0.293

†

Haddam Neck Plant B&W or Westinghouse stainless steel clad fuel assemblies.

Table 4.4.2

SUMMARY OF BWR FUEL ASSEMBLY EFFECTIVE
THERMAL CONDUCTIVITIES

Fuel	@ 200°F (Btu/ft-hr-°F)	@ 450°F (Btu/ft-hr-°F)	@ 700°F (Btu/ft-hr-°F)
Dresden 1 - 8x8 [†]	0.119	0.201	0.319
Dresden 1 - 6x6 [†]	0.126	0.215	0.345
GE - 7x7	0.171	0.286	0.449
GE - 7x7R	0.171	0.286	0.449
GE - 8x8	0.168	0.278	0.433
GE - 8x8R	0.166	0.275	0.430
GE10 - 8x8	0.168	0.280	0.437
GE11 - 9x9	0.167	0.273	0.422
AC ^{††} -10x10 SS	0.152	0.222	0.309
Exxon-10x10 SS	0.151	0.221	0.308
Damaged Dresden-1 8x8 [†] (in a Holtec damaged fuel container)	0.107	0.169	0.254
Humboldt Bay-7x7 [†]	0.127	0.215	0.343
Dresden-1 Thin Clad 6x6 [†]	0.124	0.212	0.343
Damaged Dresden-1 8x8 (in TN D-1 canister) [†]	0.107	0.168	0.252
8x8 Quad [†] Westinghouse [†]	0.164	0.276	0.435

† Cladding temperatures of low heat emitting Dresden (intact and damaged) SNF in the HI-STORM System will be bounded by design basis fuel cladding temperatures. Therefore, these fuel assembly types are excluded from the list of fuel assemblies (zircaloy clad) evaluated to determine the most resistive SNF type.

†† Allis-Chalmers stainless steel clad fuel assemblies.

Table 4.4.3

**MPC BASKET EFFECTIVE THERMAL CONDUCTIVITY RESULTS
FROM ANSYS MODELS**

Basket	@200°F (Btu/ft-hr-°F)	@450°F (Btu/ft-hr-°F)	@700°F (Btu/ft-hr-°F)
MPC-24 (Zircaloy Clad Fuel)	1.109	1.495	1.955
MPC-68 (Zircaloy Clad Fuel)	1.111	1.347	1.591
MPC-24 (Stainless Steel Clad Fuel) †	0.897	1.213	1.577(a)
MPC-68 (Stainless Steel Clad Fuel)†	1.070	1.270	1.451(b)
MPC-32 (Zircaloy Clad Fuel)	1.015	1.271	1.546
MPC-32 (Stainless Steel Clad Fuel)†	0.806	0.987	1.161 (c)
MPC-24E (Zircaloy Clad Fuel)	1.216	1.637	2.133
MPC-24E (Stainless Steel Clad fuel)†	0.991	1.351	1.766 (d)

- (a) Conductivity is 19% less than corresponding zircaloy fueled basket.
- (b) Conductivity is 9% less than corresponding zircaloy fueled basket.
- (c) Conductivity is 25% less than corresponding zircaloy fueled basket.
- (d) Conductivity is 17% less than corresponding zircaloy fueled basket.

† Evaluated in a damaged fuel canister (conservatively bounding)

Table 4.4.4

CLOSED CAVITY NUSSOLT NUMBER RESULTS
FOR HELIUM-FILLED MPC PERIPHERAL VOIDS[†]

Temperature (°F)	Nusselt Number (PWR Baskets)	Nusselt Number (BWR Basket)
200	3.17	2.41
450	2.56	1.95
700	2.21	1.68

[†] For conservatism the Rayleigh effect is ignored in the MPC thermal analyses.

Table 4.4.5

SUMMARY OF 10x10 ARRAY TYPE BWR FUEL ASSEMBLY
EFFECTIVE THERMAL CONDUCTIVITIES[†]

Fuel Assembly	@ 200°F (Btu/ft-hr-°F)	@ 450°F (Btu/ft-hr-°F)	@ 700°F (Btu/ft-hr-°F)
GE-12/14	0.166	0.269	0.412
Atrium-10	0.164	0.266	0.409
SVEA-96	0.164	0.269	0.416

[†] The conductivities reported in this table are obtained by the simplified method described in the beginning of Subsection 4.4.1.1.2.

Table 4.4.6

COMPARISON OF ARTIUM-10 BWR FUEL ASSEMBLY CONDUCTIVITY[†] WITH
THE BOUNDING^{††} BWR FUEL ASSEMBLY CONDUCTIVITY

Temperature (°F)	Atrium-10 BWR Assembly		Bounding BWR Assembly	
	(Btu/ft-hr-°F)	(W/m-K)	(Btu/ft-hr-°F)	(W/m-K)
200	0.225	0.389	0.171	0.296
450	0.345	0.597	0.271	0.469
700	0.504	0.872	0.410	0.710

[†] The reported effective conductivity has been obtained from a rigorous finite-element model.

^{††} The bounding BWR fuel assembly conductivity applied in the MPC-68 basket thermal analysis.

Table 4.4.7

SUMMARY OF THERMAL CONDUCTIVITY CALCULATIONS
FOR MPC HELIUM DILUTED BY RELEASED ROD GASES

Component Gas	Molecular Weight (g/mole)	Component Gas Mole Fractions and Mixture Conductivity (Btu/hr-ft-°F)	
		MPC-24	MPC-68
MPC Backfill Helium	4	0.951	0.962
Fuel Rod Backfill Helium	4	0.023	5.750×10^{-3}
Rod Tritium	3	1.154×10^{-5}	4.483×10^{-5}
Rod Krypton	85	2.372×10^{-3}	2.905×10^{-3}
Rod Xenon	131	0.024	0.030
Rod Iodine	129	1.019×10^{-3}	1.273×10^{-3}
Mixture of Gases (diluted helium)	N/A	0.088 at 200°F 0.116 at 450°F 0.142 at 700°F	0.086 at 200°F 0.113 at 450°F 0.139 at 700°F

SHADED TEXT INDICATES CONFIDENTIAL INFORMATION PURSUANT TO 10 CFR 2.790

Table 4.4.8

COMPARISON OF COMPONENT THERMAL CONDUCTIVITIES
WITH AND WITHOUT BACKFILL HELIUM DILUTION

	@ 200°F (Btu/hr-ft-°F)	@ 450°F (Btu/hr-ft-°F)	@ 700°F (Btu/hr-ft-°F)
GE-11 9×9 Fuel Assembly with Undiluted Helium	0.171	0.271	0.410
GE-11 9×9 Fuel Assembly with Diluted Helium	0.158	0.254	0.385
W 17×17 OFA Fuel Assembly with Undiluted Helium	0.257	0.406	0.604
W 17×17 OFA Fuel Assembly with Diluted Helium	0.213	0.347	0.537
<hr/>			
MPC-24 Fuel Basket with Undiluted Helium	1.109	1.495	1.955
MPC-24 Fuel Basket with Diluted Helium	1.047	1.425	1.883
MPC-24 Basket Periphery with Undiluted Helium	0.2050	0.3522	0.5644
MPC-24 Basket Periphery with Diluted Helium	0.1967	0.3417	0.5502
<hr/>			
MPC-68 Fuel Basket with Undiluted Helium	1.111	1.347	1.591
MPC-68 Fuel Basket with Diluted Helium	1.090	1.326	1.562
MPC-68 Basket Periphery with Undiluted Helium	0.1143	0.2020	0.3316
MPC-68 Basket Periphery with Diluted Helium	0.1090	0.1954	0.3234

SHADED TEXT INDICATES CONFIDENTIAL INFORMATION PURSUANT TO 10 CFR 2.790

Table 4.4.9

**HI-STORM[†] SYSTEM LONG-TERM NORMAL
STORAGE MAXIMUM TEMPERATURES
(MPC-24 BASKET) (Note 1)**

Component	Normal Condition Temp. (°F)	Long-Term Temperature Limit (°F)
Fuel Cladding	691	787 ^{††}
MPC Basket	650	725 ^{†††}
Basket Periphery	486	725 ^{†††}
MPC Outer Shell	344	450

Note 1:

The temperatures provided in this table are based on one thermal analysis for a uniform storage scenario. The option to store SNF in a regionalized configuration wherein the heat generation rates in Region 2 and Region 1 can vary within a wide range (See Table 4.4.30), a large number of heat generation scenarios are possible. However prescription of a maximum value for the peak cladding temperature ensures that the changes to the highest metal temperatures obtained inside an MPC are small. In as much as the corresponding temperature limits (Table 2.2.3) are considerably larger than the temperatures obtained over the entire universe of design basis SNF storage scenarios, a robust margin of safety with respect to the metal temperature limit remains.

[†] Bounding overpack temperatures are provided in Table 4.4.36.

^{††} The *tabulated* temperature limit is in accordance with DCCG (gross rupture) criteria. Permissible peak cladding temperature *used, however is based on the PNL method is (equal to 691°F (Table 4.3.7))(PNL Criteria).*

^{†††} The ASME Code allowable temperature of the fuel basket Alloy X materials is 800°F. This lower temperature limit is imposed to add additional conservatism to the analysis of the HI-STORM System.

Table 4.4.10

HI-STORM[†] SYSTEM LONG-TERM NORMAL
STORAGE MAXIMUM TEMPERATURES
(MPC-68 BASKET)(*Note 1*)

Component	Normal Condition Temp. (°F)	Long-Term Temperature Limit (°F)
Fuel Cladding	740	824 ^{††}
MPC Basket	720	725 ^{†††}
Basket Periphery	501	725 ^{†††}
MPC Outer Shell	347	450

Note 1:

The temperatures provided in this table are based on one thermal analysis for a uniform storage scenario. The option to store SNF in a regionalized configuration wherein the heat generation rates in Region 2 and Region 1 can vary within a wide range (See Table 4.4.30), a large number of heat generation scenarios are possible. However prescription of a maximum value for the peak cladding temperature ensures that the changes to the highest metal temperatures obtained inside an MPC are small. In as much as the corresponding temperature limits (Table 2.2.3) are considerably larger than the temperatures obtained over the entire universe of design basis SNF storage scenarios, a robust margin of safety with respect to the metal temperature limit remains.

† Bounding overpack temperatures are provided in Table 4.4.36.

†† The tabulated temperature limit is in accordance with DCCG (gross rupture) criteria. Permissible cladding temperature used, however is based on the PNL method is (equal to 742 740°F (Table 4.3.7)) (PNL criteria).

††† The ASME Code allowable temperature of the fuel basket Alloy X materials is 800°F. This lower temperature limit is imposed to add additional conservatism to the analysis of the HI-STORM System.

Table 4.4.11

INTENTIONALLY DELETED

Table 4.4.12

SUMMARY OF MPC-24 FREE VOLUME CALCULATIONS

Item	Volume (ft ³)
Cavity Volume	368.3
Basket Metal Volume	47.0
Bounding Fuel Assemblies Volume	78.8
Basket Supports and Fuel Spacers Volume	6.1
Aluminum Conduction Elements	5.9[‡]
Net Free Volume	230.5 (6,529 liters) 236.4 (6694 liters)

[‡] ~~Bounding 1,000 lbs weight assumed.~~

Table 4.4.13

SUMMARY OF MPC-68 FREE VOLUME CALCULATIONS

Item	Volume (ft ³)
Cavity Volume	367.3
Basket Metal Volume	45.6
Bounding Fuel Assemblies Volume	93.0
Basket Supports and Fuel Spacers Volume	11.3
Aluminum Conduction Elements	5.9 [†]
Net Free Volume	211.5 (5,989 liters) 217.4 (6156 liters)

[†] ~~Bounding 1,000 lbs weight assumed.~~

Table 4.4.14
SUMMARY OF MPC CONFINEMENT BOUNDARY PRESSURES[†]
FOR LONG-TERM STORAGE

Condition	Pressure (psig)
MPC-24:	
Initial backfill (at 70°F)	31.3 42.8
Normal condition	66.4 89.6
With 1% rods rupture	66.1 90.4
With 10% rods rupture	72.2 96.7
With 100% rods rupture	132.5 160.5
MPC-68:	
Initial backfill (at 70°F)	31.3 42.8
Normal condition	67.1 92.7
With 1% rods rupture	67.5 93.2
With 10% rods rupture	71.1 97.6
With 100% rods rupture	107.4 141.6
MPC-32:	
Initial backfill (at 70°F)	31.3 42.8
Normal Condition	65.6 89.8
With 1% rods rupture	66.5 90.8
With 10% rods rupture	75.0 99.8
With 100% rods rupture	160.1 189.4
MPC-24E:	
Initial backfill (at 70°F)	31.3 42.8
Normal Condition	65.8 89.6
With 1% rods rupture	66.4 90.4
With 10% rods rupture	72.5 96.7
With 100% rods rupture	133.5 160.5

[†] Per NUREG-1536, pressure analyses with ruptured fuel rods (including BPRA rods for PWR fuel) is performed with release of 100% of the ruptured fuel rod fill gas and 30% of the significant radioactive gaseous fission products.

Table 4.4.15

SUMMARY OF HI-STORM SYSTEM COMPONENT TEMPERATURES
FOR LONG-TERM STORAGE (°F) (Note 1)

Location	MPC-24	MPC-68	MPC-32	MPC-24E
MPC Basket Top:				
Basket periphery	485	501	496	488
MPC shell	344	348	351	346
Overpack Inner Shell	199	199	199	199
Overpack Outer Shell	124	124	124	124
MPC Basket Bottom:				
Basket periphery	281	280	290	284
MPC shell	256	258	261	258
Overpack Inner Shell	106	106	106	106
Overpack Outer Shell	107	107	107	107

Note 1:

The temperatures provided in this table are based on one thermal analysis for a uniform storage scenario. The option to store SNF in a regionalized configuration wherein the heat generation rates in Region 2 and Region 1 can vary within a wide range (See Table 4.4.30), a large number of heat generation scenarios are possible. However prescription of a maximum value for the peak cladding temperature ensures that the changes to the highest metal temperatures obtained inside an MPC are small. In as much as the corresponding temperature limits (Table 2.2.3) are considerably larger than the temperatures obtained over the entire universe of design basis SNF storage scenarios, a robust margin of safety with respect to the metal temperature limit remains.

Table 4.4.16

INTENTIONALLY DELETED

Table 4.4.17

INTENTIONALLY DELETED

Table 4.4.18

INTENTIONALLY DELETED

Table 4.4.19

**SUMMARY OF MPC CONFINEMENT BOUNDARY
TEMPERATURE DISTRIBUTIONS (Note 1)**

Location	MPC-24 (°F)	MPC-68 (°F)	MPC-32 (°F)	MPC-24E (°F)
MPC Lid Inside Surface at Centerline	463	502	487	462
MPC Lid Outside Surface at Centerline	427	454	447	425
MPC Lid Inside Surface at Periphery	371	381	383	372
MPC Lid Outside Surface at Periphery	360	375	372	358
MPC Baseplate Inside Surface at Centerline	207	209	214	209
MPC Baseplate Outside Surface at Centerline	200	203	208	202
MPC Baseplate Inside Surface at Periphery	243	246	249	245
MPC Baseplate Outside Surface at Periphery	194	196	199	195

Note 1:

The temperatures provided in this table are based on one thermal analysis for a uniform storage scenario. The option to store SNF in a regionalized configuration wherein the heat generation rates in Region 2 and Region 1 can vary within a wide range (See Table 4.4.30), a large number of heat generation scenarios are possible. However prescription of a maximum value for the peak cladding temperature ensures that the changes to the highest metal temperatures obtained inside an MPC are small. In as much as the corresponding temperature limits (Table 2.2.3) are considerably larger than the temperatures obtained over the entire universe of design basis SNF storage scenarios, a robust margin of safety with respect to the metal temperature limit remains.

SHADED TEXT INDICATES CONFIDENTIAL INFORMATION PURSUANT TO 10 CFR 2.790

Table 4.4.20

MPC-24 DESIGN-BASIS MAXIMUM HEAT LOAD†
 VERSUS FUEL AGE AT LOADING (MODERATE BURNUP)

Fuel Age At Loading (years)	Permissible Heat Load (kW)
5	27.77 37.80
6	26.96 36.60
7	24.74 33.44
10	24.23 32.70
15	23.66 31.88

† The cask heat load limits (Q_c) presented in this table pertain to loading the MPC with uniformly aged fuel assemblies emitting heat at the design basis maximum rate (q_v), where “ τ ” is the age of the fuel at the start of dry storage. For a cask loaded with a mix of fuel ages, the cask heat load limit shall be the sum of the individual assembly decay heat limits (as a function of τ) as specified in the Appendix B to COC 1014.

SHADED TEXT INDICATES CONFIDENTIAL INFORMATION PURSUANT TO 10 CFR 2.790

Table 4.4.21

MPC-68 DESIGN-BASIS MAXIMUM HEAT LOAD†
 VERSUS FUEL AGE AT LOADING (MODERATE BURNUP)

Fuel Age At Loading (years)	Permissible Heat Load (kW)
5	28.19 41.22
6	26.81 39.09
7	24.71 35.82
10	24.18 34.98
15	23.60 34.11

† The cask heat load limits (Q_t) presented in this table pertain to loading the MPC with uniformly aged fuel assemblies emitting heat at the design basis maximum rate (q_t), where “ τ ” is the age of fuel at the start of dry storage. For a cask loaded with a mix of fuel ages, the cask heat load limit shall be the sum of the individual assembly decay heat limits (as a function of fuel age) as specified in the Appendix B to COC 1014.

Table 4.4.22
MATRIX OF HI-STORM SYSTEM THERMAL EVALUATIONS

Scenario	Description	Ultimate Heat Sink	Analysis Type	Principal Input Parameters	Results in FSAR Subsection
1	Long Term Normal	Ambient	SS	N_T, Q_D, ST, SC, I_O	4.4.2
2	Off-Normal Environment	Ambient	SS(B)	O_T, Q_D, ST, SC, I_O	11.1.2
3	Extreme Environment	Ambient	SS(B)	E_T, Q_D, ST, SC, I_O	11.2.15
4	Partial Ducts Blockage	Ambient	SS(B)	$N_T, Q_D, ST, SC, I_{1/4}$	11.1.4
5	Ducts Blockage Accident	Overpack	TA	N_T, Q_D, ST, SC, I_C	11.2.13
6	Fire Accident	Overpack	TA	Q_D, F	11.2.4
7	Tip Over Accident	Overpack	AH	Q_D	11.2.3
8	Debris Burial Accident	Overpack	AH	Q_D	11.2.14

Legend:

<p>N_T - Maximum Annual Average (Normal) Temperature (80°F) O_T - Off-Normal Temperature (100°F) E_T - Extreme Hot Temperature (125°F) Q_D - Design Basis Maximum Heat Load SS - Steady State SS(B) - Bounding Steady State TA - Transient Analysis AH - Adiabatic Heating</p>	<p>I_O - All Inlet Ducts Open $I_{1/2}$ - Half of Inlet Ducts Open $I_{1/4}$ - Quarter of Inlet Ducts Open I_C - All Inlet Ducts Closed ST - Insolation Heating (Top) SC - Insolation Heating (Curved) F - Fire Heating (1475°F)</p>
---	--

Table 4.4.23

PLANT SPECIFIC BWR FUEL TYPES EFFECTIVE CONDUCTIVITY[†]

Fuel	@200°C [Btu/ft-hr-°F]	@450°F [Btu/ft-hr-°F]	@700°F [Btu/ft-hr-°F]
Oyster Creek (7x7)	0.161	0.269	0.422
Oyster Creek (8x8)	0.162	0.266	0.413
TVA Browns Ferry (8x8)	0.160	0.264	0.411
SPC-5 (9x9)	0.149	0.245	0.380
ANF 8x8	0.167	0.277	0.433
ANF-9X (9x9)	0.165	0.272	0.423

[†] The conductivities reported in this table are obtained by a simplified analytical method in Subsection 4.4.1.1.2.

Table 4.4.24

SUMMARY OF MPC-32 FREE VOLUME CALCULATIONS

Item	Volume (ft ³)
Cavity Volume	367.9
Basket Metal Volume	29.6
Bounding Free Assemblies Volume	105.0
Basket Supports and Fuel Spacers Volume	9.0
Aluminum Conduction Elements	5.9†
Net Free Volume	218.4 (6184 liters) 224.3 (6351 liters)

Table 4.4.25

SUMMARY OF MPC-24E FREE VOLUME CALCULATIONS

Item	Volume (ft ³)
Cavity Volume	368.3
Basket Metal Volume	48.3
Bounding Fuel Assemblies Volume	78.8
Basket Supports and Fuel Spacers Volume	6.1
Aluminum Conduction Elements	5.9
Net Free Volume	229.3 (6490 liters) 235.1 (6657 liters)

Table 4.4.26

**HI-STORM[†] SYSTEM LONG-TERM NORMAL STORAGE MAXIMUM
TEMPERATURES
(MPC-32 BASKET) (Note 1)**

Component	Normal Condition Temp. (°F)	Long-Term Temperature Limit (°F)
Fuel Cladding	691	787 ^{††}
MPC Basket	660	725 ^{†††}
Basket Periphery	496	725 ^{†††}
MPC Outer Shell	351	450

Note 1:

The temperatures provided in this table are based on one thermal analysis for a uniform storage scenario. The option to store SNF in a regionalized configuration wherein the heat generation rates in Region 2 and Region 1 can vary within a wide range (See Table 4.4.30), a large number of heat generation scenarios are possible. However prescription of a maximum value for the peak cladding temperature ensures that the changes to the highest metal temperatures obtained inside an MPC are small. In as much as the corresponding temperature limits (Table 2.2.3) are considerably larger than the temperatures obtained over the entire universe of design basis SNF storage scenarios, a robust margin of safety with respect to the metal temperature limit remains.

[†] Bounding overpack temperatures are provided in Table 4.4.36.

^{††} The *tabulated* temperature limit is in accordance with DCCG (gross rupture) criteria. Permissible peak cladding temperature used, however is based on the PNL method is- (equal to 691°F (Table 4.3.7)) PNL Criteria).

^{†††} The ASME Code allowable temperature of the fuel basket Alloy X materials is 800°F. This lower temperature limit is imposed to add additional conservatism in the analysis of the HI-STORM Systems.

Table 4.4.27

HI-STORM† SYSTEM LONG-TERM NORMAL STORAGE MAXIMUM
TEMPERATURES
(MPC-24E BASKET) (Note 1)

Component	Normal Condition Temp. (°F)	Long-Term Temperature Limit (°F)
Fuel Cladding	691	787 ^{††}
MPC Basket	650	725 ^{†††}
Basket Periphery	492	725 ^{†††}
MPC Outer Shell	347	450

Note 1:

The temperatures provided in this table are based on one thermal analysis for a uniform storage scenario. The option to store SNF in a regionalized configuration wherein the heat generation rates in Region 2 and Region 1 can vary within a wide range (See Table 4.4.30), a large number of heat generation scenarios are possible. However prescription of a maximum value for the peak cladding temperature ensures that the changes to the highest metal temperatures obtained inside an MPC are small. In as much as the corresponding temperature limits (Table 2.2.3) are considerably larger than the temperatures obtained over the entire universe of design basis SNF storage scenarios, a robust margin of safety with respect to the metal temperature limit remains.

† Bounding overpack temperatures are provided in Table 4.4.36.

†† The tabulated temperature limit is in accordance with DCCG (gross rupture) criteria. Permissible peak cladding temperature used, however is based on the PNL method is (equal to 691°F (Table 4.3.7)) (PNL Criteria).

††† The ASME Code allowable temperature of the fuel basket Alloy X materials is 800°F. This lower temperature limit is imposed to add additional conservatism to the analysis of the HI-STORM System.

Table 4.4.28

MPC-32 DESIGN BASIS MAXIMUM HEAT LOAD[†] VERSUS FUEL AGE AT
LOADING
(MODERATE BURNUP)

Fuel Age at Loading (years)	Permissible Heat Load (kW)
5	28.74 38.90
6	27.95 37.73
7	25.79 34.54
10	25.26 33.81
15	24.68 32.99

† The cask heat load limits (Q_c) presented in this table pertain to loading the MPC with uniformly aged fuel assemblies emitting heat at the design basis maximum rate (q_v) where “ τ ” is the age of fuel at the start of dry storage. For a cask loaded with a mix of fuel ages, the cask heat load limit shall be the sum of the individual assembly decay heat limits (as a function of fuel age) as specified in the Appendix B to CoC 1014.

Table 4.4.29

MPC-24E DESIGN BASIS MAXIMUM HEAT LOAD[†] VERSUS FUEL AGE AT
LOADING
(MODERATE BURNUP)

Fuel Age at Loading (years)	Permissible Heat Load (kW)
5	28.17 37.79
6	27.33 36.61
7	25.05 33.47
10	24.53 32.73
15	23.95 31.92

[†] The cask heat load limits (Q_c) presented in this table pertain to loading the MPC with uniformly aged fuel assemblies emitting heat at the design basis maximum rate (q_c), where “ τ ” is the age of fuel at the start of dry storage. For a cask loaded with a mix of fuel ages, the cask heat load limit shall be the sum of the individual assembly decay heat limits (as a function of fuel age) as specified in the Appendix B to the COC 1014.

Table 4.4.30

REGIONALIZED LOADING OUTER REGION HEAT LOAD LIMITS

MPC Type	Inner Region Assemblies	Outer Region Assemblies	<i>Range of Permissible Outer Region Heat Load Limit (kW)</i>
MPC-24	4	20	18 – 26
MPC-24E	4	20	18 – 26
MPC-32	12	20	12 – 20
MPC-68	32	36	9.9 – 18

Table 4.4.31
 [INTENTIONALLY DELETED]

~~REGIONALIZED LOADING INNER REGION HEAT LOAD LIMITS (kW)~~

Fuel Age (years)	MPC-24	MPC-24E	MPC-32	MPC-68
5	5.88 [†]	6.16 [†]	13.58	16.02
6	5.88 [†]	6.16 [†]	12.87	14.99
7	5.34	5.58	11.92	13.40
10	4.94	5.16	11.40	12.99
15	4.66	4.86	11.02	12.54

[†] Inner region heat load governed by interface cladding temperature limit.

Table 4.4.32

MPC-24 DESIGN BASIS MAXIMUM HEAT LOAD† VERSUS FUEL AGE
AT LOADING (HIGH BURNUP)

Fuel Age at Loading (yrs)	Permissible Heat Load (kW)
5	27.12 36.84
6	26.09 35.32
7	24.74 33.44
10	24.02 32.40
15	23.50 31.65

† The cask heat load limits (Q_c) presented in this table pertain to loading the MPC with uniformly aged fuel assemblies emitting heat at the design basis maximum rate (q_c), where “ τ ” is the age of fuel at the start of dry storage. For a cask loaded with a mix of fuel ages, the cask heat load limit shall be the sum of the individual assembly decay heat limits (as a function of fuel age) as specified in the Appendix B to the COC 1014.

Table 4.4.33

MPC-24E DESIGN BASIS MAXIMUM HEAT LOAD†
VERSUS FUEL AGE AT LOADING (HIGH BURNUP)

Fuel Age at Loading (yrs)	Permissible Heat Load (kW)
5	27.50 36.84
6	26.44 35.34
7	25.05 33.47
10	24.31 32.44
15	23.79 31.70

† The cask heat load limits (Q_c) presented in this table pertain to loading the MPC with uniformly aged fuel assemblies emitting heat at the design basis maximum rate (q_c), where “ τ ” is the age of fuel at the start of dry storage. For a cask loaded with a mix of fuel ages, the cask heat load limit shall be the sum of the individual assembly decay heat limits (as a function of fuel age) as specified in the Appendix B to the COC 1014.

Table 4.4.34

MPC-32 DESIGN BASIS MAXIMUM HEAT LOAD†
 VERSUS FUEL AGE AT LOADING (HIGH BURNUP)

Fuel Age at Loading (yrs)	Permissible Heat Load (kW)
5	28.10 37.96
6	27.10 36.47
7	25.79 34.54
10	25.05 33.51
15	24.53 32.77

† The cask heat load limits (Q_c) presented in this table pertain to loading the MPC with uniformly aged fuel assemblies emitting heat at the design basis maximum rate (q_τ), where “ τ ” is the age of fuel at the start of dry storage. For a cask loaded with a mix of fuel ages, the cask heat load limit shall be the sum of the individual assembly decay heat limits (as a function of fuel age) as specified in the Appendix B to the COC 1014.

Table 4.4.35

MPC-68 DESIGN BASIS MAXIMUM HEAT LOAD†
 VERSUS FUEL AGE AT LOADING (HIGH BURNUP)

Fuel Age at Loading (yrs)	Permissible Heat Load (kW)
5	28.19 41.22
6	26.81 39.09
7	24.71 35.82
10	24.18 34.98
15	23.60 34.11

† The cask heat load limits (Q_{τ}) presented in this table pertain to loading the MPC with uniformly aged fuel assemblies emitting heat at the design basis maximum rate (q_{τ}), where “ τ ” is the age of fuel at the start of dry storage. For a cask loaded with a mix of fuel ages, the cask heat load limit shall be the sum of the individual assembly decay heat limits (as a function of fuel age) as specified in the Appendix B to the COC 1014.

Table 4.4.36

BOUNDING LONG-TERM NORMAL STORAGE
HI-STORM OVERPACK TEMPERATURES

Component/Item†	Local Section Temperature†† (°F)	Long-Term Temperature Limit (°F)
Inner shell (<i>Carbon Steel</i>)	199 240	350
Outer shell (<i>Carbon Steel</i>)	145 159	350
Lid bottom plate (<i>Carbon Steel</i>)	339 374	350 400
Lid top plate (<i>Carbon Steel</i>)	196 214	350
MPC pedestal plate (<i>Carbon Steel</i>)	208 253	350
Baseplate (<i>Carbon Steel</i>)	111 123	350
Radial shield (<i>Concrete</i>)	172 180	200
Air outlet†††	206 241	

† See Figure 1.2.8 for a description of HI-STORM overpack components.

†† Section temperature is defined as the through-thickness average temperature.

††† Reported herein for the option of temperature measurement surveillance of the inlet-to-outlet ducts air temperature rise (equal to $241^{\circ}\text{F} - 80^{\circ}\text{F} = 161^{\circ}\text{F}$) as set forth in the Technical Specifications.

4.5 THERMAL EVALUATION FOR NORMAL HANDLING AND ONSITE TRANSPORT

Prior to placement in a HI-STORM overpack, an MPC must be loaded with fuel, outfitted with closures, dewatered, ~~vacuum~~-dried, backfilled with helium and transported to the HI-STORM module. In the unlikely event that the fuel needs to be returned to the spent fuel pool, these steps must be performed in reverse. Finally, if required, transfer of a loaded MPC between HI-STORM overpacks or between a HI-STAR transport overpack and a HI-STORM storage overpack must be carried out in an assuredly safe manner. All of the above operations are short duration events that would likely occur no more than once or twice for an individual MPC.

The device central to all of the above operations is the HI-TRAC transfer cask that, as stated in Chapter 1, is available in two anatomically identical weight ratings (100- and 125-ton). The HI-TRAC transfer cask is a short-term host for the MPC; therefore it is necessary to establish that, during all thermally challenging operation events involving either the 100-ton or 125-ton HI-TRAC, the permissible temperature limits presented in Section 4.3 are not exceeded. The following discrete thermal scenarios, all of short duration, involving the HI-TRAC transfer cask have been identified as warranting thermal analysis.

- i. Normal Onsite Transport
- ii. MPC Cavity Vacuum Drying
- iii. Post-Loading Wet Transfer Operations
- iv. MPC Cooldown and Reflood for Unloading Operations

The above listed conditions are described and evaluated in the following subsections. Subsection 4.5.1 describes the individual analytical models used to evaluate these conditions. Due to the simplicity of the conservative evaluation of wet transfer operations, Subsection 4.5.1.1.5 includes both the analysis model and analysis results discussions. The maximum temperature analyses for onsite transport and vacuum drying are discussed in Subsection 4.5.2. Subsections 4.5.3, 4.5.4 and 4.5.5, respectively, discuss minimum temperature, MPC maximum internal pressure and thermal data for stress analyses during onsite transport.

4.5.1 Thermal Model

The HI-TRAC transfer cask is used to load and unload the HI-STORM concrete storage overpack, including onsite transport of the MPCs from the loading facility to an ISFSI pad. Section views of the HI-TRAC have been presented in Chapter 1. Within a loaded HI-TRAC, heat generated in the MPC is transported from the contained fuel assemblies to the MPC shell in the manner described in Section 4.4. From the outer surface of the MPC to the ambient air, heat is transported by a combination of conduction, thermal radiation and natural convection. It has been demonstrated in Section 4.3 that from a thermal standpoint, storage of stainless steel clad fuel assemblies is bounded by storage of zircaloy clad fuel assemblies. Thus, only zircaloy clad fuel assemblies shall be considered in the HI-TRAC thermal performance evaluations. Analytical modeling details of all the various thermal transport mechanisms are provided in the following subsection.

Two HI-TRAC transfer cask designs, namely, the 125-ton and the 100-ton versions, are developed for onsite handling and transport, as discussed in Chapter 1. The two designs are principally different in terms of lead thickness and the thickness of radial connectors in the water jacket region. The analytical model developed for HI-TRAC thermal characterization conservatively accounts for these differences by applying the higher shell thickness and thinner radial connectors' thickness to the model. In this manner, the HI-TRAC overpack resistance to heat transfer is overestimated, resulting in higher predicted MPC internals and fuel cladding temperature levels.

4.5.1.1 Analytical Model

From the outer surface of the MPC to the ambient atmosphere, heat is transported within HI-TRAC through multiple concentric layers of air, steel and shielding materials. Heat must be transported across a total of six concentric layers, representing the air gap, the HI-TRAC inner shell, the lead shielding, the HI-TRAC outer shell, the water jacket and the enclosure shell. From the surface of the enclosure shell heat is rejected to the atmosphere by natural convection and radiation.

A small diametral air gap exists between the outer surface of the MPC and the inner surface of the HI-TRAC overpack. Heat is transported across this gap by the parallel mechanisms of conduction and thermal radiation. Assuming that the MPC is centered and does not contact the transfer overpack walls conservatively minimizes heat transport across this gap. Additionally, thermal expansion that would minimize the gap is conservatively neglected. Heat is transported through the cylindrical wall of the HI-TRAC transfer overpack by conduction through successive layers of steel, lead and steel. A water jacket, which provides neutron shielding for the HI-TRAC overpack, surrounds the cylindrical steel wall. The water jacket is composed of carbon steel channels with welded, connecting enclosure plates. Conduction heat transfer occurs through both the water cavities and the channels. While the water jacket channels are sufficiently large for natural convection loops to form, this mechanism is conservatively neglected. Heat is passively rejected to the ambient from the outer surface of the HI-TRAC transfer overpack by natural convection and thermal radiation.

In the vertical position, the bottom face of the HI-TRAC is in contact with a supporting surface. This face is conservatively modeled as an insulated surface. Because the HI-TRAC is not used for long-term storage in an array, radiative blocking does not need to be considered. The HI-TRAC top lid is modeled as a surface with convection, radiative heat exchange with air and a constant maximum incident solar heat flux load. Insolation on cylindrical surfaces is conservatively based on 12-hour levels prescribed in 10CFR71 averaged on a 24-hour basis. Concise descriptions of these models are given below.

4.5.1.1.1 Effective Thermal Conductivity of Water Jacket

The 125-ton HI-TRAC water jacket is composed of fourteen formed channels equispaced along the circumference of the HI-TRAC and welded along their length to the HI-TRAC outer shell. Enclosure plates are welded to these channels, creating twenty-eight water compartments. The 100-ton HI-TRAC water jacket has 15 formed channels and enclosure plates creating thirty compartments. Holes in the channel legs connect all the individual compartments in the water jacket. Thus, the annular region between the HI-TRAC outer shell and the enclosure shell can be considered as an array of steel ribs and water spaces.

The effective radial thermal conductivity of this array of steel ribs and water spaces is determined by combining the heat transfer resistance of individual components in a parallel network. A bounding calculation is assured by using the minimum number of channels and channel thickness as input values. The thermal conductivity of the parallel steel ribs and water spaces is given by the following formula:

$$K_{ne} = \frac{K_r N_r t_r \ln\left(\frac{r_o}{r_i}\right)}{2\pi L_R} + \frac{K_w N_r t_w \ln\left(\frac{r_o}{r_i}\right)}{2\pi L_R}$$

where:

K_{ne} = effective radial thermal conductivity of water jacket

r_i = inner radius of water spaces

r_o = outer radius of water spaces

K_r = thermal conductivity of carbon steel ribs

N_r = minimum number of channel legs (equal to number of water spaces)

t_r = minimum (nominal) rib thickness (lower of 125-ton and 100-ton designs)

L_R = effective radial heat transport length through water spaces

K_w = thermal conductivity of water

t_w = water space width (between two carbon steel ribs)

Figure 4.5.1 depicts the resistance network to combine the resistances to determine an effective conductivity of the water jacket. The effective thermal conductivity is computed in the manner of the foregoing, and is provided in Table 4.5.1.

4.5.1.1.2 Heat Rejection from Overpack Exterior Surfaces

The following relationship for the surface heat flux from the outer surface of an isolated cask to the environment applied to the thermal model:

$$q_s = 0.19 (T_s - T_A)^{4/3} + 0.1714\epsilon \left[\left(\frac{T_s + 460}{100} \right)^4 - \left(\frac{T_A + 460}{100} \right)^4 \right]$$

where:

T_S = cask surface temperatures ($^{\circ}\text{F}$)

T_A = ambient atmospheric temperature ($^{\circ}\text{F}$)

q_s = surface heat flux ($\text{Btu}/\text{ft}^2 \times \text{hr}$)

ϵ = surface emissivity

The second term in this equation is the Stefan-Boltzmann formula for thermal radiation from an exposed surface to ambient. The first term is the natural convection heat transfer correlation recommended by Jacob and Hawkins [4.2.9]. This correlation is appropriate for turbulent natural convection from vertical surfaces, such as the vertical overpack wall. Although the ambient air is conservatively assumed to be quiescent, the natural convection is nevertheless turbulent.

Turbulent natural convection correlations are suitable for use when the product of the Grashof and Prandtl ($Gr \times Pr$) numbers exceeds 10^9 . This product can be expressed as $L^3 \times \Delta T \times Z$, where L is the characteristic length, ΔT is the surface-to-ambient temperature difference, and Z is a function of the surface temperature. The characteristic length of a vertically oriented HI-TRAC is its height of approximately 17 feet. The value of Z , conservatively taken at a surface temperature of 340°F , is 2.6×10^5 . Solving for the value of ΔT that satisfies the equivalence $L^3 \times \Delta T \times Z = 10^9$ yields $\Delta T = 0.78^{\circ}\text{F}$. For a horizontally oriented HI-TRAC the characteristic length is the diameter of approximately 7.6 feet (minimum of 100- and 125-ton designs), yielding $\Delta T = 8.76^{\circ}\text{F}$. The natural convection will be turbulent, therefore, provided the surface to air temperature difference is greater than or equal to 0.78°F for a vertical orientation and 8.76°F for a horizontal orientation.

4.5.1.1.3 Determination of Solar Heat Input

As discussed in Section 4.4.1.1.8, the intensity of solar radiation incident on an exposed surface depends on a number of time varying terms. A twelve-hour averaged insolation level is prescribed in 10CFR71 for curved surfaces. The HI-TRAC cask, however, possesses a considerable thermal inertia. This large thermal inertia precludes the HI-TRAC from reaching a steady-state thermal condition during a twelve-hour period. Thus, it is considered appropriate to use the 24-hour averaged insolation level.

4.5.1.1.4 MPC Temperatures During Moisture Removal Operations

4.5.1.1.4.1 Vacuum Drying

The initial loading of SNF in the MPC requires that the water within the MPC be drained and replaced with helium. For MPCs containing moderate burnup fuel assemblies only, this operation may be carried out using the conventional vacuum drying approach. In this method, removal of the last traces of residual moisture from the MPC cavity is accomplished by evacuating the MPC for a short time after draining the MPC. As stipulated in the Technical Specifications, vacuum drying may not be performed on MPCs containing high burnup fuel assemblies. High burnup fuel drying is

performed by a forced flow helium drying process as described in Section 4.5.1.1.4.2 and Appendix 2.B.

Prior to the start of the MPC draining operation, both the HI-TRAC annulus and the MPC are full of water. The presence of water in the MPC ensures that the fuel cladding temperatures are lower than design basis limits by large margins. As the heat generating active fuel length is uncovered during the draining operation, the fuel and basket mass will undergo a gradual heat up from the initially cold conditions when the heated surfaces were submerged under water.

The vacuum condition effective fuel assembly conductivity is determined by procedures discussed earlier (Subsection 4.4.1.1.2) *with due recognition of the attenuation of thermosiphon effect with the decrease in the quantity of helium and reduction in the conductivity of helium at extremely low gas pressures. after setting the thermal conductivity of the gaseous medium to a small fraction (one part in one thousand) of helium conductivity.* The MPC basket cross sectional effective conductivity is determined for vacuum conditions according to the procedure discussed in 4.4.1.1.4. Basket periphery-to-MPC shell heat transfer occurs through conduction and radiation.

~~As described in Chapter 8 (Operating Procedures) vacuum drying of the MPC is performed with the annular gap between the MPC and the HI-TRAC continuously flushed with water. The water movement in this annular gap will maintain the MPC shell temperature at about the temperature of flowing water. Thus, the thermal analysis of the MPC during vacuum drying is performed with cooling of the MPC shell with water at a bounding maximum temperature of 125°F.~~

To ensure safe fuel temperatures within the MPC during the drying operation, a graded approach towards annulus heat removal requirements based on MPC heat duty is proposed. For those canisters having a very low heat duty (10 kW or less), presence of water in the HI-TRAC annulus is optional. Canisters with a low heat duty (greater than 10 kW and less than or equal to 22 kW), the HI-TRAC annulus must be filled with water. For medium heat load canisters (greater than 22 kW and less than or equal to 29 kW), vacuum drying is performed with the annulus gap continuously flushed with water at a rate sufficient to ensure that the mean water temperature is below 125°F. For high MPC heat loads (greater than 29 kW), a forced helium dehydration system is employed (See Sub-Section 4.5.1.1.4.2). The MPC cooling requirements stipulated herein for fuel drying are summarized in Table 4.5.10.

An axisymmetric FLUENT thermal model of the MPC is constructed, employing the MPC in-plane conductivity as an isotropic fuel basket conductivity (i.e. conductivity in the the basket radial and axial directions is equal), to determine peak cladding temperature at ~~design basis heat an upperbound vacuum condition heat load of 29 kw loads.~~ To avoid excessive conservatism in the computed FLUENT solution, partial recognition for higher axial heat dissipation is adopted in the peak cladding calculations. The boundary conditions applied to this evaluation are:

- i. A bounding steady-state analysis is performed with the MPC decay heat load set equal to the largest design-basis decay heat load.

- ii. The entire outer surface of the MPC shell is postulated to be at a bounding maximum temperature of 125°F
- iii. The top and bottom surfaces of the MPC are adiabatic.

Results of vacuum condition analyses are provided in Subsection 4.5.2.2.

4.5.1.1.4.2 Forced Helium Recirculation

To reduce moisture to trace levels in the MPC using a Forced Helium Dehydration (FHD) system, a conventional, closed loop dehumidification system consisting of a condenser, a demister, a compressor, and a pre-heater is utilized to extract moisture from the MPC cavity through repeated displacement of its contained helium, accompanied by vigorous flow turbulence. A vapor pressure of 3 torr or less is assured by verifying that the helium temperature exiting the demister is maintained at or below the psychrometric threshold of 21°F for a minimum of 30 minutes. See Appendix 2.B for detailed discussion of the design criteria and operation of the FHD system.

The FHD system provides concurrent fuel cooling during the moisture removal process through forced convective heat transfer. The attendant forced convection-aided heat transfer occurring during operation of the FHD system ensures that the fuel cladding temperature will remain below the applicable peak cladding temperature limit for normal conditions of storage, which is well below the high burnup cladding temperature limit 752°F (400°C) for all combinations of SNF type, burnup, decay heat, and cooling time. Because the FHD operation induces a state of forced convection heat transfer in the MPC, (in contrast to the quiescent mode of natural convection in long term storage), it is readily concluded that the peak fuel cladding temperature under the latter condition will be greater than that during the FHD operation phase. In the event that the FHD system malfunctions, the forced convection state will degenerate to natural convection, which corresponds to the conditions of normal storage. As a result, the peak fuel cladding temperatures will approximate the values reached during normal storage as described elsewhere in this chapter.

4.5.1.1.5 Maximum Time Limit During Wet Transfer Operations

In accordance with NUREG-1536, water inside the MPC cavity during wet transfer operations is not permitted to boil. Consequently, uncontrolled pressures in the de-watering, purging, and recharging system that may result from two-phase conditions are completely avoided. This requirement is accomplished by imposing a limit on the maximum allowable time duration for fuel to be submerged in water after a loaded HI-TRAC cask is removed from the pool and prior to the start of vacuum drying operations.

When the HI-TRAC transfer cask and the loaded MPC under water-flooded conditions are removed from the pool, the combined water, fuel mass, MPC, and HI-TRAC metal will absorb the decay heat emitted by the fuel assemblies. This results in a slow temperature rise of the entire system with time, starting from an initial temperature of the contents. The rate of temperature rise is limited by the

thermal inertia of the HI-TRAC system. To enable a bounding heat-up rate determination for the HI-TRAC system, the following conservative assumptions are imposed:

- i. Heat loss by natural convection and radiation from the exposed HI-TRAC surfaces to the pool building ambient air is neglected (i.e., an adiabatic temperature rise calculation is performed).
- ii. Design-basis maximum decay heat input from the loaded fuel assemblies is imposed on the HI-TRAC transfer cask.
- iii. The smaller of the two (i.e., 100-ton and 125-ton) HI-TRAC transfer cask designs is credited in the analysis. The 100-ton design has a significantly smaller quantity of metal mass, which will result in a higher rate of temperature rise.
- iv. The smallest of the minimum MPC cavity-free volumes among the two MPC types is considered for flooded water mass determination.
- v. Only fifty percent of the water mass in the MPC cavity is credited towards water thermal inertia evaluation.

Table 4.5.5 summarizes the weights and thermal inertias of several components in the loaded HI-TRAC transfer cask. The rate of temperature rise of the HI-TRAC transfer cask and contents during an adiabatic heat-up is governed by the following equation:

$$\frac{dT}{dt} = \frac{Q}{C_h}$$

where:

- Q = decay heat load (Btu/hr) [Design Basis maximum ~~28.74~~ 41.22 kW = 98,205
1.408*10⁵ Btu/hr]
- C_h = combined thermal inertia of the loaded HI-TRAC transfer cask (Btu/°F)
- T = temperature of the contents (°F)
- t = time after HI-TRAC transfer cask is removed from the pool (hr)

A bounding heat-up rate for the HI-TRAC transfer cask contents is determined to be equal to ~~3.77~~
5.41 °F/hr. From this adiabatic rate of temperature rise estimate, the maximum allowable time duration (t_{max}) for fuel to be submerged in water is determined as follows:

$$t_{\max} = \frac{T_{\text{boil}} - T_{\text{initial}}}{(dT/dt)}$$

where:

- T_{boil} = boiling temperature of water (equal to 212°F at the water surface in the MPC cavity)

$T_{initial}$ = initial temperature of the HI-TRAC contents when the transfer cask is removed from the pool

Table 4.5.6 provides a summary of t_{max} at several representative HI-TRAC contents starting temperature.

As set forth in the HI-STORM operating procedures, in the unlikely event that the maximum allowable time provided in Table 4.5.6 is found to be insufficient to complete all wet transfer operations, a forced water circulation shall be initiated and maintained to remove the decay heat from the MPC cavity. In this case, relatively cooler water will enter via the MPC lid drain port connection and heated water will exit from the vent port. The minimum water flow rate required to maintain the MPC cavity water temperature below boiling with an adequate subcooling margin is determined as follows:

$$M_w = \frac{Q}{C_{pw} (T_{max} - T_{in})}$$

where:

- M_w = minimum water flow rate (lb/hr)
- C_{pw} = water heat capacity (Btu/lb-°F)
- T_{max} = maximum MPC cavity water mass temperature
- T_{in} = temperature of pool water supply to MPC

With the MPC cavity water temperature limited to 150°F, MPC inlet water maximum temperature equal to 125°F and at the design basis maximum heat load, the water flow rate is determined to be 3928 5632 lb/hr (7.9-11.2 gpm).

4.5.1.1.6 Cask Cooldown and Reflood Analysis During Fuel Unloading Operation

NUREG-1536 requires an evaluation of cask cooldown and reflood procedures to support fuel unloading from a dry condition. Past industry experience generally supports cooldown of cask internals and fuel from hot storage conditions by direct water quenching. The extremely rapid cooldown rates to which the hot MPC internals and the fuel cladding are subjected during water injection may, however, result in uncontrolled thermal stresses and failure in the structural members. Moreover, water injection results in large amounts of steam generation and unpredictable transient two-phase flow conditions inside the MPC cavity, which may result in overpressurization of the confinement boundary. To avoid potential safety concerns related to rapid cask cooldown by direct water quenching, the HI-STORM MPCs will be cooled in a gradual manner, thereby eliminating thermal shock loads on the MPC internals and fuel cladding.

In the unlikely event that a HI-STORM storage system is required to be unloaded, the MPC will be transported on-site via the HI-TRAC transfer cask back to the fuel handling building. Prior to

reflooding the MPC cavity with water[†], a forced flow helium recirculation system with adequate flow capacity shall be operated to remove the decay heat and initiate a slow cask cooldown lasting for several days. The operating procedures in Chapter 8 (Section 8.3) provide a detailed description of the steps involved in the cask unloading. An analytical method that provides a basis for determining the required helium flow rate as a function of the desired cooldown time is presented below, to meet the objective of eliminating thermal shock when the MPC cavity is eventually flooded with water.

Under a closed-loop forced helium circulation condition, the helium gas is cooled, via an external chiller, down to 100°F. The chilled helium is then introduced into the MPC cavity, near the MPC baseplate, through the drain line. The helium gas enters the MPC basket from the bottom oversized flow holes and moves upward through the hot fuel assemblies, removing heat and cooling the MPC internals. The heated helium gas exits from the top of the basket and collects in the top plenum, from where it is expelled through the MPC lid vent connection to the helium recirculation and cooling system. The MPC contents bulk average temperature reduction as a function of time is principally dependent upon the rate of helium circulation. The temperature transient is governed by the following heat balance equation:

$$C_h \frac{dT}{dt} = Q_D - m C_p (T - T_i) - Q_c$$

Initial Condition: $T = T_o$ at $t = 0$

where:

- T = MPC bulk average temperature (°F)
- T_o = initial MPC bulk average temperature in the HI-TRAC transfer cask
(equal to 586 670°F)
- t = time after start of forced circulation (*hrs*)
- Q_D = decay heat load (Btu/hr)
(equal to Design Basis maximum 28.74 41.22 kW (i.e., 98,2051.408*10⁵ Btu/hr)
- m = helium circulation rate (lb/hr)
- C_p = helium heat capacity (Btu/lb-°F)
(equal to 1.24 Btu/lb-°F)
- Q_c = heat rejection from cask exposed surfaces to ambient (Btu/hr) (conservatively neglected)
- C_h = thermal capacity of the loaded MPC (Btu/°F)
(For a bounding upper bound 100,000 lb loaded MPC weight and heat capacity of Alloy X equal to 0.12 Btu/lb-°F, the heat capacity is equal to 12,000 Btu/°F.)
- T_i = MPC helium inlet temperature (°F)

[†] Prior to helium circulation, the HI-TRAC annulus is flooded with water to substantially lower the MPC shell temperature (approximately 100°F). For low decay heat MPCs (~10 kW or less) the annulus cooling is adequate to lower the MPC cavity temperature below the boiling temperature of water.

The differential equation is analytically solved, yielding the following expression for time-dependent MPC bulk temperature:

$$T(t) = \left(T_i + \frac{Q_D}{m C_p}\right) \left(1 - e^{-\frac{m C_p}{C_h} t}\right) + T_o e^{-\frac{m C_p}{C_h} t}$$

This equation is used to determine the minimum helium mass flow rate that would cool the MPC cavity down from initially hot conditions to less than 200°F (i.e., with a subcooling margin for normal boiling temperature of water† (212°F)). For example, to cool the MPC to less than 200°F in 72 hours using 0°F helium would require a helium mass flow rate of 432 586 lb/hr (i.e., 647-878 SCFM).

Once the helium gas circulation has cooled the MPC internals to less than 200°F, water can be injected to the MPC without risk of boiling and the associated thermal stress concerns. Because of the relatively long cooldown period, the thermal stress contribution to the total cladding stress would be negligible, and the total stress would therefore be bounded by the normal (dry) condition. The elimination of boiling eliminates any concern of overpressurization due to steam production.

4.5.1.1.7 Study of Lead-to-Steel Gaps on Predicted Temperatures

Lead, poured between the inner and outer shells, is utilized as a gamma shield material in the HI-TRAC on-site transfer cask designs. Lead shrinks during solidification requiring the specification and implementation of appropriate steps in the lead installation process so that the annular space is free of gaps. Fortunately, the lead pouring process is a mature technology and proven methods to insure that radial gaps do not develop are widely available. This subsection outlines such a method to achieve a zero-gap lead installation in the annular cavity of the HI-TRAC casks.

The 100-ton and 125-ton HI-TRAC designs incorporate 2.5 inch and 4.5 inch annular spaces, respectively, formed between a 3/4-inch thick steel inner shell and a 1-inch thick steel outer shell. The interior steel surfaces are cleaned, sandblasted and fluxed in preparation for the molten lead that will be poured in the annular cavity. The appropriate surface preparation technique is essential to ensure that molten lead sticks to the steel surfaces, which will form a metal to lead bond upon solidification. The molten lead is poured to fill the annular cavity. The molten lead in the immediate vicinity of the steel surfaces, upon cooling by the inner and outer shells, solidifies forming a melt-solid interface. The initial formation of a gap-free interfacial bond between the solidified lead and steel surfaces initiates a process of lead crystallization from the molten pool onto the solid surfaces. Static pressure from the column of molten lead further aids in retaining the solidified lead layer to the steel surfaces. The melt-solid interface growth occurs by freezing of successive layers of molten lead as the heat of fusion is dissipated by the solidified metal and steel structure enclosing it. This growth stops when all the molten lead is used up and the annulus is filled with a solid lead plug. The shop fabrication procedures, being developed in conjunction with the designated manufacturer of the HI-TRAC transfer casks, shall contain detailed step-by-step instructions devised to eliminate the

† Certain fuel configurations in PWR MPCs are required to be flooded with borated water, which has a higher boiling temperature. Thus, greater subcooling margins are present in this case.

incidence of annular gaps in the lead space of the HI-TRAC.

In the spirit of a defense-in-depth approach, however, a conservatively bounding lead-to-steel gap is assumed herein and the resultant peak cladding temperature under design basis heat load is computed. It is noted that in a non-bonding lead pour scenario, the lead shrinkage resulting from phase transformation related density changes introduces a tendency to form small gaps. This tendency is counteracted by gravity induced slump, which tends to push the heavy mass of lead against the steel surfaces. If the annular molten mass of lead is assumed to contract as a solid, in the absence of gravity, then a bounding lead-to-steel gap is readily computed from density changes. This calculation is performed for the 125-ton HI-TRAC transfer cask, which has a larger volume of lead and is thus subject to larger volume shrinkage relative to the 100-ton design, and is presented below.

The densities of molten (ρ_l) and solid (ρ_s) lead are given on page 3-96 of Perry's Handbook (6th Edition) as 10,430 kg/m³ and 11,010 kg/m³, respectively. The fractional volume contraction during solidification ($\delta v/v$) is calculated as:

$$\frac{\delta v}{v} = \frac{(\rho_s - \rho_l)}{\rho_l} = \frac{(11,010 - 10,430)}{10,430} = 0.0556$$

and the corresponding fractional linear contraction during solidification is calculated as:

$$\frac{\delta L}{L} = \left[1 + \frac{\delta v}{v} \right]^{1/3} - 1 = 1.0556^{1/3} - 1 = 0.0182$$

The bounding lead-to-steel gap, which is assumed filled with air, is calculated by multiplying the nominal annulus radial dimension (4.5 inches in the 125-ton HI-TRAC) by the fractional linear contraction as:

$$\delta = 4.5 \times \frac{\delta L}{L} = 4.5 \times 0.0182 = 0.082 \cdot \text{inches}$$

In this hypothetical lead shrinkage process, the annular lead cylinder will contract towards the inner steel shell, eliminating gaps and tightly compressing the two surfaces together. Near the outer steel cylinder, a steel-to-lead air gap will develop as a result of volume reduction in the liquid to solid phase transformation. The air gap is conservatively postulated to occur between the inner steel shell and the lead, where the heat flux is higher relative to the outer steel shell, and hence the computed temperature gradient is greater. The combined resistance of an annular lead cylinder with an air gap (R_{cyl}) is computed by the following formula:

$$R_{cyl} = \frac{\ln(R_o / R_i)}{2\pi K_{pb}} + \frac{\delta}{2\pi R_i [K_{air} + K_r]}$$

where:

R_i = inner radius (equal to 35.125 inches)

- R_o = outer radius (equal to 39.625 inches)
- K_{pb} = bounding minimum lead conductivity (equal to 16.9 Btu/ft-hr-°F, from Table 4.2.2)
- δ = lead-to-steel air gap, computed above
- K_{air} = temperature dependent air conductivity (see Table 4.2.2)
- K_r = effective thermal conductivity contribution from radiation heat transfer across air gap

The effective thermal conductivity contribution from radiation heat transfer (K_r) is defined by the following equation:

$$K_r = 4 \times \sigma \times F_\epsilon \times T^3 \times \delta$$

where:

- σ = Stefan-Boltzmann constant
- $F_\epsilon = (1/\epsilon_{cs} + 1/\epsilon_{pb} - 1)^{-1}$
- ϵ_{cs} = carbon steel emissivity (equal to 0.66, HI-STORM FSAR Table 4.2.4)
- ϵ_{pb} = lead emissivity (equal to 0.63 for oxidized surfaces at 300°F from McAdams, Heat Transmission, 3rd Ed.)
- T = absolute temperature

Based on the total annular region resistance (R_{cyl}) computed above, an equivalent annulus conductivity is readily computed. This effective temperature-dependent conductivity results are tabulated below:

Temperature (°F)	Effective Annulus Conductivity (Btu/ft-hr-°F)
200	1.142
450	1.809

The results tabulated above confirm that the assumption of a bounding annular air gap grossly penalizes the heat dissipation characteristics of lead filled regions. Indeed, the effective conductivity computed above is an order of magnitude lower than that of the base lead material. To confirm the heat dissipation adequacy of HI-TRAC casks under the assumed overly pessimistic annular gaps, the HI-TRAC thermal model described earlier is altered to include the effective annulus conductivity computed above for the annular lead region. The peak cladding temperature results are tabulated below:

Annular Gap Assumption	Peak Cladding Temperature (°F)	Cladding Temperature Limit (°F)
None	872 871	1058
Bounding Maximum	924 926	1058

From these results, it is readily apparent that the stored fuel shall be maintained within safe temperature limits by a substantial margin of safety (in excess of 100°F).

4.5.1.2 Test Model

A detailed analytical model for thermal design of the HI-TRAC transfer cask was developed using the FLUENT CFD code, the industry standard ANSYS modeling package and conservative adiabatic calculations, as discussed in Subsection 4.5.1.1. Furthermore, the analyses incorporate many conservative assumptions in order to demonstrate compliance to the specified short-term limits with adequate margins. In view of these considerations, the HI-TRAC transfer cask thermal design complies with the thermal criteria established for short-term handling and onsite transport. Additional experimental verification of the thermal design is therefore not required.

4.5.2 Maximum Temperatures

4.5.2.1 Maximum Temperatures Under Onsite Transport Conditions

An axisymmetric FLUENT thermal model of an MPC inside a HI-TRAC transfer cask was developed to evaluate temperature distributions for onsite transport conditions. A bounding steady-state analysis of the HI-TRAC transfer cask has been performed using the hottest MPC, the highest design-basis decay heat load (Table 2.1.6), and design-basis insolation levels. While the duration of onsite transport may be short enough to preclude the MPC and HI-TRAC from obtaining a steady-state, a steady-state analysis is conservative. Information listing all other thermal analyses pertaining to the HI-TRAC cask and associated subsection of the FSAR summarizing obtained results is provided in Table 4.5.8.

~~A converged temperature contour plot is provided in Figure 4.5.2. Maximum fuel clad temperatures are listed in Table 4.5.2, which also summarizes maximum calculated temperatures in different parts of the HI-TRAC transfer cask and MPC. As described in Subsection 4.4.2, the FLUENT calculated peak temperature in Table 4.5.2 is actually the peak pellet centerline temperature, which bounds the peak cladding temperature. We conservatively assume that the peak clad temperature is equal to the peak pellet centerline temperature. An axial temperature plot of the hottest fuel rod is provided in Figure 4.5.2.~~

The maximum computed temperatures listed in Table 4.5.2 are based on the HI-TRAC cask at Design Basis Maximum heat load, passively rejecting heat by natural convection and radiation to a hot ambient environment at 100°F in still air in a vertical orientation. In this orientation, there is apt to be a less of metal-to-metal contact between the physically distinct entities, viz., fuel, fuel basket, MPC shell and HI-TRAC cask. For this reason, the gaps resistance between these parts is higher than in a horizontally oriented HI-TRAC. To bound gaps resistance, the various parts are postulated to be in a centered configuration. MPC internal convection at a postulated low cavity pressure of 5.7 atm is included in the thermal model. The peak cladding temperature computed under these adverse Ultimate Heat Sink (UHS) assumptions is 872-871°F which is substantially lower than the short-term temperature limit of 1058°F. Consequently, cladding integrity assurance is provided by large safety margins (in excess of 100°F) during onsite transfer of an MPC emplaced in a HI-TRAC cask.

As a defense-in-depth measure, cladding integrity is demonstrated for a theoretical bounding scenario. For this scenario, all means of convective heat dissipation within the canister are neglected in addition to the bounding relative configuration for the fuel, basket, MPC shell and HI-TRAC overpack assumption stated earlier for the vertical orientation. This means that the fuel is centered in the basket cells, the basket is centered in the MPC shell and the MPC shell is centered in the HI-TRAC overpack to maximize gaps thermal resistance. The peak cladding temperature computed for this scenario (1025 1009°F) is below the short-term limit of 1058°F.

As discussed in Sub-section 4.5.1.1.6, MPC fuel unloading operations are performed with the MPC inside the HI-TRAC cask. For this operation, a helium cooldown system is engaged to the MPC via lid access ports and a forced helium cooling of the fuel and MPC is initiated. With the HI-TRAC cask external surfaces dissipating heat to a UHS in a manner in which the ambient air access is not restricted by bounding surfaces (*for example in a cask pit*) or large objects in the immediate vicinity of the cask, the temperatures reported in Table 4.5.2 will remain bounding during fuel unloading operations. *To evaluate the effect of restricted cooling, a theoretical bounding scenario in which a vertically situated HI-TRAC cask is surrounded by an insulating boundary is postulated. As an additional measure of conservatism, the boundary is modeled as a low emissivity surface ($\epsilon = 0.1$) so that most of the radiant energy emitted by cask is reflected back to the cask (in this case reflected fraction = $1 - \epsilon = 0.9$). The principal means of cask cooling in this situation is via infiltration of ambient air (at 100°F) from above the HI-TRAC space into a narrow annular space (assumed 2 ft) between the HI-TRAC and a bounding cylindrical surface (the insulating boundary). A FLUENT model of this scenario is constructed at design basis maximum heat load (41.22 kW). In order to conservatively maximize air heating in the annular space, the HI-TRAC top is assumed to be insulated. The cumulative effect of conservatisms and the imposed severe restrictions to ambient air access is to elevate the mean temperature of air in the annulus by 160°F. Under this postulated scenario, the steady state maximum cladding temperature ($871^{\circ}\text{F} + 160^{\circ}\text{F} = 1031^{\circ}\text{F}$) is below the short term temperature limit (1058°F). In other words, ambient air access restriction does not unduly limit the coolability of fuel. Therefore additional means for cask cooling are not necessary.* Under a scenario in which the cask is emplaced in a area with ambient air access restrictions (*for example in a cask pit area*), additional means shall be devised to limit the cladding temperature rise arising from such restrictions to less than 100°F. These means are discussed next.

~~The time duration allowed for the cask to be emplaced in a ambient air restricted area with the helium cooling system non operational shall be limited to 22 hours. Conservatively postulating that the rate of passive cooling is substantially degraded by 90% (i.e., 10% of decay heat is dissipated to ambient), cladding integrity is demonstrated based on cask heating considerations from the undissipated heat. At a bounding heat load of 28.74kW, the HI-TRAC cask system thermal inertia (19,532 Btu/°F, Table 4.5.5), limits the temperature rise to 4.52°F/hr. Thus, the computed cladding temperature rise during this time period will be less than 100°F.~~

~~A forced supply of ambient air near the bottom of the cask pit to aid heat dissipation by the natural convection process is another adequate means to maintain the fuel cladding within safe operating limits. Conservatively assuming this column of moving air as the UHS (i.e. to which all heat~~

~~dissipation occurs) with no credit for enhanced cooling as a result of forced convection heat transfer, a nominal air supply of 1000 SCFM (4850 lbs/hr) adequately meets the cooling requirement. At this flow rate, the temperature rise of the UHS resulting from cask decay heat input to the airflow will be less than 100°F. The cladding temperature elevation will consequently be bounded by this temperature rise.~~

4.5.2.2 Maximum MPC Basket Temperature Under Vacuum Conditions

As stated in Subsection 4.5.1.1.4, above, an axisymmetric FLUENT thermal model of the MPC is developed with an isotropic fuel basket thermal conductivity for the vacuum condition.. Each MPC is analyzed at ~~its respective design maximum~~ *an upperbound vacuum condition heat load (29 kW) with an added conservative assumption that the conductivity of helium is a very small fraction of its nominal value.* The steady-state peak cladding results, with partial recognition for higher axial heat dissipation, are summarized in Table 4.5.9. The peak fuel clad temperatures during short-term vacuum drying operations ~~with design basis maximum~~ *at an upperbound vacuum condition* heat loads are calculated to be less than 1058°F for all MPC baskets by a significant margin..

4.5.3 Minimum Temperatures

In Table 2.2.2 and Chapter 12, the minimum ambient temperature condition required to be considered for the HI-TRAC design is specified as 0°F. If, conservatively, a zero decay heat load (with no solar input) is applied to the stored fuel assemblies then every component of the system at steady state would be at this outside minimum temperature. Provided an antifreeze is added to the water jacket (required by Technical Specification for ambient temperatures below 32°F), all HI-TRAC materials will satisfactorily perform their intended functions at this minimum postulated temperature condition. Fuel transfer operations are controlled by Technical Specifications in Chapter 12 to ensure that onsite transport operations are not performed at an ambient temperature less than 0°F.

4.5.4 Maximum Internal Pressure

After fuel loading and vacuum drying, but prior to installing the MPC closure ring, the MPC is initially filled with helium. During handling in the HI-TRAC transfer cask, the gas temperature within the MPC rises to its maximum operating temperature as determined based on the thermal analysis methodology described previously. The gas pressure inside the MPC will also increase with rising temperature. The pressure rise is determined based on the ideal gas law, which states that the absolute pressure of a fixed volume of gas is proportional to its absolute temperature. *The thermal analysis of the bounding MPC heat load (MPC-68) under the on-site transport scenario also provides the MPC cavity internal pressure. In reality the steady state condition in the onsite transport evolution that is characterized by a short duration, will not be achieved. A steady state condition, however, was assumed to obtain an upperbound on the MPC cavity pressure. Results show that the maximum MPC internal pressure will remain bounded by the short duration pressure*

permitted in the MPC under the on-the-pad storage mode (defined as off-normal pressure in Table 2.2.1). The net free volumes of the four MPC designs are determined in Section 4.4.

The maximum MPC internal pressure is determined for normal onsite transport conditions, as well as off-normal conditions of a postulated accidental release of fission product gases caused by fuel rod rupture. Based on NUREG-1536 [4.4.10] recommended fission gases release fraction data, net free volume and initial fill gas pressure, the bounding maximum gas pressures with 1% and 10% rod rupture are given in Table 4.5.3. The MPC maximum gas pressures listed in Table 4.5.3 are all below the MPC design internal pressure listed in Table 2.2.1.

4.5.5 Maximum Thermal Stresses

Thermal expansion induced mechanical stresses due to non-uniform temperature distributions are reported in Chapter 3. Tables 4.5.2 and 4.5.4 provide a summary of MPC and HI-TRAC transfer cask component temperatures for structural evaluation.

4.5.6 Evaluation of System Performance for Normal Conditions of Handling and Onsite Transport

The HI-TRAC transfer cask thermal analysis is based on a detailed heat transfer model that conservatively accounts for all modes of heat transfer in various portions of the MPC and HI-TRAC. The thermal model incorporates several conservative features, which are listed below:

- i. The most severe levels of environmental factors - bounding ambient temperature (100°F) and constant solar flux - were coincidentally imposed on the thermal design. A bounding solar absorptivity of 1.0 is applied to all insolation surfaces.
- ii. The HI-TRAC cask-to-MPC annular gap is analyzed based on the nominal design dimensions. No credit is considered for the significant reduction in this radial gap that would occur as a result of differential thermal expansion with design basis fuel at hot conditions. The MPC is considered to be concentrically aligned with the cask cavity. This is a worst-case scenario since any eccentricity will improve conductive heat transport in this region.
- iii. No credit is considered for cooling of the HI-TRAC baseplate while in contact with a supporting surface. An insulated boundary condition is applied in the thermal model on the bottom baseplate face.

Temperature distribution results (Tables 4.5.2 and 4.5.4, and Figure 4.5.2) obtained from this highly conservative thermal model show that the short-term fuel cladding and cask component temperature limits are met with adequate margins. Expected margins during normal HI-TRAC use will be larger due to the many conservative assumptions incorporated in the analysis. Corresponding MPC internal pressure results - evaluation (Table 4.5.3) shows that the MPC confinement boundary remains well below the short-term condition design pressure. Stresses induced due to imposed temperature gradients are within ASME Code limits (Chapter 3). The maximum local axial neutron shield

temperature is lower than design limits. Therefore, it is concluded that the HI-TRAC transfer cask thermal design is adequate to maintain fuel cladding integrity for short-term onsite handling and transfer operations.

The water in the water jacket of the HI-TRAC provides necessary neutron shielding. During normal handling and onsite transfer operations this shielding water is contained within the water jacket, which is designed for an elevated internal pressure. It is recalled that the water jacket is equipped with pressure relief valves set at 60 psig. This set pressure elevates the saturation pressure and temperature inside the water jacket, thereby precluding boiling in the water jacket under normal conditions. Under normal handling and onsite transfer operations, the bulk temperature inside the water jacket reported in Table 4.5.2 is less than the coincident saturation temperature at 60 psig (307°F), so the shielding water remains in its liquid state. The bulk temperature is determined via a conservative analysis, presented earlier, with design-basis maximum decay heat load. One of the assumptions that render the computed temperatures extremely conservative is the stipulation of a 100°F steady-state ambient temperature. In view of the large thermal inertia of the HI-TRAC, an appropriate ambient temperature is the "time-averaged" temperature, formally referred to in this FSAR as the normal temperature.

Note that during hypothetical fire accident conditions (see Section 11.2) these relief valves allow venting of any steam generated by the extreme fire flux, to prevent overpressurizing the water jacket. In this manner, a portion of the fire heat flux input to the HI-TRAC outer surfaces is expended in vaporizing a portion of the water in the water jacket, thereby mitigating the magnitude of the heat input to the MPC during the fire.

~~During vacuum drying operations, the annular gap between the MPC and the HI-TRAC is filled with water. The saturation temperature of the annulus water bounds the maximum temperatures of all HI-TRAC components, which are located radially outside the water-filled annulus. As previously stated (see Subsection 4.5.1.1.4) the maximum annulus water temperature is only 125°F, so the HI-TRAC water jacket temperature will be less than the 307°F saturation temperature.~~

Table 4.5.1

EFFECTIVE RADIAL THERMAL CONDUCTIVITY OF THE WATER JACKET

Temperature (°F)	Thermal Conductivity (Btu/ft-hr-°F)
200	1.376
450	1.408
700	1.411

Table 4.5.2

HI-TRAC TRANSFER CASK STEADY-STATE
MAXIMUM TEMPERATURES

Component	Temperature [°F]	Design Limit [°F]*
Fuel Cladding	872 871	1058
MPC Basket	852 851	950
Basket Periphery	600 675	950
MPC Outer Shell Surface	455 539	775
HI-TRAC Overpack Inner Surface	322 401	600
Water Jacket Inner Surface	314 371	700
Enclosure Shell Outer Surface	224 255	700
Water Jacket Bulk Water	258 292	307
Axial Neutron Shield†	258 271	300

* Obtained from Tables 2.2.3 and 4.3.1.

† Local neutron shield section temperature.

Table 4.5.3

[INTENTIONALLY DELETED]

SUMMARY OF MPC CONFINEMENT BOUNDARY PRESSURES FOR
NORMAL HANDLING AND ONSITE TRANSPORT

Condition	Pressure (psig)
MPC 24: Initial backfill (at 70°F) Normal condition With 1% rod rupture With 10% rod rupture	31.3 76.0 76.8 83.7
MPC 68: Initial backfill (at 70°F) Normal condition With 1% rods rupture With 10% rod rupture	31.3 76.0 76.5 80.5
MPC 32: Initial backfill (at 70°F) Normal condition With 1% rods rupture With 10% rod rupture	31.3 76.0 77.1 86.7
MPC 24E: Initial backfill (at 70°F) Normal condition With 1% rods rupture With 10% rod rupture	31.3 76.0 76.8 83.7

* Includes gas from BPPA rods for PWR MPCs

Table 4.5.4

SUMMARY OF HI-TRAC TRANSFER CASK AND MPC COMPONENTS
NORMAL HANDLING AND ONSITE TRANSPORT TEMPERATURES (Note 1)

Location	Temperature (°F)
MPC Basket Top:	
Basket periphery	590
MPC shell	445
O/P [†] inner shell	280
O/P enclosure shell	196
MPC Basket Bottom:	
Basket periphery	334
MPC shell	302
O/P inner shell	244
O/P enclosure shell	199

Note 1:

The temperatures provided in this table are based on one thermal analysis for a uniform storage scenario. The option to store SNF in a regionalized configuration wherein the heat generation rates in Region 2 and Region 1 can vary within a wide range (See Table 4.4.30), a large number of heat generation scenarios are possible. However prescription of a maximum value for the peak cladding temperature ensures that the changes to the highest metal temperatures obtained inside an MPC are small. In as much as the corresponding temperature limits (Table 2.2.3) are considerably larger than the temperatures obtained over the entire universe of design basis SNF storage scenarios, a robust margin of safety with respect to the metal temperature limit remains.

[†] O/P is an abbreviation for HI-TRAC overpack.

Table 4.5.5

SUMMARY OF LOADED 100-TON HI-TRAC TRANSFER CASK
 BOUNDING COMPONENT
 WEIGHTS AND THERMAL INERTIAS

Component	Weight (lbs)	Heat Capacity (Btu/lb-°F)	Thermal Inertia (Btu/°F)
Water Jacket	7,000	1.0	7,000
Lead	52,000	0.031	1,612
Carbon Steel	40,000	0.1	4,000
Alloy-X MPC (empty)	39,000	0.12	4,680
Fuel	40,000	0.056	2,240
MPC Cavity Water [†]	6,500	1.0	6,500
			26,032 (Total)

[†] Conservative lower bound water mass.

Table 4.5.6

MAXIMUM ALLOWABLE TIME DURATION FOR WET
TRANSFER OPERATIONS

Initial Temperature (°F)	Time Duration (hr)
115	25.7 17.9
120	24.4 17.0
125	23.1 16.1
130	21.7 15.1
135	20.4 14.2
140	19.1 13.3
145	17.8 12.4
150	16.4 11.5

Table 4.5.7

INTENTIONALLY DELETED

Table 4.5.8
MATRIX OF HI-TRAC TRANSFER CASK THERMAL EVALUATIONS

Scenario	Description	Ultimate Heat Sink	Analysis Type	Principal Input Parameters	Results in FSAR Subsection
1	Onsite Transport	Ambient	SS(B)	O _T , Q _D , ST, SC	4.5.2.1
2	Lead Gaps	Ambient	SS(B)	O _T , Q _D , ST, SC	4.5.1.1.7
3	Vacuum	HI-TRAC annulus water	SS(B)	Q _D	4.5.2.2
4	Wet Transfer Operation	Cavity water and Cask Internals	AH	Q _D	4.5.1.1.5
5	Fuel Unloading	Helium Circulation	TA	Q _D	4.5.1.1.6
6	Fire Accident	Jacket Water, Cask Internals	TA	Q _D , F	11.2.4
7	Jacket Water Loss Accident	Ambient	SS(B)	O _T , Q _D , ST, SC	11.2.1

Legend:

O_T - Off-Normal Temperature (100°F)
Q_D - Design Basis Maximum Heat Load

SS(B) - Bounding Steady State
TA - Transient Analysis
AH - Adiabatic Heating

ST - Insolation Heating (Top)
SC - Insolation Heating (Curved)
F - Fire Heating (1475°F)

Table 4.5.9

PEAK CLADDING TEMPERATURE IN VACUUM[†]

MPC	Temperature (°F)
MPC-24	960 997
MPC-68	1014 1039
MPC-32	1040 1049
MPC-24E	942 966

[†] Steady state temperatures at the MPC design maximum ~~an upperbound vacuum condition~~ heat load reported.

Table 4.5.10

HI-TRAC ANNULUS COOLING REQUIREMENT DURING VACUUM DRYING

<i>MPC Heat Load</i>	<i>Annulus Cooling Requirement</i>
<i>Very Low (≤ 10 kW)</i>	<i>None</i>
<i>Low (> 10 kW and ≤ 22 kW)</i>	<i>Water in the annulus</i>
<i>Medium (> 22 kW and ≤ 29 kW)</i>	<i>Annulus continuously flushed with water</i>
<i>High (> 29 kW)</i>	<i>NA (Vacuum Drying Not Permitted)</i>

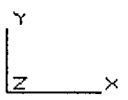
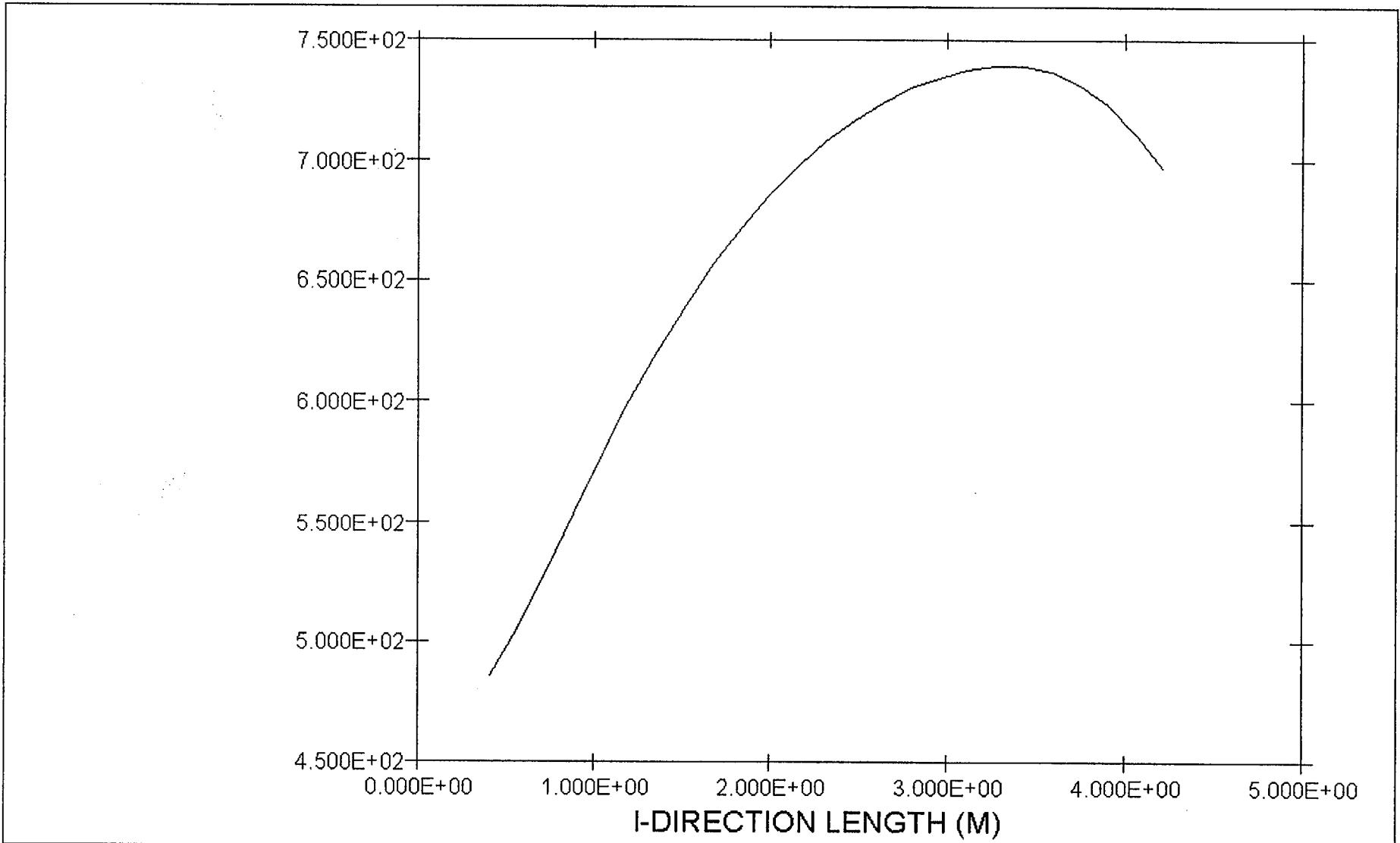


FIGURE 4.5.2: Hottest Rod Axial Temperature Plot
Temperature (K) vs. axial distance from cask bottom [m]

Feb 27 2002
Fluent 4.56
Fluent Inc.

APPENDIX 4.A: CLAD TEMPERATURE LIMITS FOR HIGH-BURNUP FUEL

4.A.1 INTRODUCTION

The current revision of NUREG-1536 [4.A.1] for storage of spent fuel in dry storage casks essentially limits fuel burnup to 45 GWd/MTU. In light of the continuous improvements in fuel bundle design and manufacturing technologies and longer fuel cycles, the quantity of fuel assemblies with burnups in excess of 45 GWd/MTU stored in the spent fuel pools is expected to rise at a rapid pace. It is therefore necessary to address the storage of these high-burnup fuel assemblies in Holtec's storage system. This appendix presents a summary of the methodology developed by Holtec for determining suitable clad temperature limits consistent with the intent of the regulatory review guidelines presented in ISG-15 [4.A.2]. *Permissible peak clad temperature limits are computed for a fuel burnup of limit of 75,000 MWD/MTU (PWR) and 70,000 MWD/MTU (BWR).* The governing mode for cladding failure, as specified in ISG-15, is assumed to be thermal creep, and the strain limit is set equal to 1% in spite of growing scientific evidence that supports a 2% minimum strain limit. Finally, an alternative criterion for categorizing a spent nuclear fuel (SNF) as "damaged" is proposed in lieu of the ISG-15 criterion which, based on recent data, would needlessly classify a large quantity of high burnup intact SNF as "damaged". This deviation from the guidance contained in ISG-15 has been added to the list of deviations from NUREG-1536 in Table 1.0.3.

4.A.2 REGULATORY GUIDANCE

NRC ISG-15 [4.A.2] presents the current regulatory position on storage and transport of high-burnup spent fuel assemblies. For the purpose of storage in the HI-STORM system, we define high-burnup spent fuel as any fuel assembly with an assembly average burnup greater than 45 GWd/MTU. This definition is consistent with ISG-15.

The mode of failure is postulated to be excessive hoop dilation of the pressurized tubes (fuel rods). Failure is postulated to occur when the cumulative strain reaches 1%. ISG-15 does not prescribe a mathematical model to compute the creep rate: It is incumbent on the certificate holder or licensee to propose an appropriate correlation. In this appendix, we present such a correlation along with the necessary justifications to substantiate its veracity.

ISG-15 also provides a set of fuel integrity criteria predicated on the extent of corrosion (oxidation) of the fuel cladding to define when a high burnup spent nuclear fuel should be treated as damaged. We discuss the ISG integrity criteria vis-à-vis our proposed criteria in a later section in this appendix.

4.A.3 CREEP DEFORMATION MECHANISM AND FAILURE STRAIN

Failure of the fuel cladding in dry storage is postulated to occur from the visco-elastic-plastic effect known as creep. The fuel cladding very gradually dilates in the manner of a pressurized tube under the influence of internal pressure of the contained gas. The predominant stress component in the cladding is the hoop stress, σ , which is readily computed by the classical Lamé's formula:

$$\sigma = pr/t \quad (1)$$

where p , r and t are, respectively, the net outward pressure acting on the cladding in dry storage, inside cladding radius and cladding wall thickness.

Classical creep mechanics instructs us that the magnitude of stress, σ , and the coincident metal temperature, T , are the most significant variables in determining the rate of creep for a given material. The development in predicting creep behavior of pure metals and alloys has traditionally followed the path of measuring the creep rate while holding the stress and temperatures constant and then developing a compact mathematical correlation that accords with the measured data. This process, quite logical in light of the absence of an identifiable fundamental constitutive relation for metal creep, has spawned numerous creep equations in the past ninety years. Lin, in his text on creep mechanics [4.A.7] published in 1968, cites eight general correlations: Many more have followed in the years since then. Attempts by the American Society of Metals to correlate the multitude of correlations [4.A.8], each purporting to represent the creep behavior of certain metals and alloys with precision, ended up in an essentially non-specific recommendation that recognizes creep rate as a complex and non-linear function of stress and temperature.

To propose a creep equation for irradiated zircaloy, an appropriate relationship for strain as a function of stress, temperature and time must be defined. Then the available experimental data on irradiated zircaloy must be used to correlate and benchmark the functional relationship.

Having developed an experimentally corroborated creep rate functional relationship, the next step in the analysis process is to determine the permissible peak cladding temperature at the start of dry storage that will limit the total creep strain accumulation in the hottest fuel rod in forty years of dry storage to ~~0.01~~ 1%.

Holtec International has proposed 1% uniform circumferential creep strain of the fuel cladding as a conservative limit for the purpose of establishing the permissible peak cladding temperature, T_p , in dry storage, even though independent work by EPRI [4.A.9], citing several references, including a recent experimental work by Goll [4.A.10], asserts that the 1% strain limit is "overly conservative."

The test creep experiments by Goll et al. [4.A.10] appear to have been expressly performed to establish the failure strain limit of high burnup SNF (54 to 64 GWD/MTU) with a heavy oxide

layer (up to $\sim 100 \mu\text{m}$). To achieve circumferential strains in the range of 2% in a short period, the samples were subjected to a much higher stress (400 to 600 MPa) than would be obtained in dry storage of spent nuclear fuel ($<150 \text{ MPa}$). The experiments included 21 creep tests on samples of two rods, none of which failed at 2% hoop strain. Ductility tests on cladding containing radially oriented hydrides also exhibited unbreached integrity at 100 MPa and 423°K, indicating that the increased vulnerability of the fuel cladding in the presence of radially oriented hydride lenses is not a cladding integrity limiting condition.

Oxidation of the cladding during reactor operations is an immutable fact. Oxidation leads to flaking or spalling of the cladding, resulting in a reduction of the tube wall, t , development of a rough external surface (stress raisers) and incursion of hydrogen into the cladding microstructure.

Spalling of the fuel cladding, associated with oxidation of zirconium, is a function of numerous variables, including reactor operation history, water chemistry, areal power density, coolant temperature, and burnup. Spalling or flaking introduces a local surface discontinuity on the cladding surface. However, burst test data on spalled cladding by Garde et al. [4.A.11], if interpreted properly, as shown by EPRI [4.A.9], support the conclusion that a 1% creep strain limit is conservative even for spalled cladding where the hydride lenses, formed as a byproduct of the oxidation process, have penetrated as far as the cladding mid-wall. EPRI [4.A.9] computes the Critical Strain Energy Density (CSED) [4.A.15, 4.A.16] corresponding to the Garde data to be 5 MPa, which corresponds to the fracture toughness value, K_{IC} , of $7.8 \text{ MPa}\sqrt{m}$. EPRI computes the K_{IC} for the heavily spalled cladding (up to 50% hydride penetration) at 1% creep to be $3.8 \text{ MPa}\sqrt{m}$, thus demonstrating that 1% creep strain limit is conservative. Recent work by Jarheiff, Manzel, and Ortlieb [4.A.17] corroborates EPRI's position by showing that at even up to 2,000 ppm hydride concentration (which will develop only under extremely high levels of burnup), the ductility of irradiated zircaloy is essentially undiminished.

Failure strain under rapidly applied mechanical loading is a measure of the ductility of the material, which can be significantly lower than the creep strain limit. EPRI [4.A.9] suggests using the strain energy density at failure in burst tests as the invariant parameter to estimate the corresponding creep strain limit for the material. Using this method and typical temperatures and pressures attendant to dry storage, the creep strain limit may be as much as five to ten times the plastic failure strain under burst tests.

Burst tests on irradiated fuel cladding from commercial reactors (Calvert Cliffs Unit 1, ANO Unit 2, Ft. Calhoun) by Garde et al. [4.A.11] show that "ductility of zircaloy-4 irradiated to fluence levels of $1.2 \times 10^{22} \text{ n/cm}^2$ ($E > 1 \text{ MeV}$) at LWR operating temperatures of roughly 600°K is about 3 to 4% and depends on the hydride precipitate local volume."

It is generally recognized that the tertiary creep stage [4.A.7, pp. 60-61] is essentially obviated if the material is subject to a constant stress (rather than a constant load, which is common in most engineering applications). Andrade explained the difference between constant load and constant stress creep in 1910: His classical curve [4.A.7, p. 61] is reproduced herein as Figure 4.A.1. The

case of irradiated fuel cladding in dry storage, however, belongs to the special class of problems wherein the stress would decrease as the fuel rod containing a fixed quantity of gas at a constant temperature increases in diameter with passage of time due to creep. This is due to the fact that, based on the perfect gas law, the increase in the cladding diameter due to creep reduces the pressure exerted by the contained gas. The increase in diameter also causes a concomitant reduction in the cladding wall thickness. Since the hoop stress σ , governed by Lamé's formula (Equation 4.A.1) is proportional to the radius and internal pressure, and inversely proportional to the wall thickness, it is shown in the following that the hoop stress will remain essentially constant as the cladding radius increases due to creep if the fuel rod were a hollow tube (no fuel pellets) and will decrease if the gas is contained in the annulus between the pellets and the rod.

To quantify the reduction in gas pressure, p , due to creep-induced increase in the rod diameter, let us consider a unit length of a fuel rod of inside radius, r , and initial wall thickness, t , containing a fuel pellet of radius a . The pellet is assumed to be rigid and the gas is assumed to be confined to the annular region defined by radii r and a . If the inner radius of the rod expands to $(r+\Delta r)$ due to creep, then the annular space will accordingly increase, reducing the gas pressure to say, p' . p' is related to p by the perfect gas law:

$$p' [(r + \Delta r)^2 - a^2] = p (r^2 - a^2)$$

Neglecting the terms of second order, we have

$$p' = \frac{p b^2}{b^2 + 2 r \Delta r} \quad (2)$$

where we have defined

$$b^2 = r^2 - a^2 \quad (3)$$

Since the increase in circumference of the rod due to increase in radius by Δr causes a corresponding decrease in the rod wall thickness by Δt to maintain a constant metal volume, we have

$$2\pi (r + \Delta r) (t - \Delta t) = 2\pi r t$$

or
$$r \Delta t = t \Delta r \quad (4)$$

The initial stress σ is given by Equation (1), the final stress σ' after creep to radius Δr is given by

$$\sigma' = \frac{p' (r + \Delta r)}{(t - \Delta t)} \quad (5)$$

Substituting for p' from Equation (2), utilizing Equation (4), and neglecting terms of higher order, we obtain

$$\sigma' = \frac{pr}{t} \left[1 - \frac{2\Delta r}{r} \frac{a^2}{b^2} \right] \quad (6)$$

The fractional decrease in stress is given by Eqs. (1) and (6); we have

$$\frac{\sigma - \sigma'}{\sigma} = \frac{\Delta\sigma}{\sigma} = 2c\chi^2 \quad (7)$$

where

$$c = \frac{\Delta r}{r} \quad (8)$$

and:

$$\chi^2 = \frac{a^2}{r^2 - a^2} \quad (9)$$

We note that in the case of a hollow tube (i.e., no pellets, $a = 0$), $\chi=0$ and $\Delta\sigma = 0$, i.e., the hoop stress will not change with creep. However, for the case of a fuel rod containing pellets (the real life case), the drop in the stress level with creep is a strong function of χ . If we assume that $a = .99r$, then $\chi^2 = 49.25$. Using Equation (7), we find that the percentage reduction in stress is 98.5%, corresponding to 1% creep ($c=\Delta r/r = .01$). In a fuel rod, the gas is in the annulus as well as in the plenum. For a typical fuel rod, EPRI [4.A.9] estimates that the reduction in stress is 17% for 1% creep.

In view of the foregoing, the condition of rapid straining leading to gross rupture that characterizes failure in the tertiary creep domain can be ruled out for fuel cladding in dry storage (Figure 4.A.1). In fact the state of hoop stress in the fuel cladding suffers additional decrease as the heat emission rate from the fuel declines, resulting in the decrease of the gas temperature (and hence, pressure) inside the rods.

To summarize:

- The process of creep will result in a reduction in the cladding hoop stress even if the gas temperature were to remain constant.
- The continuous reduction in the heat emission rate from the fuel correspondingly reduces the gas temperature in the fuel rods, leading to an additional reduction in the hoop stress.

- Creep in fuel rods in dry storage belongs to the special class of problems where the actuating stress decreases with time, thus inoculating the fuel rod against tertiary creep (which is characterized by rapid deformation).

Finally, a fundamental characteristic of creep in metals is its relationship to the mechanical properties of the material. The rate of creep is known to decrease monotonically with the increase in yield strength. The creep strain limit also reduces as the ductility of the material (measured by its “elongation” in the terminology of ASTM) is reduced. The effect of irradiation is to modify zircaloy’s microstructure resulting in an increase in the yield strength and reduction in the ductility. This would imply a reduced rate of creep and a lower creep limit for the irradiated cladding than its unirradiated counterpart. However, both the yield strength and elongation curves tend to flatten out at high burnup levels (fluence $\approx 10^{22}$ N/cm² (E > 1 MeV)) [4.A.12, 4.A.13], suggesting that the Holtec creep equation and 1% creep limit will remain conservative for burnups up to ~~68,400~~ 75,000 MWD/MTU. *In other words, a zircaloy cladding at 75,000 MWD/MTU burnup should reasonably be expected to exhibit a somewhat smaller rate of creep compared to test data (upto 64,000 MWD/MTU (Goll et al. [4.A.10])). Therefore, the total accumulated creep in 40 years should be less for the 75,000 MWD/MTU fuel than its 64,000 MWD/MTU counterpart. Furthermore, it is recalled, that by assuming 40 years, which is twice the 20-year license limit, we have imputed an additional margin of safety in the computed value of accumulated creep.*

In summary, the accumulated creep for 75,000 MWD/MTU burnup SNF is expected to be much less than 1% in the 20-year license period, if permissible cladding temperature is computed using a 40-year storage life and creep rate based on a correlation that is conservatively constructed employing available high burnup SNF data. Therefore the PCT limits that are developed in this Appendix from upto 64,000 MWD/MTU SNF data can be conservatively applied to 75,000 MWD/MTU SNF as well.

4.A.4 ZIRCALOY CREEP STRAIN MODELING: PRIOR WORK

An experimental program to compile creep data on internally pressurized irradiated zircaloy fuel cladding has been carried out jointly by GNB and Siemens AG [4.A.3]. In this experimental study, internally pressurized zircaloy samples were irradiated for 10,000 hours at a variety of temperatures and hoop stresses. Test temperatures for each sample were held constant over the entire irradiation period and ranged from 250°C to 400°C. Hoop stresses are temperature dependent and were also, therefore, held constant for each sample over the entire irradiation period and ranged from 80 MPa to 150 MPa. Creep was measured for up to 10,000 hours.

The GNB/Siemens researchers also proposed an empirical model that could be used to predict cladding creep as a function of the cladding hoop stress and temperature. Their model, which we henceforth refer to as the “Siemen’s model”, is fully described in Reference [4.A.3] and is, therefore, merely summarized in this subsection. The Siemen’s creep equation is given as:

$$\epsilon = At^m \tag{10}$$

where:

- ϵ = the total creep strain at time t (%)
- A = the so-called "initial creep strain" (%)
- t = the storage time (hr)

The exponent 'm' on the time value in Equation (10) is expressed as a high-order polynomial function as:

$$m = \sum_{i=1}^{11} c_i \times T_f^{i-1} \quad (11)$$

In Equation (11), the c_i values are constants and T_f is a function of hoop stress and the temperature. The constants are given as:

$c_1 = 0.361705 \times 10^{-13}$	$c_7 = -0.126131 \times 10^{-12}$
$c_2 = 0.500028 \times 10^{-3}$	$c_8 = 0.433320 \times 10^{-15}$
$c_3 = -0.555901 \times 10^{-6}$	$c_9 = -0.835848 \times 10^{-18}$
$c_4 = 0.715481 \times 10^{-7}$	$c_{10} = 0.842689 \times 10^{-21}$
$c_5 = -0.181897 \times 10^{-8}$	$c_{11} = -0.345181 \times 10^{-24}$
$c_6 = 0.207254 \times 10^{-10}$	

and T_f is given as:

$$T_f = T + (\sigma - 80) \times \frac{45}{70} \quad (12)$$

where:

- T is the cladding temperature (°C)
- σ is the cladding hoop stress (MPa)

Equation (12) is held in the Siemen's formulation to be valid for temperatures between 100°C and 400°C and for hoop stresses between 80 MPa and 150 MPa.

As stated above, we refer to the modeling approach embodied in Equations (10) through (12) as the Siemen's model. This model does, however, have some shortcomings.

Figure 10 of a paper by Dr. Martin Peehs [4.A.4], using the recommended [4.A.3] initial creep strain (A) of 0.04% shows that the Siemen's model more closely approximates the creep behavior of unirradiated zircaloy and is inordinately conservative for irradiated zircaloy. As the model is intended for use in determining clad temperature limits for high-burnup fuel assemblies, this might result in erroneous low temperature limits.

The perceived over-conservatism in the Siemen's correlation was empirically remedied in the recent WESFLEX application [4.A.5] by dividing the cumulative creep predicted by the Siemen's model by a factor of two.

Unfortunately, the Siemen's model correlates poorly with the recent creep data published by Goll et al. [4.A.10]. Therefore, it was decided to develop a creep equation for irradiated zircaloy, using standard procedures, that benchmarks satisfactorily with *all* publicly available data.

4.A.5 IRRADIATED ZIRCALOY TEST DATA

In this section, we provide a listing of all test data that is utilized herein to benchmark the proposed Holtec creep model. The test data that we are seeking to utilize pertains to experimentally measured creep in irradiated zircaloy. Although the published data in this area are admittedly sparse, cited bibliographies and public-domain documents have been reviewed to adequately cover the range of stress and temperature conditions in dry storage.

Five sources of creep data are identified for benchmarking the Holtec creep model. The first data source is from the published creep results by Spilker et al. [4.A.3]. The test conditions are:

Temperature: 400°C
Stress: 70 MPa
Time: 1,000-6,000 hrs.

The second data source is from the Kaspar et al. high temperature creep data reported in a docketed dry storage document [4.A.22]. The test conditions for this data are:

Stress: 86 MPa
Temperature: 380°C (0-1,000 hrs)
395°C (>1,000 hrs)
Time: 1,000-8,000 hrs

The third source of data is from the accelerated creep testing by Goll et al. [4.A.10]. The testing was done on samples of zircaloy cladding from fuel rods of up to 64,000 MWD/MTU burnup. The test conditions are summarized below:

Stress: 320 MPa to 630 MPa
Temperature: 300°C to 370°C
Time: 2 to 189 hrs

The fourth source of data is from the low temperature creep testing by Einziger and Kohli [4.A.20] on irradiated Turkey Point fuel rods. A total of five pressurized rods were tested at 323°C for a time period of between 31 to 2,101 hrs, and stress of between 146 MPa to 157 MPa. Four of the rods lost their pressure because of an end cap brazing failure.

The test conditions for the rod (TPD04-H6) that retained its pressure are:

Temperature: 323°C
Stress: 146 MPa

Time: 2,101 hrs
 Cladding Strain: 0.157%

The fifth data source is from the low temperature creep testing by Kaspar et al. [4.A.21] on irradiated KWO samples. The test conditions are:

Temperature: 350°C
 Stress: 50 MPa
 Time: 1,000 to 8,000 hrs

4.A.6 PROPOSED CORRELATION (HOLTEC MODEL)

The experimental data cited in the foregoing provides us with creep data for different stress levels up to about 600 MPa and for different temperatures (up to 400°C). While the database is admittedly not copious, it is adequate to provide the means to establish the coefficients in a creep equation of standard form, which, according to classical creep mechanics [4.A.7; 4.A.19, p. 95] should have the following key characteristics:

- i. The accumulated creep bears a hyperbolic function relationship to the hoop stress, σ , i.e.,

$$\epsilon \sim \sinh(\gamma\sigma)$$

- ii. The temperature dependence (T) of the accumulated creep follows the Arrhenius equation; $\epsilon \sim \exp\left(-\frac{\zeta}{RT}\right)$

where ζ is the activation energy, R is the universal gas constant, and T is the absolute temperature.

- iii. Recognizing that the test data exhibits continuously decreasing creep rate (i.e., the slope of the creep-time curve is continuously decreasing), the correlation should be appropriate for primary creep of the form $\epsilon \sim \tau^\beta$ where $\beta < 1$, and τ is the time coordinate.

In other words, the Holtec creep model constructed from the above three functional elements is of the form:

$$\epsilon = \alpha \exp\left(-\frac{\zeta}{RT}\right) \sinh(\gamma\sigma) \tau^\beta \quad (13)$$

where α , ζ , γ , and β are creep constants with values suitably selected to bound all relevant irradiated cladding creep data and R is the Universal Gas constant (8.31 J/(g-mol°K)). Differentiating ϵ with τ will give the rate of creep, ϕ , as a function of time.

$$\phi = \frac{d\varepsilon}{d\tau} \quad (14)$$

The correlation provided in Equation (13) is applicable in the primary creep stage. Creep is assumed to transition into the secondary regime when ε reaches 0.5%.

Figures 4.A.2-4.A.5 show the creep rate predicted by the proposed Holtec creep model against the previously discussed test data. Five principal sources of creep data are identified for benchmarking the creep model. The first data source is shown plotted in Figure 4.A.2 from the Spilker et al. experiments on irradiated fuel rods. The second data source is the Kaspar et al. irradiated cladding creep strain results shown plotted in Figure 4.A.3. The third source of data is by Goll et al. [4.A.10]. The data from the first two sources was essentially at constant stress and temperature and strain was measured at several instants in time. The family of creep strain vs. time relationships are therefore amenable to a graphical representation in a single plot. In contrast, the Goll et al. data is a single creep strain measurement at the end of each experiment at a stress and temperature that was different in each experiment. The stress and temperature range for the experiments covered a large band (320 to 630 MPa & 300 to 370°C). Therefore, to display the benchmark results from the collected data, a scatter plot of the experimental creep strain vs. Holtec model creep strain is provided in Figure 4.A.4. A straight line representing the ordinate equal to experimental creep strain is shown to aid the reader in confirming that in *all* cases the Holtec model correlates with the measured creep strain with suitable margins.

For the Einziger and Kohli [4.A.20] creep strain data on the intact TPD04-H6 rod sample, the Holtec Creep Model computes a creep strain of 0.191%. This bounds the measured creep strain of 0.157% by a respectable margin (21.6%). A comparison of the Holtec creep model predictions for the KWO creep testing conditions [Kaspar et al., 4.A.21] is shown in Figure 4.A.5. The Holtec predictions bound the KWO creep curve over the range of time (0 to 8,000 hrs). In the 4,000 to 8,000 hrs time interval, the Holtec model exhibits a diverging trend from the KWO creep curve in the conservative direction. In other words, the slope of the Holtec creep model is steeper than the Kaspar et al. creep curve. Thus, creep strain beyond 8,000 hrs is overestimated by the Holtec creep model.

It is quite obvious from the foregoing that the proposed correlation accords well with the available test data, bounding some with large margins. It is thus established that the proposed creep equation is suitable to bound (not predict) the rate of creep that high burnup fuel in dry storage will sustain with the passage of time.

4.A.7 APPLICATION TO STORAGE IN HI-STORM

Equation (13) provides an appropriate vehicle for computing the accumulated creep over a time, say τ^* , if the stress σ and metal temperature, T , are known. If σ and T are varying with time, then the accumulated creep ε will be calculated by integrating the rate of creep ϕ ($\phi = d\varepsilon/d\tau$) over

the time period in dry storage. Therefore, in the HI-STORM system, where σ and T decrease with time, the total creep ϵ is computed by

$$\epsilon = \int_0^T \phi \, d\tau \quad (15)$$

where
$$\phi = \frac{d\epsilon}{d\tau}$$

ϵ is given by Equation (13). The creep rate, ϕ , like ϵ , is a function of σ and T .

Hoop stress is directly proportional to internal pressure, which itself is a function of the gas temperature. The fuel temperatures in dry storage casks like the HI-STORM system, however, are not constant but rather decrease over the duration of the dry storage period. To accurately predict the fuel cladding creep strain, this time-varying temperature behavior must be properly incorporated.

It is recognized that the stress σ in a fuel rod will depend on its radius to cladding thickness ratio and internal pressure. Referring to the table of SNF types (Tables 4.3.3 and 4.3.6), it is evident that the r/t ratio varies widely among the various SNF types. To establish a common peak cladding temperature (PCT) limit for all SNF of a given type, we select one upper bound r/t ratio for PWR fuel and one for BWR fuel so that all SNF types included in this FSAR are covered. We assume:

$$w = r/t = 10.5 \text{ (PWR fuel)} \quad (16a)$$

$$w = r/t = 9.5 \text{ (BWR fuel)} \quad (16b)$$

For a specific SNF, defined by cladding thickness t_g and internal radius r , Equations 16a and 16b imply that a certain amount of its wall thickness, Δ , is not recognized in the hoop stress computation. Δ is given by:

$$\text{For PWR fuel; } \Delta = t_g - \frac{r}{10.5} \quad (17a)$$

$$\text{For BWR fuel; } \Delta = t_g - \frac{r}{9.5} \quad (17b)$$

Δ represents the cladding unused thickness not accounted for in the creep analysis and, hence, can be viewed as the "corrosion reserve" in the specific SNF type. Having defined an upper bound r/t , we now need to use an upper bound internal pressure at the start of dry storage to establish the hoop stress, σ , at the beginning of dry storage. In Section 4.3.1, the upper bound of the internal pressure p_r is set at 2,000 psi and 1,000 psi, respectively, for PWR and BWR SNF at

the reference temperature θ_r ($\theta_r = 387^\circ\text{C}$ (PWR), 311°C (BWR)). Both the PWR and BWR cladding internal pressure values, as discussed in Section 4.3.1, are quite conservative.

The stress in the fuel cladding is given by the Lamé's formula (Equation (1)).

Using the r/t value given by Equations (16a) and (16b) above, the hoop stress in the cladding at the gas temperature, θ_r , is given as:

$$\begin{aligned}\sigma &= (10.5) (2,000) = \del{20,500} 21,000 \text{ psi or } 144.7 \text{ MPa (PWR)} \\ &= (9.5) (1,000) = 9,500 \text{ psi or } 65.5 \text{ MPa (BWR)}\end{aligned}\tag{18}$$

In the next step it is necessary to define the variation of hoop stress σ with time. The internal pressure, p , in the fuel rod (and, therefore, σ through Lamé's equation) will decrease with the passage of time due to two discrete effects: (i) creep-induced increase in the cladding diameter explained in Equation (7) and Subsection 4.A.3 above, and (ii) reduction in the bulk temperature of the contained gas due to the monotonic decline in the heat generated by the stored SNF.

For conservatism, the creep-induced pressure reduction is neglected completely. The reduction in the cladding internal pressure due to the continuing reduction in the heat emission rate is determined by ascertaining the rod bulk gas temperature, θ , as a function of time (in storage in HI-STORM).

The internal gas pressure p corresponding to gas temperature θ (in $^\circ\text{C}$) is given by the perfect gas law

$$p = \frac{p_r (\theta + 273)}{(\theta_r + 273)}\tag{19}$$

where $p_r = 2,000$ psi and $1,000$ psi for PWR and BWR SNF, respectively.

Using Equation (1), the corresponding stress σ is given by

$$\sigma = \frac{p_r (\theta + 273)}{(\theta_r + 273)} \frac{r}{t}\tag{20}$$

It is recognized that both the cladding temperature, T , and gas temperature, θ , depend on the system heat generation rate, Q , and the thermal characteristics of the storage system (HI-STORM). Because the HI-STORM system is certified to store a large array of PWR and BWR SNF types, it is necessary that the T and θ functions be defined in a conservative manner to bound all SNF types (a conservative T or θ function means one whose attenuation with time is "less steep" than all SNF types covered by the CoC.) For this purpose, we must first define the heat generation decay function (η) in a conservative manner. Recognizing that the $Q(\tau)$ function

will attenuate least rapidly with time, τ , for bounding burnup (b) and uranium content in the SNF, we select $b=70$ 75 GWD/MTU and the B&W 15x15 SNF (uranium content = 495 kg) as the reference PWR SNF. Henceforth, we will refer the SNF with the bounding burnup and uranium content simply as the “bounding SNF”. For the same reason, we select GE 7x7 as the reference BWR SNF. The η functions for the reference PWR and BWR SNF are shown in Figure 4.A.6 and 4.A.7, respectively. In Figures 4.A.6 and 4.A.7, η is plotted as the ratio of heat generation of the “bounding SNF” to that at PCDT = 5 years.

In the next step, the HI-STORM 100 thermal model (described in Chapter 4) was used for discrete values of Q to determine T and θ as a function of Q . Strictly speaking, the T and θ functions will be very slightly different for the different MPC types (because of the small differences in their gross heat dissipation capacities). The analytical (curve fit) relationships developed for $T(Q)$ and $\theta(Q)$ are accordingly developed to bound the curves obtained by the HI-STORM thermal model analysis. Figure 4.A.8 shows the postulated $T(Q)$ curve and the computed $T(Q)$ curve using FLUENT for MPC-24 to illustrate the conservatism*. Likewise, Figure 4.A.9 shows the postulated $\theta(Q)$ curve and the computed $\theta(Q)$ using FLUENT for hottest PWR canister (MPC-24). $T(Q)$ and $\theta(Q)$ plots for BWR fuel are provided in Figures 4.A.10 and 4.A.11.

These enveloping $\theta(Q)$ and $T(Q)$ curves along with the appropriate $\eta(\tau)$ curve (Figure 4.A.6 for PWR SNF and Figure 4.A.7 for BWR SNF) are essential for utilizing the Holtec creep model. The T curve (cladding metal temperature), of course, is the direct input variable in the creep equation. The θ curve, through Equation (20), provides the means to compute the hoop stress, σ , as a function of the time coordinate.

The procedure to compute the peak cladding temperature (PCT) limit using the creep equation (Equation 13) for the HI-STORM system to store an MPC containing SNF of a certain age (post-core decay time (PCDT)) can now be outlined.

Let τ_0 denote the PCDT at which the SNF is placed in dry storage in HI-STORM. The object is to calculate the PCT, T_p , such that the accumulated creep in 40 years of storage is 1%.

In other words, the mathematical problem resolves to computing T at $\tau = \tau_0$ such that ϵ_s is 1%; i.e.,

Determine T at $\tau = \tau_0$ such that

$$\epsilon_s = \int_{\tau_0}^{\tau_0 + \tau} \phi(\sigma, T) d\tau \leq 1\% \quad (21)$$

* The FLUENT curves depicted in the $T(Q)$ and $\theta(Q)$ plots do not recognize the relaxation of certain elements of conservatism in the thermal solutions (See Chapter 4, Section 4.1 and Appendix 4.B). Therefore the conservative margins are understated in these plots.

where τ_0 is the PCDT at which the SNF is placed in dry storage, $\tau^* =$ the design life of 40 years.

The problem of determining the permissible initial cladding temperature T_p when the fuel is placed in dry storage such that the value of the integral (in Equation 21) is equal to 1% requires an iterative analysis with assumed values of the initial fuel cladding temperature, T_0 . The computation proceeds as follows:

- i. Assume a value of the peak cladding temperature at τ_0 (say T_0). (τ_0 is the post-core decay time at which the SNF is placed into dry storage)
- ii. Use the T-Q curve (Figure 4.A.8 or 4.A.10, as applicable) to obtain the associated value of the heat generation rate, Q_0 .
- iii. From Figure 4.A.9 or 4.A.11 as applicable, obtain the associated value of the gas temperature, θ_0 . Equation (20) provides the associated hoop stress, σ_0 .
- iv. With T_0 and σ_0 defined, the rate of creep, ϕ , is provided by Equation (14).
- v. To compute the value of ϕ , at the next time step ($\tau_0 + \Delta\tau$), updated values of σ and T are required. For this purpose, the coincident heat generation rate Q is obtained by using Figure 4.A.6 or 4.A.7, as applicable, which provides Q at any time τ through the simple algebraic relationship

$$Q = \frac{Q_0 \eta}{\eta_0} \quad (22)$$

where η is the value of the dimensionless heat generation rate at the PCDT of interest, and η_0 is the corresponding value at τ_0 (PCDT at the initiation of dry storage). Figure 4.A.8 (or 4.A.10) and 4.A.9 (or 4.A.11), respectively, provide the associated T and θ . Equation (20) provides the associated σ . This process is repeated at incremental time steps. In this manner, time history of σ and T as a function of τ (starting at σ_0 and T_0 computed for $\tau = \tau_0$) is obtained for the 40-year duration.

- vi. Equation (21) is used to compute the total accumulated creep, ϵ_s , in 40 years ($\tau^* = 40$ years).
- vii. If the value of ϵ_s is greater than 1%, then the initial assumed value of the peak cladding temperature, T_0 , is appropriately adjusted and the calculation returns to Step (i) above.

- viii. The process is repeated until the computed ϵ_s is close to 1% within a small tolerance (set equal to 0.001) in the numerical analysis. The converged value of T_o is the permissible cladding temperature (T_p) for fuel placed in dry storage at $PCDT = \tau_o$.

4.A.8 ALLOWABLE CLAD TEMPERATURE LIMITS

Using the Holtec creep model described in the preceding section, allowable peak clad temperature limits for high-burnup fuel assemblies (75,000 MWD/MTU (PWR) and 70,000 MWD/MTU (BWR)) have been determined. These calculated temperature limits are presented in Table 4.A.1, below.

Table 4.A.1
Allowable Peak Clad Temperature Limits for High Burnup Fuel from Holtec Creep Model

Fuel Age at Initial Loading	PWR Fuel Limit	BWR Fuel Limit
5 years	361.55°C [682.79°F] 361.37 [682.47]	397.63°C [747.73°F]
6 years	358.00°C [676.40°F] 357.50 [675.50]	393.49°C [740.28°F]
7 years	354.80°C [670.64°F] 354.84 [670.71]	390.26°C [734.47°F]
10 years	349.15°C [660.47°F] 349.23 [660.61]	384.49°C [724.08°F]
15 years	345.78°C [654.40°F] 345.94 [654.69]	380.95°C [717.71°F]

The temperature limits in Table 4.A.1, it should be recalled, are obtained using a most conservative equation of state for creep, a bounding value of internal gas pressure at the start of fuel storage, an upper bound value for cladding radius-to-thickness ratio (10.5 for PWR and 9.5 for BWR fuel), and a 1% limit on creep deformation in 40 years of storage. To build in even additional margins in the allowable heat load for the MPCs, the PCT limit is further reduced, as shown in Table 4.A.2. The values in Table 4.A.2 are the ones used in the thermal analysis in Chapter 4. The PCT limits in Table 4.A.2, as can be ascertained by direct comparison with Table 4.A.1, are as much as 39.85°C less. This additional margin in the PCT limits, admittedly not typical in dry storage applications, has been provided as a first step in addressing the issue of dry storage of high burnup fuel, and may be re-visited.

Table 4.A.2
High Burnup Fuel Allowable Peak Clad Temperature Limits Used in the Thermal Analysis
in Chapter 4

Fuel Age at Initial Loading	PWR Fuel Limit	BWR Fuel Limit
5 years	359.7°C [679°F]	393.2°C [740°F]
6 years	348.7°C [660°F]	377.9°C [712°F]
7 years	335.0°C [635°F]	353.7°C [669°F]
10 years	327.2°C [621°F]	347.9°C [658°F]
15 years	321.9°C [611°F]	341.1°C [646°F]

4.A.9 INTACT AND DAMAGED FUEL

ISG-15 requires that for a fuel assembly to be considered intact, the following criteria must be met:

- “A1. No more than 1% of the rods in the assembly have peak cladding oxide thicknesses greater than 80 micrometers.
- A2. No more than 3% of the rods in the assembly have peak cladding oxide thicknesses greater than 70 micrometers.”

ISG-15 provides the bases for the conditions and guidelines presented above. The limits on cladding oxide thickness are intended to ensure that the hydrogen concentration in the cladding micro-structure does not exceed 400 to 500 parts per million. The creep strain limit of 1%, along with hydrogen concentration limits, are intended to ensure that cladding perforation does not occur. Specifically, ISG-15 states:

“The staff believes that Zircaloy cladding can withstand uniform creep strains (i.e., creep prior to tertiary or accelerating creep strain rates) of about 1% before the cladding can become perforated if the average hydrogen concentration in the cladding is less than about 400 to 500 parts per million (ppm). This amount of hydrogen corresponds to an oxide thickness of approximately 70-80 micrometers using the recommended hydrogen pickup fraction of 0.15 from Lanning, et al, and Garde. The staff also believes that the strength and ductility of irradiated Zircaloy do not appear to be significantly affected by corrosion-induced hydrides at hydrogen concentrations up to approximately 400 ppm.

According to ISG-15, the thickness of the cladding oxide layer needs to be determined prior to loading for high burnup fuel. Only those high-burnup fuel assemblies that meet both of the oxidation conditions presented above may be stored as intact; all other assemblies must be treated as potentially damaged fuel. This, as we discuss below, is an overly restrictive

requirement, which has prompted Holtec to propose an alternative criterion for damaged fuel as an approved deviation from this regulatory guidance.

Available cladding thickness measurement data on high burnup SNF is quite sparse. However, recent data collected by a Westinghouse PWR owner indicates that the oxidation-induced cladding metal loss can be well in excess of 80 μ m in a substantial fraction of the population of high burnup fuel. All fuel rods that had experienced a heavy oxide corrosion, however, were found to be intact, i.e., none exhibited loss of pressure boundary integrity. Corrosion data compiled in Japan [4.A.23] reproduced in Figures 4.A.12 and 13 show that the corrosion loss increases rapidly with increasing burnup. In view of the data in Figures 4.A.12 and 13, applying the ISG-15 criteria will a priori consign hundreds of undamaged, high burnup fuel assemblies already stored in the plant's fuel pool to the potentially damaged category. This experience is sure to be repeated at other plants when measurements are taken. Clearly, the oxidation threshold for defining damaged SNF warrants additional consideration.

To propose a technically sound cladding corrosion limit, we must consider two underlying facts, namely: (i) the collateral effect of cladding oxidation on its creep capacity and (ii) the increase in circumferential stress due to loss in the cladding wall thickness.

The effect of cladding oxidation on the creep limit of the cladding material has been assayed by EPRI [4.A.18]. EPRI recommends a 2% creep strain limit for high burnup fuel that may have sustained spallation in the reactor core. Our proposed strain limit of 1% quite clearly provides a significant additional margin over the EPRI/NEI recommendation.

If the 1% creep strain limit is accepted for the spalled cladding, then it is possible to define the acceptable metal loss (oxidation loss) using the hoop stress as the guiding parameter. It is recalled that the computation of the creep strain in Section 4.A.8 in the foregoing has been performed for $\sigma_0 = 144.7$ MPa for PWR SNF and 65.5 MPa for BWR SNF, where σ_0 = the hoop stress in the fuel cladding at the beginning of dry storage. Furthermore, the internal gas pressure in the cladding, at the beginning of dry storage, p_0 , has been assumed to be equal to 2000 psi and 1000 psi for PWR and BWR SNF, respectively. Using Lamé's formula, the maximum cladding stress (σ_0) is computed as the product of p and cladding radius to thickness ratio, w . The value of w has been set as 10.5 and 9.5 for PWR and BWR fuel, respectively, in the calculation of accumulated creep (Section 4.A.8).

In other words, the initial stress σ_0 used in the creep analysis in this appendix uses the limiting values of p and r/t as shown in Table 4.A.3.

Table 4.A.3

Assumed Pressure Geometry Parameters for Creep Analysis

	Internal Pressure at the Start of Storage	w = r/t	Stress σ_0 Computed by Lame Formula
PWR Fuel	2,000 psi	10.5	144.7 MPa
BWR Fuel	1,000 psi	9.5	65.5 MPa

PWR and BWR fuel assemblies used in commercial reactors in the U.S. have lower values of w than the number used in the creep analysis herein (Table 4.A.3). The metal wall in the as-fabricated fuel in excess of that implied by the value of w in the above table therefore is the available corrosion allowance, Δ . Tables 4.A.4 and 4.A.5 provide the values of Δ using Equation (17) for different PWR and BWR fuel classes using the thinnest cladding assembly type within each class (fuel assembly types in any one class have the same rod O.D. and pitch, but may have different cladding thicknesses). It is evident from these tables that the available Δ in all fuel assembly array/classes is well in excess of 100 μ m.

In view of the information presented in the foregoing, it is proposed that the permitted maximum cladding corrosion be specified so that the value of w in Table 4.A.3 for high burnup fuel is preserved.

Table 4.A.4

Available Corrosion Reserve in PWR Fuel Cladding

Holtec Fuel Assembly Array/Class*	Nominal Cladding Outer Diameter (in.)	Nominal Cladding Thickness (in.)	Available Corrosion* Reserve (μm),Δ
14x14A	0.4	0.0243	192
14x14B	0.422	0.0243	165
14x14C	0.44	0.026	191
15x15A	0.418	0.026	217
15x15B	0.42	0.024	159
15x15C	0.424	0.03	321
15x15D	0.43	0.025	175
15x15E	0.428	0.0245	163
15x15F	0.428	0.023	122

* Any form of corrosion that produces non-adherent (flaked or spalled) metal layers should be considered to be lost for load (pressure) bearing purposes.

Table 4.A.4

Available Corrosion Reserve in PWR Fuel Cladding

Holtec Fuel Assembly Array/Class*	Nominal Cladding Outer Diameter (in.)	Nominal Cladding Thickness (in.)	Available Corrosion* Reserve (μm),Δ
15×15H	0.414	0.022	111
16×16A	0.382	0.025	233
17×17A	0.36	0.0225	190
17×17B	0.372	0.0205	120
17×17C	0.377	0.022	156

* Fuel Assembly Array Classes are defined in Section 6.2

Table 4.A.5

Available Corrosion Reserve in BWR Fuel Cladding

Holtec Fuel Assembly Array/Class*	Nominal Cladding Outer Diameter (in.)	Nominal Cladding Thickness (in.)	Available Corrosion* Reserve (μm),Δ
7×7B	0.563	0.032	145
8×8B	0.493	0.034	295
8×8C	0.483	0.032	252
8×8D	0.483	0.03	196
8×8E	0.493	0.034	295
9×9A	0.440	0.028	197
9×9B	0.433	0.026	151
9×9C	0.423	0.0295	262
9×9D	0.424	0.03	275
9×9E	0.417	0.0265	186
9×9F	0.417	0.0265	186
9×9G	0.424	0.03	275
10×10A	0.404	0.026	189

* Any form of corrosion that produces non-adherent (flaked or spalled) metal layers should be considered to be lost for load (pressure) bearing purposes.

Table 4.A.5

Available Corrosion Reserve in BWR Fuel Cladding

Holtec Fuel Assembly Array/Class*	Nominal Cladding Outer Diameter (in.)	Nominal Cladding Thickness (in.)	Available Corrosion* Reserve (μm), Δ
10x10B	0.3957	0.0239	141
10x10C	0.378	0.0243	176

* Fuel Assembly Array Classes are defined in Section 6.2

4.A.10 CLOSURE

A mathematical relationship to conservatively estimate the extent of primary creep in the irradiated zircaloy cladding has been proposed. The form of proposed creep equation is consistent with the classical metal creep formulation wherein the two principal variables, stress and temperature, respectively, bear an exponential and Arrhenius-type relationship to creep accumulation. The creep equation has been validated against available irradiated cladding creep data and shown to correlated with the measured data in the temperature range (300 to 400°C) and stress range (70 MPa – 630 MPa) with considerable margins. This benchmarked creep equation is used to compute the PCT limits for SNF placed in dry storage after a given amount of time in wet storage (wet storage time is also referred to as “fuel age”). In computing the PCT limits, several assumptions have been made to render a conservative prediction. The key conservatisms (in addition to the use of a creep equation that overpredicts creep for a given stress and temperature) are:

- i. The maximum permissible creep is set at 1%.
- ii. The internal pressure (hence the hoop stress) in the cladding is assumed to remain unchanged due to the creep induced dilation of the rod radius (Equation 7 in Subsection 4.A.3).
- iii. The primary creep that is characterized by a monotonically decreasing creep rate with time is assumed to cease when 0.5% creep has been accumulated and the transition to secondary creep is assumed to begin. Thereafter, the creep rate is conservatively held constant for constant stress and temperature.
- iv. The bounding burnup of 70 and 75 GWD/MTU is used to construct the relationship for decay of heat generation from the BWR and PWR stored spent nuclear fuel respectively (Figure 4.A.6 and 4.A.7).
- v. The assumed internal rod pressure, which directly affects the level of hoop stress, has been set at a bounding high value for both PWR and BWR SNF.

4.A.11 NOMENCLATURE

- K_{IC} : Fracture Toughness
- p : Internal gas pressure in the fuel rod
- Q : The total heat generation in the HI-STORM 100 MPC.
- r : Inside radius of the fuel rod
- T : Peak cladding temperature
- t : Cladding wall thickness recognized in the hoop stress calculation
- t_g : Nominal thickness of the fuel cladding
- w : Ratio of r to t
- ϵ : Accumulated creep in dry storage (%)
- ϵ_s : Total accumulated creep in 40 years of storage (%)
- τ : Post Core Decay Time (PCTD), i.e., the time elapsed after reactor shutdown
- τ_o : PCDT at the time the SNF is placed in dry storage (also known as “fuel age”)
- θ : Bulk gas temperature in the fuel rod, °C
- ϕ : Rate of creep
- σ : Hoop stress in the fuel cladding
- η : Ratio of $Q(\tau)$ to Q_o

Subscripts

- o : Value of the variable at $\tau = \tau_o$
- a : Ambient
- r : Reference point

4.A.12 REFERENCES

- [4.A.1] “Standard Review Plan for Dry Cask Storage Systems,” NUREG-1536, January 1997.
- [4.A.2] USNRC Interim Staff Guidance -15, “Materials Evaluation,” Revision 0, January 10, 2001.
- [4.A.3] Spilker et al., “Spent LWR fuel dry storage in large transport and storage casks after extended burnup,” *Journal of Nuclear Materials* 250 (1997) 63-74.
- [4.A.4] Peehs, Martin, “Assessment of Dry Storage Performance of Spent LWR Fuel Assemblies with Increasing Burn-Up,” CRP on Spent Fuel Performance Assessment and Research (SPAR): 1st RCM in Washington D.C., April 20 through 24, 1998.
- [4.A.5] Gilbert et al., “Technical Evaluation Report of WCAP-15168 (Dry Storage of High Burnup Spent Nuclear Fuel),” PNNL, February 2000.
- [4.A.6] Levy et al., “Recommended Temperature Limits for Dry Storage of Spent Light Water Reactor Zircaloy-Clad Fuel Rods in Inert Gas,” PNL-6189, May 1987.
- [4.A.7] Lin, T.H., “Theory of Inelastic Structures”, Wiley (1968).
- [4.A.8] M.A. Meyers and K.K. Chawla, “Mechanical Metallurgy”, Chapter 20, page 667, Prentice Hall (1984).
- [4.A.9] “Storage and Transportation of Spent LWR Fuel Having Burnup in Excess of 45 GWD/MTU”, NEI submittal to the SFPO dated October 2, 2000 (L. Hendricks to E.W. Brach).
- [4.A.10] W. Goll et al., “Short-Time Creep and Rupture Tests on High Burnup Fuel Rod Cladding, *Journal of Nuclear Materials*”, to be published.
- [4.A.11] Garde, A.M., Smith, G.P. and Pirek, R.C., “Effects of Hydride Precipitate Localization and Neutron Fluence on the Ductility of Irradiated Zircaloy-4”, ASTM, STP 1295 (1996) pp 407-428.
- [4.A.12] J.H. Schemel, “ASTM Manual Zirconium and Hafnium”, STP 639, ASTM (1977).
- [4.A.13] Zirconium in the Nuclear Industry, ASTM 1354, edited by G.P. Sabol and G.D. Moan (January 2000).

- [4.A.14] J.A.L. Robertson, "Learning from History: A Case Study in Nuclear Fuel", ASTM STP 1295, edited by E.R. Bradley and G.A. Sabol (1996).
- [4.A.15] Montgomery R.O. and Rashid Y.R., "Evaluation of Irradiated Fuel During RIA Simulation Tests", EPRI TR-106387, August 1996.
- [4.A.16] Rashid, Y.R., "Montgomery R.O. and Yang, R.L., "A Cladding Failure Model for Fuel Rods Subjected to Operational and Accident Transients", IAEA Specialists Meeting on Fuel Modeling, Windmere, U.K., June 2000.
- [4.A.17] J. Jarheiff, R., Manzel, and E. Ortlieb, "Influence of Hydrogen Content and Irradiation on the Mechanical Behavior of Fuel Assembly Structural Members Made of Zircaloy", 1993, Annual Nuclear Engineering Convention, Cologne, Germany, May 1993.
- [4.A.18] EPRI Report 1001207, "Creep As the Limiting Mechanism for Spent Fuel Dry Storage" (Progress Report, December, 2000).
- [4.A.19] Franklin, D.G., Lucas G.E. and Bement, A.L., "Creep of Zirconium Alloys in Nuclear Reactors", ASTM STP 815 (1985).
- [4.A.20] "Low-Temperature Rupture Behavior of Zircaloy-clad Pressurized Water Reactor Spent Fuel Rods Under Dry Storage Conditions," R.E. Einziger and R. Kohli, Nuclear Technology, Vol. 67, Oct. 1984, 107-123.
- [4.A.21] "Release of Fission Products and Post-Pile Creep Behavior of Irradiated Fuel Rods Stored Under Dry Conditions", Kaspar et al., BMFT-KWA 2100 BO, 1985, Erlangen, Germany.
- [4.A.22] "Dry Storage of High Burnup Spent Nuclear Fuel", (Wesflex Docket 72-1026), WCAP-15211, (page 4-20).
- [4.A.23] Inter Company Communication from T. Miyazaki, Manager Nuclear Fuel Cycle Group, Kansai Electric Power Co. to K. P. Singh, Holtec International, Dated December 26, 2000.

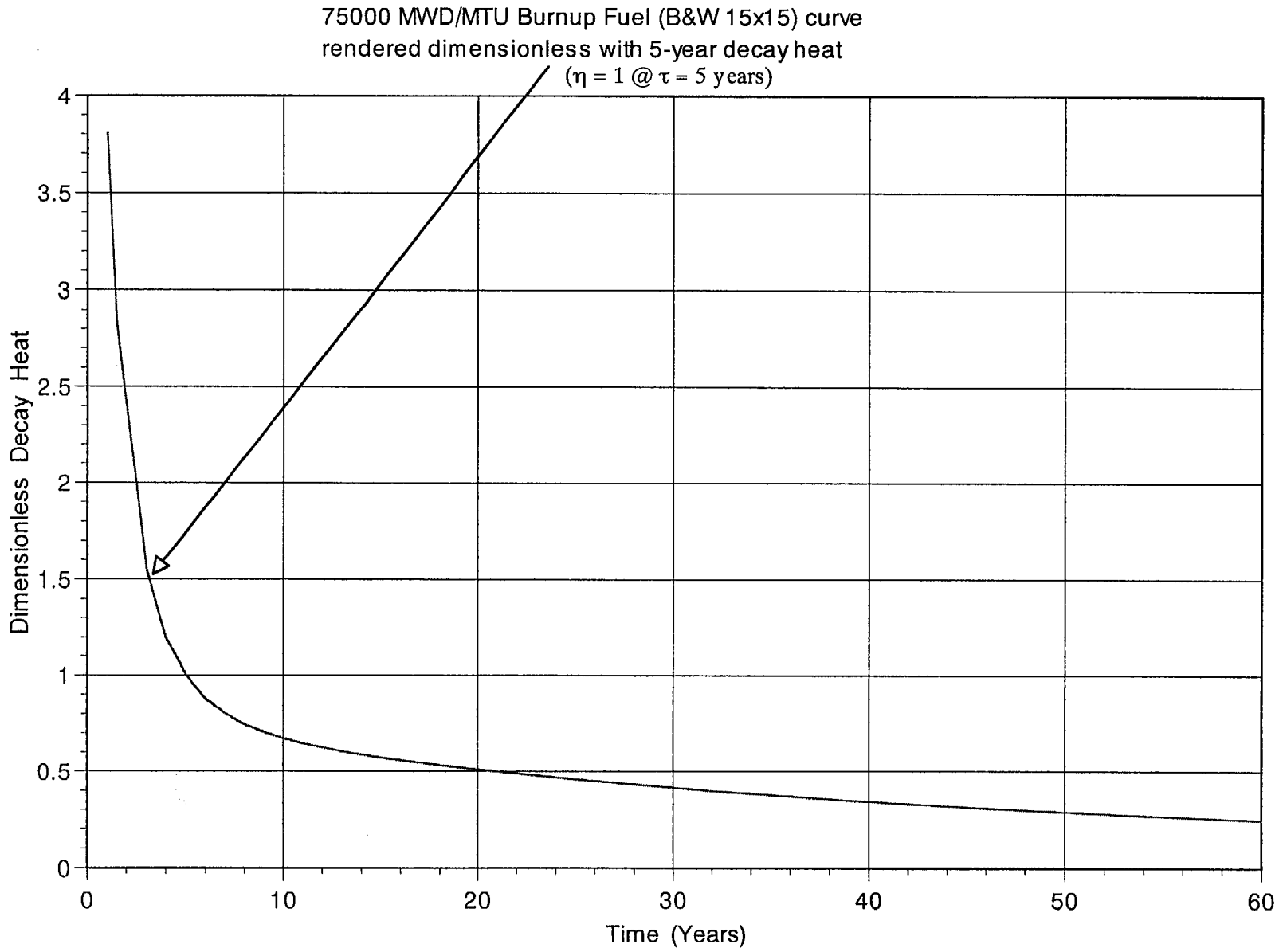


FIGURE 4.A.6: PWR FUEL DECAY HEAT VS. POST CORE DECAY TIME

APPENDIX 4.B: CONSERVATISMS IN THE THERMAL ANALYSIS OF THE HI-STORM 100 SYSTEM

4.B.1 OVERVIEW OF CASK HEAT REMOVAL SYSTEM

The HI-STORM 100 overpack is a large, cylindrical structure with an internal cavity suited for emplacement of a cylindrical canister containing spent nuclear fuel (SNF). The canister is arrayed in an upright manner inside the vertically oriented overpack. The design of the system provides for a small radial gap between the canister and the cylindrical overpack cavity. One principal function of a fuel storage system is to provide a means for ensuring fuel cladding integrity under long-term storage periods (20 years or more). The HI-STORM 100 overpack is equipped with four large ducts near its bottom and top extremities. The ducted overpack construction, together with an engineered annular space between the MPC cylinder and internal cavity in the HI-STORM 100 overpack structure, ensures a passive means of heat dissipation from the stored fuel via ventilation action (i.e., natural circulation of air in the canister-to-overpack annulus). In this manner a large structure physically interposed between the hot canister and ambient air (viz. the concrete overpack engineered for radiation protection) is rendered as an air flow device for convective heat dissipation. The pertinent design features producing the air ventilation ("chimney effect") in the HI-STORM 100 cask are shown in Figure 4.B.1.

A great bulk of the heat emitted by the SNF is rejected to the environment (Q_1) by convective action. A small quantity of the total heat rejection occurs by natural convection and radiation from the surface of the overpack (Q_2), and an even smaller amount is dissipated by conduction to the concrete pad upon which the HI-STORM 100 overpack is placed (Q_3). From the energy conservation principle, the sum of heat dissipation to all sinks (convective cooling (Q_1), surface cooling (Q_2) and cooling to pad (Q_3)) equals the sum of decay heat emitted from the fuel stored in the canister (Q_d) and the heat deposited by insolation, Q_s (i.e., $Q_d + Q_s = Q_1 + Q_2 + Q_3$). This situation is illustrated in Figure 4.B.2. In the HI-STORM 100 System, Q_1 is by far the dominant mode of heat removal, accounting for well over 80% of the decay heat conveyed to the external environment. Figure 4.B.3 shows the relative portions of Q_d transferred to the environs via Q_1 , Q_2 , and Q_3 in the HI-STORM 100 System under the design basis heat load.

The heat removal through convection, Q_1 , is similar to the manner in which a fireplace chimney functions: Air is heated in the annulus between the canister and the overpack through contact with the canister's hot cylindrical surface causing it to flow upward toward the top (exit) ducts and inducing the suction of the ambient air through the bottom ducts. The flow of air sweeping past the cylindrical surfaces of the canister has sufficient velocity to create turbulence that aids in the heat extraction process. It is readily recognized that the chimney action relies on a fundamental and immutable property of air, namely that air becomes lighter (i.e., more buoyant) as it is heated. If the canister contained no heat emitting fuel, then there would be no means for the annulus air to heat and rise. Similarly, increasing the quantity of heat produced in the

canister would make more heat available for heating of annulus air, resulting in a more vigorous chimney action. Because the heat energy of the spent nuclear fuel itself actuates the chimney action, ventilated overpacks of the HI-STORM 100 genre are considered absolutely safe against thermal malfunction. While the removal of heat through convective mass transport of air is the dominant mechanism, other minor components, labeled Q_2 and Q_3 in the foregoing, are recognized and quantified in the thermal analysis of the HI-STORM 100 System.

Heat dissipation from the exposed surfaces of the overpack, Q_2 , occur principally by natural convection and radiation cooling. The rate of decay heat dissipation from the external surfaces is, of course, influenced by several factors, some of which aid the process (e.g., wind, thermal turbulence of air), while others oppose it (for example, radiant heating by the sun or blocking of radiation cooling by surrounding casks). In this appendix, the relative significance of Q_2 and Q_3 and the method to conservatively simulate their effect in the HI-STORM 100 thermal model is discussed.

The thermal problem posed for the HI-STORM 100 System in the system's Final Safety Analysis Report (FSAR) is as follows: Given a specified maximum fuel cladding temperature, T_c , and a specified ambient temperature, T_a what is the maximum permissible heat generation rate Q_d , in the canister under steady state conditions? Of course, in the real world, the ambient temperature, T_a , varies continuously, and the cask system is rarely in a steady state (i.e., temperatures vary with time). Fortunately, fracture mechanics of spent fuel cladding instruct us that it is the time-integrated effect of elevated temperature, rather than an instantaneous peak value, that determines whether fuel cladding would rupture. The most appropriate reference ambient temperature for cladding integrity evaluation, therefore, is the average ambient temperature for the entire duration of dry storage. For conservatism, the reference ambient temperature is, however, selected to be the maximum yearly average for the ISFSI site. In the general certification of HI-STORM 100, the reference ambient temperature (formally referred to as the normal temperature) is set equal to 80°F, which is greater than the annual average for any power plant location in the U.S.*

The thermal analysis of the cask system leads to a computed value of the fuel cladding temperature greater than T_a by an amount C . In other words, $T_c = T_a + C$, where C decreases slightly as T_a (assumed ambient temperature) is increased. The thermal analysis of HI-STORM 100 is carried out to compute C in a most conservative manner. In other words, the mathematical model seeks to calculate an upper bound on the value of C .

Dry storage scenarios are characterized by relatively large temperature elevations (C) above ambient (650°F or so). The cladding temperature rise is the cumulative sum of temperature increments arising from individual elements of thermal resistance. To protect cladding from overheating, analytical assumptions adversely impacting heat transfer are chosen with particular

* According to the U.S. National Oceanic and Atmospheric Administration (NOAA) publication, "Comparative Climatic Data for the United States through 1998", the highest annual average temperature for any location in the continental U.S. is 77.8°F in Key West, Florida.

attention given to those temperature increments which form the bulk of the temperature rise. In this appendix, the principal conservatisms in the thermal modeling of the HI-STORM 100 System and their underlying theoretical bases are presented. This overview is intended to provide a physical understanding of the large margins buried in the HI-STORM 100 design which are summarized in Section 4.4.6 of this FSAR.

4.B.2 CONSERVATISM IN ENVIRONMENTAL CONDITION SPECIFICATION

The ultimate heat sink for decay heat generated by stored fuel is ambient air. The HI-STORM 100 System defines three ambient temperatures as the environmental conditions for thermal analysis. These are, the Normal (80°F), the Off-Normal (100°F) and Extreme Hot (125°F) conditions. Two factors dictate the stipulation of an ambient temperature for cladding integrity calculations. One factor is that ambient temperatures are constantly cycling on a daily basis (night and day). Furthermore, there are seasonal variations (summer to winter). The other factor is that cladding degradation is an incremental process that, over a long period of time (20 years), has an accumulated damage resulting from an "averaged-out" effect of the environmental temperature history. The 80°F normal temperature stated in the HI-STORM 100 FSAR is defined as the highest annual average temperature at a site established from past records. This is a principal design parameter in the HI-STORM 100 analysis because it establishes the basis for demonstrating long-term SNF integrity. The choice of maximum annual average temperature is conservative for a 20-year period. Based on meteorological data, the 80°F is chosen to bound annual average temperatures reported within the continental US.

For short periods, it is recognized that ambient temperature excursions above 80°F are possible. Two scenarios are postulated and analyzed in the FSAR to bound such transient events. The Off-Normal (100°F) and Extreme Hot (125°F)* cases are postulated as continuous (72-hour average) conditions. Both cases are analyzed as steady-state conditions (i.e., thermal inertia of the considerable concrete mass, fuel and metal completely neglected) occurring at the start of dry storage when the decay heat load to the HI-STORM 100 System is at its peak value with fuel emitting heat at its design basis maximum level.

4.B.3 CONSERVATISM IN MODELING THE ISFSI ARRAY

Traditionally, in the classical treatment of the ventilated storage cask thermal problem, the cask to be analyzed (the subject cask) is modeled as a stand-alone component that rejects heat to the ambient air through chimney action (Q_1) by natural convection to quiescent ambient air and radiation to the surrounding open spaces (Q_2), and finally, a small amount through the concrete pad into the ground (Q_3). The contributing effect of the sun (addition of heat) is considered, but the dissipative effect of wind is neglected. The interchange of radiative heat between proximate casks is also neglected (the so-called "cask-to-cask interactions"). In modeling the HI-STORM

* According to NOAA, the highest daily mean temperature for any location in the continental U.S. is 93.7°F, which occurred in Yuma, Arizona.

100 System, Holtec International extended the classical cask thermal model to include the effect of the neighboring casks in a most conservative manner. This model represents the flow of supply air to the inlet ducts for the subject cask by erecting a cylinder around the subject cask. The model blocks all lateral flow of air from the surrounding space into the subject cask's inlet ducts. This mathematical artifice is illustrated in Figure 4.B.4, where the lateral air flow arrows are shown "dotted" to indicate that the mathematical cylinder constructed around the cask has blocked off the lateral flow of air. Consequently, the chimney air must flow down the annulus from the air plenum space above the casks, turn around at the bottom and enter the inlet ducts. Because the vertical downflow of air introduces additional resistance to flow, an obvious effect of the hypothetical enclosing cylinder construct is an increased total resistance to the chimney flow which, it is recalled, is the main heat conveyance mechanism in a ventilated cask. Throttling of the chimney flow by the hypothetical enclosing cylinder is an element of conservatism in the HI-STORM modeling.

Thus, whereas air flows toward the bottom ducts from areas of supply which are scattered in a three dimensional continuum with partial restriction from neighboring casks, the analytical model blocks the air flow completely from areas outside the hypothetical cylinder. This is illustrated in Figure 4.B.4 in which an impervious boundary is shown to limit HI-STORM 100 cask access to fresh air from an annular opening near the top.

Thus, in the HI-STORM model, the feeder air to the HI-STORM 100 System must flow down the hypothetical annulus sweeping past the external surface of the cask. The ambient air, assumed to enter this hypothetical annulus at the assumed environmental temperature, heats by convective heat extraction from the overpack before reaching the bottom (inlet) ducts. In this manner, the temperature of the feeder air into the ducts is maximized. In reality, the horizontal flow of air in the vicinity of the inlet ducts, suppressed by the enclosed cylinder construct (as shown in Figure 4.B.4) would act to mitigate the pre-heating of the feeder air. By maximizing the extent of air preheating, the computed value of ventilation flow is underestimated in the simulation.

4.B.4 CONSERVATISM IN RADIANT HEAT LOSS

In an array of casks, the external (exposed) cask surfaces have a certain "view" of each other. The extent of view is a function of relative geometrical orientation of the surfaces and presence of other objects between them. The extent of view influences the rate of heat exchange between surfaces by thermal radiation. The presence of neighboring casks also partially blocks the escape of radiant heat from a cask thus affecting its ability to dissipate heat to the environment. This aspect of Radiative Blocking (RB) is illustrated for a reference cask (shown shaded) in Figure 4.B.5. It is also apparent that a cask is a recipient of radiant energy from adjacent casks (Radiant Heating (RH)). Thus, a thermal model representative of a cask array must address the RB and RH effects in a conservative manner. To bound the physical situation, a Hypothetical Reflecting Boundary (HRB) modeling feature is introduced in the thermal model. The HRB feature

surrounds the HI-STORM 100 overpack with a reflecting cylindrical surface with the boundaries insulated.

In Figures 4.B.6 and 4.B.7 the inclusion of RB and RH effects in the HI-STORM 100 modeling is graphically illustrated. Figure 4.B.6 shows that an incident ray of radiant energy leaving the cask surface bounces back from the HRB thus preventing escape (i.e., RB effect maximized). The RH effect is illustrated in Figure 4.B.7 by superimposing on the physical model reflected images of HI-STORM 100 cask surrounding the reference cask. A ray of radiant energy from an adjacent cask directed toward the reference cask (AA) is duplicated by the model via another ray of radiant energy leaving the cask (BB) and being reflected back by the HRB (BA'). A significant feature of this model is that the reflected ray (BA') initiated from a cask surface (reference cask) assumed to be loaded with design basis maximum heat (hottest surface temperature). As the strength of the ray is directly proportional to the fourth power of surface temperature, radiant energy emission from an adjacent cask at a lower heat load will be overestimated by the HRB construct. In other words, the reference cask is assumed to be in an array of casks all producing design basis maximum heat. Clearly, it is physically impossible to load every location of every cask with fuel emitting heat at design basis maximum. Such a spent fuel inventory does not exist. This bounding assumption has the effect of maximizing cask surface temperature as the possibility of "hot" (design basis) casks being radiatively cooled by adjacent casks is precluded. The HRB feature included in the HI-STORM 100 model thus provides a bounding effect of an infinite array of casks, all at design basis maximum heat loads. No radiant heat is permitted to escape the reference cask (bounding effect) and the reflecting boundary mimics incident radiation toward the reference casks around the 360° circumference (bounding effect).

4.B.5 CONSERVATISM IN REPRESENTING BASKET AXIAL RESISTANCE

As stated earlier, the largest fraction of the total resistance to the flow of heat from the spent nuclear fuel (SNF) to the ambient is centered in the basket itself. Out of the total temperature drop of approximately 650°F (C=650°F) between the peak fuel cladding temperature and the ambient, over 400°F occurs in the fuel basket. Therefore, it stands to reason that conservatism in the basket thermal simulation would have a pronounced effect on the conservatism in the final solution. The thermal model of the fuel basket in the HI-STORM 100 FSAR was accordingly constructed with a number of conservative assumptions that are described in the HI-STORM 100 FSAR. We illustrate the significance of the whole array of conservatisms by explaining one in some detail in the following discussion.

It is recognized that the heat emission from a fuel assembly is axially non-uniform. The maximum heat generation occurs at about the mid-height region of the enriched uranium column, and tapers off toward its extremities. The axial heat conduction in the fuel basket would act to diffuse and levelize the temperature field in the basket. The axial conductivity of the basket, quite clearly, is the key determinant in how well the thermal field in the basket would be homogenized. It is also evident that the conduction of heat along the length of the basket occurs

in an uninterrupted manner in a HI-STORM 100 basket because of its continuously welded honeycomb geometry. On the other hand, the in-plane transfer of heat must occur through the physical gaps that exist between the fuel rods, between the fuel assembly and the basket walls and between the basket and the MPC shell. These gaps depress the in-plane conductivity of the basket. However, in the interest of conservatism, the axial conductivity of basket in the HI-STORM 100 thermal model is set equal to the (computed) in-plane conductivity. This assumption has the direct effect of throttling the axial flow of heat and thus of elevating the computed value of mid-height cladding temperature (where the peak temperature occurs) above its actual value. In actuality, the axial conductivity of the fuel basket is much greater than the in-plane conductivity due to the continuity of the fuel and basket structures in that direction. Had the axial conductivity of the basket been modeled less conservatively in the HI-STORM 100 thermal analysis, then the temperature distribution in the basket will be more uniform, i.e., the bottom region of the basket would be hotter than that computed. This means that the temperature of the MPC's external surface in the bottom region is hotter than computed in the HI-STORM 100 analysis. It is a well-known fact in ventilated column design that the lower the location in the column where the heat is introduced, the more vigorous the ventilation action. Therefore, the conservatism in the basket's axial conductivity assumption has the net effect of reducing the computed ventilation rate.

To estimate the conservatism in restricting the basket axial resistance, we perform a numerical exercise using mathematical perturbation techniques. The axial conductivity (K_z) of the MPC is, as explained previously, much higher than the in-plane (K_r) conductivity. The thermal solution to the MPC anisotropic conductivities problem (i.e. K_z and K_r are not equal) is mathematically expressed as a sum of a baseline isotropic solution T_o (setting $K_z = K_r$) and a perturbation T^* which accounts for anisotropic effects. From Fourier's Law of heat conduction in solids, the perturbation equation for T^* is reduced to the following form:

$$K_z \frac{d^2 T^*}{dz^2} = -\Delta K \frac{d^2 T_o}{dz^2}$$

Where, ΔK is the perturbation parameter (i.e. axial conductivity offset $\Delta K = K_z - K_r$). The boundary conditions for the perturbation solution are zero slope at peak cladding temperature location ($dT^*/dz = 0$) (which occurs at about the top of the active fuel height) and $T^* = 0$ at the bottom of the active fuel length. The object of this calculation is to compute T^* where the peak fuel cladding temperature is reached. To this end, the baseline thermal solution T_o (i.e. HI-STORM isotropic modeling solution) is employed to compute an appropriate value for $d^2 T_o/dz^2$ which characterizes the axial temperature rise over the height of the active fuel length in the hottest fuel cell. This is computed as $(-\Delta T_{ax}/L^2)$ where ΔT_{ax} is the fuel cell temperature rise and L is the active fuel length. Conservatively postulating a lower bound ΔT_{ax} of 200°F and L of 12 ft, $d^2 T_o/dz^2$ is computed as $-1.39^\circ\text{F}/\text{ft}^2$. Integrating the perturbation equation shown above, the following formula for T^* is obtained:

$$T^* = \left(\frac{\Delta K}{K_z} \right) \frac{d^2 T_o}{dz^2} L^2$$

Employing a conservative low value for the $(\Delta K/K_z)$ parameter of ~~0.15~~ 0.05, T^* is computed as -1030°F . In other words, the baseline HI-STORM solution over predicts the peak cladding temperature by approximately 1030°F .

4.B.6 HEAT DISSIPATION UNDERPREDICTION IN THE MPC DOWNCOMER

Internal circulation of helium in the sealed MPC is modeled as flow in a porous medium in the fueled region containing the SNF (including top and bottom plenums). The basket-to-MPC shell clearance space is modeled as a helium filled radial gap to include the downcomer flow in the thermal model. The downcomer region, as illustrated in Figure 4.4.2, consists of an azimuthally varying gap formed by the square-celled basket outline and the cylindrical MPC shell. At the locations of closest approach a differential expansion gap (a small clearance on the order of 1/10 of an inch) is engineered to allow free thermal expansion of the basket. At the widest locations, the gaps are on the order of the fuel cell opening ($\sim 6''$ (BWR) and $\sim 9''$ (PWR) MPCs). It is heuristically evident that heat dissipation by conduction is maximum at the closest approach locations (low thermal resistance path) and that convective heat transfer is highest at the widest gap locations (large downcomer flow). *In previous revisions of this FSAR, the downcomer area was understated in the FLUENT model by a large margin. In Revision 2 of the FSAR, the downcomer area is still slightly understated in the FLUENT model for all MPC geometries (please see the table below), but the extent of conservatism has been moderated and the increase in the downcomer area achieved from the deletion of the aluminum heat conduction elements is duly recognized.*

<i>Comparison of the Actual and Assumed Downcomer Flow Area for Different MPC Types</i>			
	<i>Actual (Based on the drawings provided in Section 1.5)</i>	<i>Assumed in the FLUENT Model (Revision 1)</i>	<i>Assumed in the FLUENT model (Revision 2)</i>
<i>MPC-24</i>	<i>700.6</i>	<i>517.1</i>	<i>677.7</i>
<i>MPC-24E and MPC-24EE</i>	<i>664.9</i>	<i>517.1</i>	<i>641.4</i>
<i>MPC-32 and MPC-32F</i>	<i>773.3</i>	<i>517.1</i>	<i>746.1</i>
<i>MPC-68 and MPC-68F, MPC-68FF</i>	<i>629.9</i>	<i>370.6</i>	<i>601.1</i>

~~In the FLUENT thermal model, a radial gap that is large compared to the basket to shell clearance and small compared to the cell opening is used. As a relatively large gap penalizes heat dissipation by conduction and a small gap throttles convective flow, the use of a single gap in the FLUENT model understates both conduction and convection heat transfer in the downcomer region. Furthermore, heat dissipation by the aluminum heat conduction elements, if used, is conservatively neglected in the thermosiphon models employed in the HI STORM modeling.~~

Heat dissipation in the downcomer region is the sum of five elements, viz. convective heat transfer (C1), helium conduction heat transfer (C2), basket-to-shell contact heat transfer (C3), radiation heat transfer (C4) and aluminum conduction elements (if used) heat transfer (C5). In the HI-STORM thermal modeling, two elements of heat transfer (C3 and C5) are *completely* neglected, C2 is severely penalized and C1 is underpredicted. In other words the HI-STORM thermosiphon model has choked the radial flow of heat in the downcomer space. This has the direct effect of raising the temperature of fuel in the thermal solutions.

4.B.7 CONSERVATISM IN MPC EXTERNAL HEAT DISSIPATION TO CHIMNEY AIR

The principle means of decay heat dissipation to the environment is by cooling of the MPC surface by chimney air flow. Heat rejection from the MPC surface is by a combination of convective heat transfer to a through flowing fluid medium (air), natural convection cooling at the outer overpack surface, and by radiation heat transfer. Because the temperature of the fuel stored in the MPC is directly affected by the rate of heat dissipation from the canister external surface, heat transfer correlations with robust conservatisms are employed in the HI-STORM simulations. The FLUENT computer code deployed for the modeling employs a so-called “wall-functions” approach for computing the transfer of heat from solid surfaces to fluid medium. This approach has the desired effect of computing heat dissipation in a most conservative manner. As this default approach has been employed in the thermal modeling, it is contextually relevant to quantify the conservatism in a classical setting to provide an additional level of assurance in the HI-STORM results. To do this, we have posed a classical heat transfer problem of a heated square block cooled in a stream of upward moving air. The problem is illustrated in Figure 4.B.8. From the physics of the problem, the maximum steady state solid interior temperature (T_{max}) is computed as:

$$T_{max} = T_{sink} + \Delta T_{air} + \Delta T_s$$

where,

T_{sink}	= Sink temperature (mean of inlet and outlet air temperature)
ΔT_{air}	= Solid surface to air temperature difference
ΔT_s	= Solid block interior temperature elevation

The sink temperature is computed by first calculating the air outlet temperature from energy conservation principles. Solid-to-air heat transfer is computed using classical natural convection correlation proposed by Jakob and Hawkins (“Elements of Heat Transfer”, John Wiley & Sons, 1957) and T_s is readily computed by an analytical solution to the equation of heat conduction in solids. By solving this same problem on the FLUENT computer code using the in-built “wall-functions”, in excess of 100°F conservative margin over the classical result for T_{max} is established. *In the HI-STORM thermal model, an estimate of the effect of this conservatism is provided in Table 4.B.1.*

4.B.8 MISCELLANEOUS OTHER CONSERVATISMS

Section 4.4.6 of the FSAR lists *an array of eleven* elements of conservatisms of which certain non-transparent and individually significant items are discussed in detail in this appendix. These conservatisms are primarily intrinsic to the solution methodology or are the product of assumptions made in the input data. Examples in the latter category are the values assumed in the thermal analysis of the key input variables such as the extent of ~~in-solution~~ *hat-insolation heat* input, the size of the entrance area available for in-flow of helium in the *bottom of the basket*, and the axial surface temperature profile of the MPC outer surface. Apart from the input data and methodology related conservatisms, the solution process makes several implicit assumptions to under represent the rate of heat transfer, an example of this type being the assumption that the helium upflow along the basket cavities is not at all turbulated by the presence of the cladding grid spacers. *A listing of principal conservatisms not discussed in the foregoing sub-sections is summarized below:*

- i) *The flow resistance factors used to simulate flow through MPC 3-D continuum are conservative bounding values.*
- ii) *Axial heat transfer through fuel pellets is neglected.*
- iii) *The upflow of Helium through the MPC is assumed to be laminar (high flow resistance, low heat transfer).*
- iv) *Turbulation of flow at grid spacers, top & bottom fittings are neglected.*
- v) *Insolation heating with a bounding absorbtivity of 1.0.*
- vi) *Permissible cladding temperature used to determine Q is less than the computed value for either high burnup or low burnup fuel of a given age (see Figure 4.B.9).*
- vii) *Contact between fuel and basket and between basket and supports neglected.*
- viii) *MPC is assumed to be loaded with the most thermally resistive fuel type in its category (BWR or PWR) as applicable.*

The assumptions inherent to the FLUENT solution methodology and to the solution process, in conjunction with those in the input data, are estimated to have an aggregate effect of ~~Out of the balance of conservatisms, the one of notable mention is the conservatism in fuel decay heat generation stipulation based on the most heat emissive fuel assembly type. This posture imputes a large conservatism for certain other fuel types, which have a much lower quantity of Uranium fuel inventory relative to the design basis fuel type. Combining this with other miscellaneous conservatisms, an aggregate effect is to overestimating~~ overestimate cladding temperatures by about 15°F to 50°F a considerable amount, as estimated in Table 4.B.1.

4.B.9 CONCLUSIONS

The foregoing narrative provides a physical description of the many elements of conservatism in the HI-STORM 100 thermal model. The conservatisms may be broadly divided into two categories:

1. Those intrinsic to the FLUENT modeling process.
2. Those arising from the input data and on the HI-STORM 100 thermal modeling.

The conservatism in Category (1) may be identified by reviewing the Holtec International Benchmark Report [4.B.1], which shows that the FLUENT solution methodology, when applied to the prototype cask (TN 24P) over-predicts the peak cladding temperature by as much as 79 °F. and as much as 37°F relative to the PNNL results (see Attachment 1 to Reference [4.B.1]) from their COBRA SFS solution as compared against Holtec's FLUENT solution.

Category (2) conservatisms are those that we have deliberately embedded in the HI-STORM 100 thermal model to ensure that the computed value of the peak fuel cladding temperature is further over-stated. Table 4.B.1 contains a listing of the major conservatisms in the HI-STORM 100 thermal model, along with an estimate of the effect (increase) of each on the computed peak cladding temperature. *In addition, the deliberately lower permissible PCT than that computed by the analysis in this FSAR (Appendix 4.A) provides additional conservatism that is directly quantified by referring to Figure 4.B.9.*

Table 4.B.1

Conservatism in the HI-STORM 100 Thermal Model

MODELING ELEMENT	ESTIMATED CONSERVATISM IN THE PREDICTED MAX. CLADDING TEMPERATURE [°F]
Long Term Ambient Temperature (<i>Sub-Section 4.B.2</i>)	2 to 30
Hypothetical Cylinder Construct (<i>Sub-Sections 4.B.3, 4.B.4</i>)	~5
Axial Heat Dissipation Restriction (<i>Sub-Section 4.B.5</i>)	30 10
MPC Downcomer Heat Dissipation Restriction (<i>Sub-Section 4.B.6</i>)	50 5
MPC External Heat Dissipation Under-prediction (<i>Sub-Section 4.B.7</i>)	50
Miscellaneous-Other Conservatisms (<i>Sub- Section 4.B.8</i>)	15 to 50 50 to 75
Rayleigh Effect (<i>Sub-Section 4.4.1.1.5</i>)	25

4.B.9 REFERENCES

- [4.B.1] "Topical Report on the HI-STAR/HI-STORM Thermal Model and its Benchmarking with Full-Size Cask Test Data", Holtec Report HI-992252, Rev. 1.

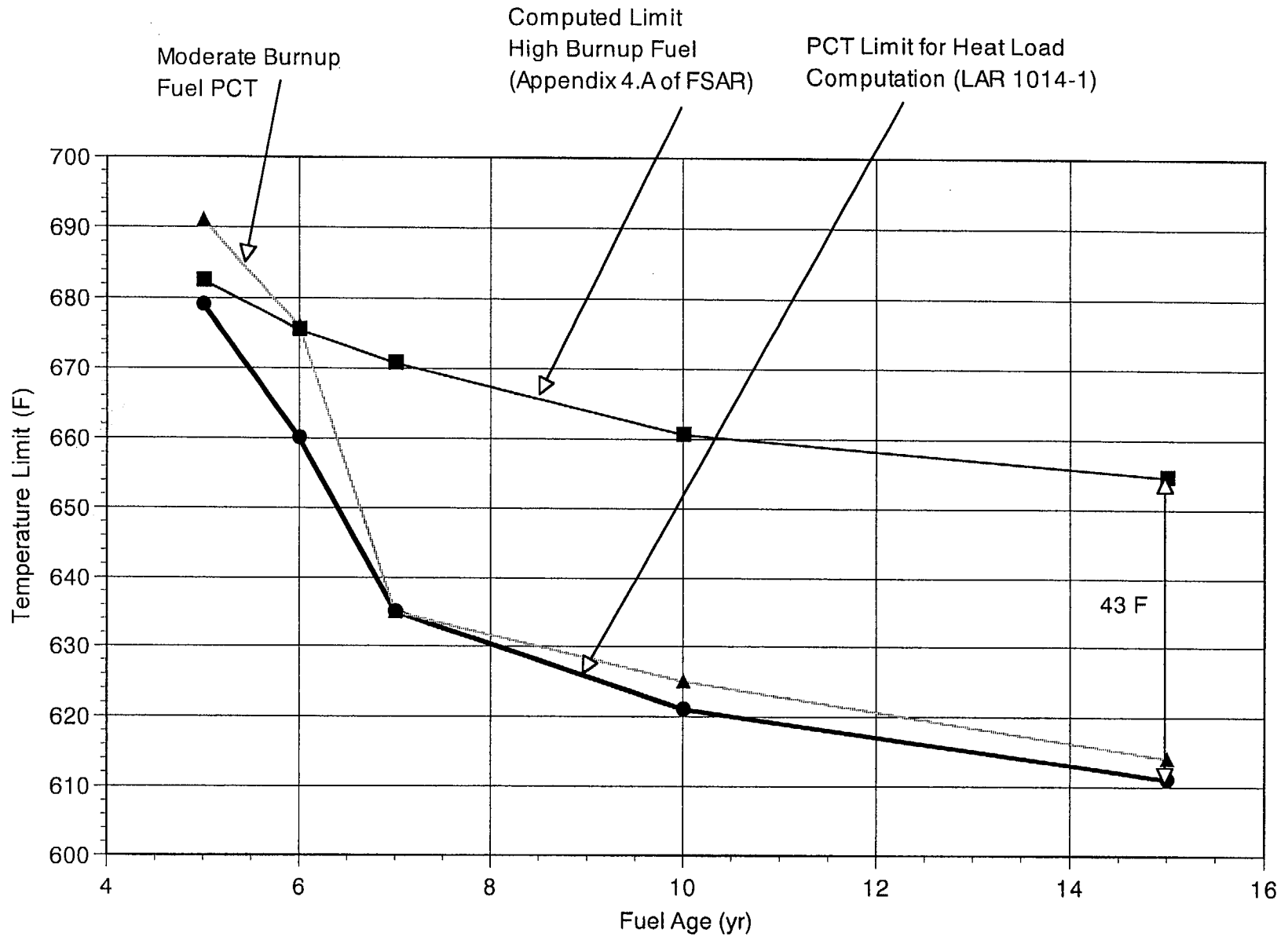


FIGURE 4.B.9: Comparison Between Computed and Specified values of the Permissible Peak Cladding Temperature Limit for High Burnup PWR Fuel